



---

<sup>b</sup>  
UNIVERSITÄT  
BERN

OESCHGER CENTRE  
CLIMATE CHANGE RESEARCH

MASTER THESIS

FACULTY OF SCIENCE

UNIVERSITY OF BERN

---

# Convective environments along Mediterranean cyclone tracks: exploring severe surface weather

---

*handed in by*  
**Andrea Angelidou**

**August, 2023**

*Supervisor:* Prof. Dr. O. Romppainen-Martius  
*Co-supervisors:* Dr. R. Rousseau-Rizzi, Dr. A. Portal

*Oeschger Centre for Climate Change Research,  
University of Bern*

## Abstract

Mediterranean cyclones may be associated with significant environmental hazards such as strong winds, heavy rain and thunderstorms. To better understand the relationship between convective environments and hazards along Mediterranean cyclone tracks, we examine their spatial and temporal characteristics from a Lagrangian viewpoint. The study differentiates among nine cyclone clusters following a recent work classifying Mediterranean cyclones based on their upper-level PV structure. Our results reveal connections between convective parameters, hazards, large-scale dynamics, and seasonal and spatial qualities of the clusters. For example, the winter cluster with the strongest convective environment displays a distinct convective rainfall pattern and higher hazard intensities compared to other winter clusters, primarily due to the presence of a warm occlusion and a deep PV structure. Further, autumn and spring clusters exhibit a convective activity and hazard intensities shaped by the specific environmental conditions within their respective geographical regions. The time evolution analysis shows a build-up of the convective environment before the mature stage of the cyclone, with hazards generally peaking before and at the time of maximum cyclone intensity, but this timing varies depending on the seasonal distribution of cyclone clusters. Overall, our results highlight the importance of considering both stability and shear when assessing convective hazards along Mediterranean cyclone tracks. Additionally, we emphasize the significance of accounting for the seasonal, spatial, and dynamical characteristics of cyclones in hazard assessment. Understanding how different types of Mediterranean cyclones are associated with convective environments, potentially leading to severe weather at the surface, is crucial for operational forecasters to issue timely alerts and prepare for the hazards.

# Contents

<b>1</b>	<b>Introduction</b>	<b>3</b>
1.1	Aims of the study . . . . .	4
<b>2</b>	<b>Literature Review</b>	<b>6</b>
2.1	Convective environments . . . . .	6
2.2	Mediterranean cyclones . . . . .	7
<b>3</b>	<b>Data</b>	<b>13</b>
3.1	Cyclone tracks and clusters . . . . .	13
3.2	Reanalysis Data . . . . .	17
3.3	Hail & Lightning proxies . . . . .	18
<b>4</b>	<b>Methods</b>	<b>20</b>
4.1	Part I: Composite analysis . . . . .	20
4.2	Part II: Time Evolution . . . . .	22
<b>5</b>	<b>Results</b>	<b>24</b>
5.1	Part I: Composite maps . . . . .	24
5.2	Part II: Time evolution . . . . .	34
<b>6</b>	<b>Discussion</b>	<b>40</b>
6.1	Winter Clusters 1-2-4 . . . . .	40
6.2	Autumn & Spring Clusters 5-8 . . . . .	45
6.3	Spring Clusters 3-7 . . . . .	48
6.4	Summer Clusters 6-9 . . . . .	50
<b>7</b>	<b>Conclusion</b>	<b>53</b>
<b>A</b>	<b>Appendix</b>	<b>55</b>
<b>B</b>	<b>Appendix</b>	<b>61</b>

# 1 Introduction

The Mediterranean region is well-known for its high frequency of cyclogenesis, with hundreds of cyclones forming each year [Petterssen, 1956; Campins et al., 2011]. The cyclones vary in their intensities, lifetimes, and structures. They are smaller in size and shorter in lifespan than extra-tropical cyclones over the open ocean [Flaounas et al., 2015, 2022]. Nevertheless, Mediterranean cyclones can have large impacts for example when they are associated with extreme winds and heavy rainfall. As highlighted by Flaounas et al. [2022], such extreme weather events threaten the region’s infrastructure, economy, and public safety.

The Mediterranean region’s distinctive geography, characterized by land-sea transitions and high mountain chains, creates an environment conducive to cyclone formation [Trigo et al., 2002; Flaounas et al., 2022]. Mediterranean cyclones vary in size, ranging from mesoscale to synoptic. Specifically, Mediterranean cyclones have a radius ranging from 200–500 km, a life cycle lasting a day or two, and intensities rarely reaching that of tropical cyclones [Trigo et al., 1999; Emanuel, 2005; Tous and Romero, 2013].

Upper-level potential vorticity (PV) intrusions influence the region and play a crucial role in the genesis and intensity of Mediterranean cyclones, while baroclinicity is established [Flaounas et al., 2015, 2021; Raveh-Rubin and Flaounas, 2017]. Once cyclogenesis initiates, the influence of baroclinic forcing can contribute to the amplification of surface cyclones, which, in turn, promotes convection at cyclone centers through induced large-scale ascent [Flaounas et al., 2021]. As a result, diabatic processes, which involve the release or absorption of heat energy, contribute to the characteristics of Mediterranean cyclones, especially during the later stages of their development [Fita et al., 2006]. For instance, the release of latent heat during the condensation of water vapor within the cyclone’s core can intensify convection [Flocas, 2000; Flaounas et al., 2021]. Convective environments are characterized by the updraft of warm, moist air, with critical parameters including temperature, humidity, atmospheric instability, and wind shear influencing the development of severe weather. Notably, Claud et al. [2012] revealed a correlation between regions of frequent deep convection over the Mediterranean and high cyclone track density. Additionally, as cyclones encounter topographic barriers, they can undergo changes in their structure and intensity. An orographic lift can enhance the ascent of moist air, triggering or intensifying convective processes and contributing to the development of heavy precipitation [Lionello et al., 2006]. Further, the presence of warm sea surface temperatures in the Mediterranean Sea can provide a favorable environment for the intensification of cyclones [Flaounas et al., 2018]. Specifically, the warm sea surface temperatures, combined with strong surface winds associated with the cyclones, fuel the sensible and latent heat fluxes in the lower troposphere. This acts to reinforce the cyclone due to diabatic processes as described above [Raveh-Rubin and Wernli, 2016]. Rigo et al. [2019] showed that higher convective activity in the western Mediterranean is connected with warmer sea surface temperatures and a high number of cyclones in the region.

Hazards occur due to processes embedded within the synoptic and mesoscale features of the cyclones. At the synoptic scale, hazards are influenced by the structure of the cyclone and characteristics such as its track, intensity, and size. At the mesoscale, Mediterranean cyclones can exhibit recognisable spatial features, such as convective bands, comma-shaped cloud formations, and spiral-shaped rainbands [Tous and Romero, 2013; Fita et al., 2007]. These features are induced by the vertical motion within the

cyclones, which can enhance the development of deep convection. The presence of convective bands within the cyclone’s core can lead to localized intense rainfall, flash flooding, and even the formation of waterspouts or tornadoes in coastal areas [Flaounas et al., 2022]. Additionally, in some cases, the interaction of cyclones and orography can result in significant rainfall disparities between windward and leeward sides of mountain ranges, leading to localized flooding or even mudslides. Moreover, studies have linked flash floods in the Mediterranean to strong and occasionally explosive cyclone activity, but also due to less intense cyclones with embedded mesoscale convective systems that interact with the unique topography of the region [Michaelides et al., 2018].

As presented above, Mediterranean cyclones are associated with environmental hazards like wind, lightning, and heavy rain. Their severe weather accounts for a sizable portion of Europe’s financial losses from natural catastrophes, including damage to infrastructure, trade, and energy supplies [Pinto et al., 2012]. Consequently, to better understand the severe surface weather of Mediterranean cyclones, it is crucial to investigate the convective environments along their tracks, which serve as the foundation for the study’s aims, outlined in the section below.

## 1.1 Aims of the study

The relationship between Mediterranean cyclones and their associated convective environments is not yet fully captured. Specifically, previous studies have shed light on the high frequency of cyclone formation in the Mediterranean, the role of both baroclinicity and diabatic processes in their development and the hazards that may derive. However, the available climatological analyses do not account for the combined dynamical, spatial and seasonal conditions leading to the development of convective activity and, potentially, of severe weather events embedded in the cyclones. To fill this gap, the present study provides a Lagrangian climatology of convective environments along the Mediterranean cyclone tracks, separating the results by cyclone dynamics and peak season together [Givon et al., 2023], in order to gain an understanding of the relation between cyclones and hazards.

In particular, this study seeks to answer the following research questions:

1. What are the spatial characteristics, in magnitude and organization, of convective environments along cyclone tracks in the Mediterranean?
2. What is the association between convective environments and severe surface weather along cyclone tracks?
3. What is the evolution of convective environments and hazards, including changes in intensity, at times before and after the mature stage of the storms?

By answering these questions, the study aims to contribute to a better understanding of the complex relationship between Mediterranean cyclones and their associated convective environments. This will ultimately enhance our ability to effectively prepare and respond to these events, leading to reduced impacts on the region.

In view of the above, the study is structured in two parts. In Part I a composite analysis will be performed to investigate spatial features of convective environments and hazards along cyclone tracks

in the Mediterranean at the time of maximum intensity. Further, in Part II we follow the evolution of convective environments and hazards, at times before and after the maximum intensity of the storms.

## 2 Literature Review

### 2.1 Convective environments

The interplay of several environmental parameters favors the development of severe convective storms. In particular, necessary conditions are (1) sufficient amount of moisture in the boundary layer, (2) steep low- to midlevel lapse rates, (3) strong vertical wind shear, and (4) low-level lifting mechanism that triggers convection [Johns and Doswell III, 1992]. The thermodynamic and kinematic factors are described below for the Mediterranean region:

1. **Moisture in the boundary layer:** The warm maritime air from the Mediterranean Sea provides a moisture source. Within the cyclone’s core, this moisture-rich air is lifted, leading to the formation of deep convection. The availability of moisture influences the potential for heavy rainfall and the overall instability of the atmosphere, which contributes to the severity of the storms [Taszarek et al., 2017].
2. **Steep low- to midlevel lapse rates:** Lapse rate refers to the rate at which temperature decreases with increasing altitude. Steep low- to midlevel lapse rates imply a rapid decrease in temperature with height. Such lapse rates contribute to the instability of the atmosphere, as they create an environment favorable for the ascent of moist air parcels [Taszarek et al., 2017]. Within Mediterranean cyclones, the presence of steep lapse rates can enhance the vertical motion and the development of convective storms, amplifying their intensity.
3. **Strong vertical wind shear:** Vertical wind shear refers to the change in wind speed and/or direction with height. Strong vertical wind shear can have a profound impact on the organization and longevity of convective storms [Taszarek et al., 2017]. In the case of Mediterranean cyclones, the presence of significant wind shear can contribute to the development of rotating updrafts. Wind shear also aids in maintaining the separation between updrafts and downdrafts, leading to the persistence of severe convective storms within the cyclone’s environment [Taszarek et al., 2017].

In the context of Mediterranean cyclones, low-level lifting mechanisms can be triggered by various factors, including the interaction of the cyclone’s circulation with local topography, frontal boundaries, or convergence zones. Orographic lifting, as mentioned earlier, can play a role in initiating convection by forcing air to ascend over mountains [Scherrmann et al., 2023]. Frontal boundaries associated with the cyclone can also provide a lifting mechanism through the interaction of air masses with different thermodynamical properties [Flaounas et al., 2021].

Pacey et al. [2021] determined the preconvective environment for severe convective windstorms in Europe by using a clustering methodology on nine convective variables. Two environments were classified: Type-1 having low-shear high-CAPE (mostly occurring in the warm season) and Type-2 having high-shear low-CAPE (mostly occurring in the cold season). Type-1 environment was characterized by higher CAPE values with an interquartile range (IQR) of 200-1040 J kg<sup>-1</sup>, moderate values of bulk wind shear with an IQR of 10-20 m/s and high surface temperatures (greater than 22°C for 90% of soundings). Type-2 environment was characterized by low CAPE (72% showing values of less than 100 J kg<sup>-1</sup>), high to very high wind shear in the range of 21-39 m/s and lower surface temperatures between 7°C-17°C.

### 2.1.1 Mesoscale convective systems

Mesoscale convective systems (MCSs) occur when convective instability merges a cluster of thunderstorms that organize into a single cloud system, with a large upper cirriform cloud structure. The system's construction enables it to persist for several hours or more. MCSs play a key role in bridging the gap between large-scale atmospheric circulation and atmospheric convection [Houze Jr, 2004]. This is largely because of the intense updrafts happening within the system, which may frequently reach the tropopause. A deep-layer ascent is dragged into the MCS as a result of the latent heating and cooling in the convective area, which causes upward motion. In response to diabatic cooling at middle-to-low levels, a middle-level layer inflow falls into the stratiform zone of the MCS from a direction indicated by the large-scale flow. A mesoscale convective vortex (MCV) can develop in the stratiform region at mid-levels. MCSs show continuous progression due to the synergy of cold pool dynamics, where outflow boundaries trigger new storm development. Also, the layer-overturning theory creates pressure gradients that sustain the MCS's forward movement and organization [Houze Jr, 2004]. However, it may also be affected by waves and disturbances that are produced both by the system itself and the large-scale flow. Large-scale waves may impact the propagation velocity and favor phase locking with the MCSs [Houze Jr, 2004]. Severe impacts from long-lasting MCS include flooding, hail, strong winds and occasionally tornadoes [Rigo et al., 2019].

Michaelides et al. [2018] showed that flash floods in the Mediterranean are also linked to relatively weak cyclones with long-lasting MCSs within their structure, where MCSs are generally associated with the presence of low-pressure systems. For the western Mediterranean, Rigo et al. [2019] showed that the primary trajectories of the MCSs resemble the tracks of the cyclones seen in the area. In addition, the sea surface temperature (SST) appeared to be a significant factor in the mechanisms behind MCSs, where MCS activity increased when SST exceeded land temperature. These previous studies outlined the need to characterize the environments that are conducive to MCSs along Mediterranean cyclone tracks.

## 2.2 Mediterranean cyclones

### 2.2.1 Spatial and seasonal distribution

Mediterranean cyclones can be regarded as a subclass of extra-tropical cyclones, distinct from those forming over the oceans, because of their smaller size and lower intensity, with the formation region confined to a much smaller area and surrounded by unique topographical characteristics. Figure 1, from Campins et al. [2011], represents the density of cyclones per season within the Mediterranean region. The storms are more common in winter, with tracks spaced over the northern and central parts of the Mediterranean basin (refer Fig. 1(c)). In winter, there is a correlation between synoptic upper-level troughs, baroclinicity and orography. Autumn shares similar characteristics with winter cyclogenesis. However, in specific autumn cases, cyclones' centers exhibit stronger convection compared to winter, largely driven by the influence of warmer SSTs [Flaounas et al., 2022]. Finally, in spring and summer, cyclogenesis arises and becomes more frequent due to thermal forcing [Trigo et al., 2002].

Intense cyclones form mostly in the northwest Mediterranean within the Gulf of Genoa, Tyrrhenian and Adriatic Seas [Homar et al., 2007]. Specifically, during winter, these regions witness a notable prevalence of deep cyclonic systems, shown as high-density areas in Fig. 1(c), which corresponds to a region known for high-impact weather events [Reale and Lionello, 2013]. Autumn shown in Fig. 1(b),



exhibits the highest concentration of cyclone centers in the Gulf of Genoa and surrounding areas. There are also some centers located in the Sahara, although their number is fewer compared to the warmer seasons. Further, mature intense cyclones may often occur within the Ionian, Aegean and Black Seas as well as the Levantine basin close to Cyprus [Homar et al., 2007]. Finally, intense cyclones can be found close to the Atlas mountains, primarily in spring and summer (refer to Fig. 1(a) & (d)), where they may propagate eastwards from southwest to the central part of the basin [Lionello et al., 2006].

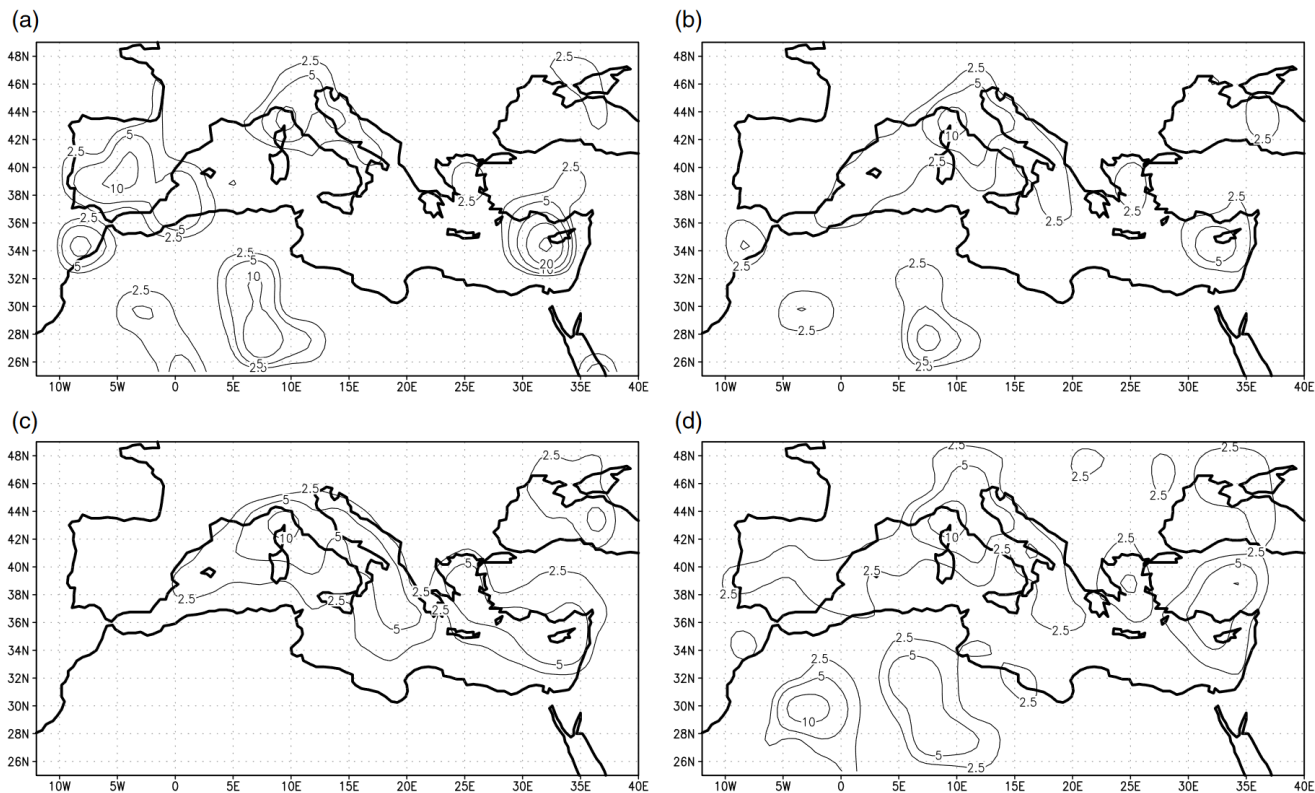


**Figure 1.** Seasonal mean number of cyclone centres in  $2.25^\circ \times 2.25^\circ$  latitude–longitude boxes, for (a) summer, (b) autumn, (c) winter and (d) spring. Contour intervals: 2.5, 5, 10, 20 and 40 centres per season. Reprinted from Campins et al. [2011].

### 2.2.2 Large-scale dynamics, fronts, and airstreams

Upper-tropospheric precursors (i.e. troughs, PV streamers, Rossby wave breaking, and cut-offs) can trigger the formation of Mediterranean cyclones primarily through baroclinic instability [Flaounas et al., 2015]. Specifically, southward deviations of the polar jet can cause air masses with high PV to intrude in the Mediterranean region. Further, Raveh-Rubin and Flaounas [2017] showed that in some cases there is a dynamical link between the warm conveyor belt (WCB) air of North Atlantic cyclones and the downstream development of Mediterranean cyclones. As the WCB ascends and amplifies the ridge, troughs are induced downstream and hence cyclogenesis occurs over Europe.

Upper-level PV anomaly can cause saturation at low levels leading to cloud and precipitation formation east of the cyclone center. Consequently, diabatic PV production takes place, amplifying the low-level positive PV anomaly. In most circumstances, the diabatically induced PV anomaly further intensifies the cyclone’s evolution [Flaounas et al., 2015, 2021]. As a result, at the mature stage of strong cyclones, there is a formation of a vertical structure known as “PV tower”, where the positive upper and low-level

PV anomalies (and surface warm anomaly) become vertically aligned.

Raveh-Rubin and Wernli [2016] created a schematic illustration of the possible features of Mediterranean cyclones bringing about combined precipitation and wind impact (refer to Fig. 2). Warm conveyor belts (feature 5 in Fig. 2) are bands of warm, moist air that ascend from lower latitudes and ahead of the cold front (i.e. to the east and north of the cyclone). WCBs have been linked to 50%-60% of severe precipitation occurrences in the Mediterranean [Pfahl et al., 2014]. Dry air intrusions (DIs; feature 3 from Fig. 2) are streams of dry air from the upper levels that descend into a region where the prevailing air mass is typically moist. They are usually found west of the cyclone centre and coincide with the region of low-level wind gusts (feature 4 from Fig. 2). Further, DIs reaching the cold front have been detected in correspondence with the region of convective wind gusts and precipitation.

In general, there are two distinct regions located to the east and west of the cyclone center, with opposing thermodynamic structures that are highly influenced by water vapor content [Flaounas et al., 2015]. On the western side, there is the presence of dry air from DIs and northward advection of PV streamer. On the other hand, the eastern side experiences the inflow of warm and moist air originating from the south, resulting in upsloping along the warm front and increased moisture in the middle and upper troposphere.

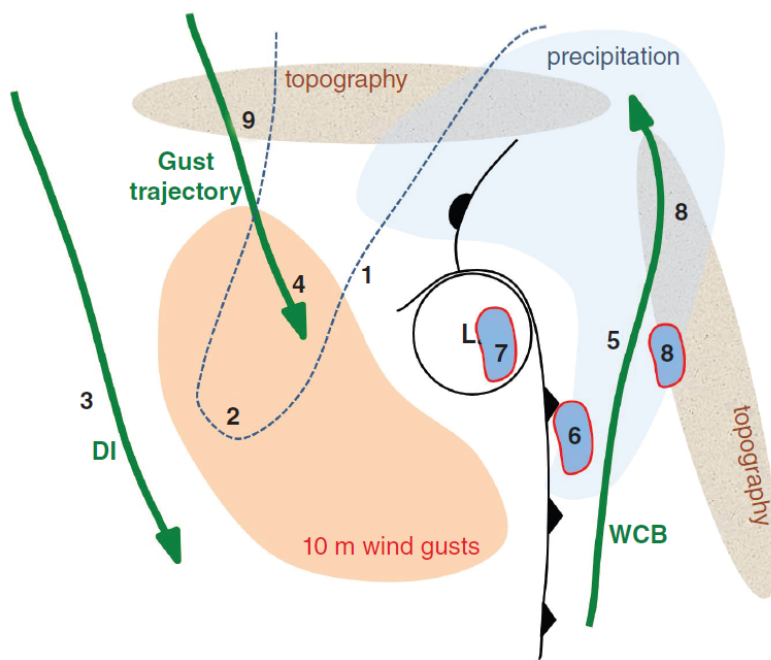


**Figure 2.** Schematic illustration of possible features related to combined precipitation and wind impact of a cyclone in the Mediterranean, based on the five events studied in Raveh-Rubin and Wernli [2016]. Note that this schematic does not represent any individual event, but rather summarizes the variable possible features of importance. The cyclone centre is denoted by the letter ‘L’, accompanied by a cold and a warm front. Shading shows areas with precipitation impact (light blue), and with 10m gust impact (light red). Areas with convection (and thus co-located precipitation and wind gust impact) are shaded blue and encircled by a red line. High topography is represented by grey regions. The 320 K 2-PVU contour is shown as a dashed line and typical WCB, DI and gust trajectories are denoted as green arrows. The numbers mark the location of: (1) a prominent upper-level feature (PV streamer/trough/ridge), (2) tropopause fold and downward momentum transfer, (3) DI trajectories around high gusts, (4) low-level gust trajectory, (5) WCB slantwise ascent associated with precipitation, (6) convective precipitation at the cold front, (7) convective precipitation in cyclone centre, (8) orography enhancing precipitation (and/or convection), (9) orography accelerating gust trajectories. Reprinted from Raveh-Rubin and Wernli [2016].

Furthermore, Raveh-Rubin and Wernli [2016] found convective precipitation in all five cases they studied, primarily seen along the cold front (feature 6), in the cyclone centre (feature 7) and in coastal regions. It was mentioned that determining convective activity is important as it may lead to compound events that combine extreme precipitation and strong wind gusts. In addition, Flaounas et al. [2018] studied the spatial variability of deep convection (DC) for 500 most intense cyclones from 2005 to 2015. Their composite analysis revealed that DC formation is favored around cyclone centres and on their eastern flanks, most likely associated with the cyclonic frontal systems. Finally, Flaounas et al. [2016] mentioned that deep convection is a prominent feature of the most intense Mediterranean cyclones, which are frequently coupled with heavy rainfall.

### 2.2.3 Cyclone subtypes

This section provides background information on cyclone subtypes that are related to the clusters used in the study (detailed later in Section 3.1). In particular, we address their physical description and dynamical characteristics.

#### 2.2.3.1 Lee-cyclogenesis

A high frequency of cyclogenesis occurs “in the lee” of the Mediterranean topography (including the Alps, Pyrenees, and Atlas Mountains). Buzzi and Tibaldi [1978] described lee-cyclogenesis as a two-step process. In the first stage (Stage A) an upper-level trough approaches the mountain range and cold air advection is obstructed on the windward side. At that time, a positive thermal anomaly and fast pressure drop are created on the lee side, coupled with wind acceleration. The atmospheric instability, mainly due to thermal advection, contributes to the strengthening of the cyclone. In Stage B, the primary wave decouples and moves away from topography. A secondary lee-cyclone forms due to the dominance of baroclinic instability (initiated at Stage A). This plays a crucial role in intensifying the cyclonic activity. Specifically, in Stage B there is a resemblance to type-B cyclogenesis [Petterssen and Smebye, 1971], where the vertical tilt and phase locking of the upper-level PV streamer and the low-level PV (or thermal) anomaly amplifies the development of the baroclinic cyclone through mutual reinforcement.

#### 2.2.3.2 Wave breaking & Cut-off lows

Mediterranean cyclones are frequently associated with elongated intrusions of high PV, known as PV streamers. PV streamers can originate from anticyclonic or cyclonic Rossby wave breaking (AWB & CWB, respectively) over the region [Flaounas et al., 2015]. Further, as the PV streamers move equatorward, they can break up into PV cut-offs, which are cyclonic PV anomalies isolated from the main stratospheric reservoir [Wernli and Sprenger, 2007]. Figure 3, from Thorncroft et al. [1993], shows the development of AWB and CWB as part of the life cycle of baroclinic waves. AWB occurs on the anticyclonic shear side i.e. equatorward of the jet stream, and CWB occurs on the cyclonic shear side i.e. poleward of the jet stream. In the case of AWB, the anticyclonic shear plays an important role in the thinning of the trough tilted to the NE-SW side and is more prone to develop into a cut-off. Conversely, in a scenario involving CWB, the trough is expected to broaden due to cyclonic shear [Thorncroft et al., 1993].

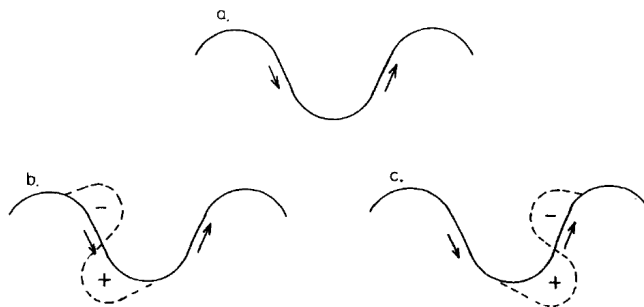


**Figure 3.** A thought experiment indicating the effects of meridional shear on the evolution of an initially sinusoidal PV-theta contour: (a) indicates a contour with implied winds before the meridional wind shear has tilted it. The dashed contours in (b) and (c) represent the configuration resulting from anticyclonic or cyclonic tilting, respectively. Reprinted from Thorncroft et al. [1993].

Cut-off lows have been identified as significant contributors to severe surface weather, including the intensification of surface cyclones and extreme precipitation (for the Mediterranean refer to Fita et al. [2006]; Porcù et al. [2007]; Toreti et al. [2016]). One example from Michaelides et al. [2018], mentions the effects of cut-off lows on hail instances in the south of France. Specifically, the occurrence of cut-off lows or troughs over the Atlantic results in south-southwest flow over the south of France. This configuration, in conjunction with a cold marine air mass coming across Aquitaine and the Pyrenees at mid-levels above a warm southern flow at lower levels, leads to an increased lapse rate between 850 and 500 hPa. These specific conditions have been previously described as highly conducive to hailstorm formation in the region [Berthet et al., 2011, 2013].

### 2.2.3.3 Daughter lows

In the Mediterranean, the majority of cyclones are referred to as “daughter” cyclones [Ziv et al., 2015], which develop in the vicinity of existing cyclones already in the region. The parents of Genoa lows are typically east of their daughters, indicating that cyclogenesis occurs within the northerly flow induced by the parent cyclone, which traverses the Alps. In contrast, the parents of Aegean Sea lows are mostly west of their daughters, showing that cyclogenesis occurs in the southerly flow ahead of the parent cyclones and hence within the warm sector of the parents. According to Saaroni et al. [2017], more than half of the daughter cyclones originate in the “parent’s” frontal system, one-third on a distinct frontal system, and the remaining within the warm sector of the parent cyclone. The warm and moist air within the warm sector provides a source of energy and moisture for the daughter cyclone to develop and intensify. Meanwhile, the cold front associated with the parent cyclone can help to steer the daughter cyclone and give it a distinct track.

### 2.2.3.4 Heat lows

Heat lows (or thermal lows) typically develop in regions with intense surface heating, such as desert areas or coastal regions affected by warm ocean currents [Johnson, 2003]. The heating in the lower troposphere leads to a low-pressure system due to rising warm air and convergence at the surface, both characteristics of convective activity. In the Mediterranean region, thermal lows are separated into continental heat

lows, referring to cyclones that form on the leeward side of the Atlas mountains (desert depressions or “Saharv cyclones”) and marine heat lows, that can occur in various areas of the basin.

The Saharv cyclones originate over arid regions of North Africa, have minimal moisture content and are frequently associated with dust storms [Fiedler et al., 2014]. They move fast with an eastward propagation and their tracks follow the North African coast, where on certain occasions they turn north and towards the southeastern Mediterranean [Alpert and Ziv, 1989]. Saharv cyclones are often accompanied by an active warm front, which is occasionally associated with extremely high temperatures, and a shallow cold front.

Marine heat lows can develop due to wind-induced surface heat exchange (WISHE; Yano and Emanuel [1991]) processes. It refers to the interaction between atmospheric circulation, surface winds, and SSTs, that lead to enhanced heat and moisture fluxes from the ocean to the atmosphere. Specifically, the region’s warm SST acts as a source of energy for these cyclones and with increased surface winds, due to cyclonic circulation, results in stronger surface heat fluxes. As a result, the latent heat released during moisture condensation further contributes to the intensification of convective activity within the cyclone. In general, diabatic processes along with low-level baroclinicity play an important role in the evolution of explosive cyclones, which are characterized by a strong deepening over a relatively short time range [Kouroutzoglou et al., 2018].

### **2.2.3.5 Medicanes**

WISHE can also play a role in the formation of Mediterranean tropical-like cyclones (referred to as “Medicanes”). Medicanes are composed of powerful mesoscale vortices that pose considerable risks upon landfall. They usually have traits that are comparable to tropical cyclones, including a warm-core, axisymmetric cloud pattern, low vertical shear of horizontal wind speed and sustained wind speeds that are nearly as strong as hurricanes [Flaounas et al., 2022]. While the definition of Medicanes remains an ongoing area of research, their classification as a distinct category or subcategory of polar and subtropical lows [Miglietta and Rotunno, 2019], underscores the Mediterranean’s unique potential for cyclogenesis. Miglietta and Rotunno [2019] categorized Medicanes in three groups based on (1) the presence of baroclinic instability and dominant warm-seclusion process, (2) the WISHE through positive feedback between air-sea interactions and atmospheric circulation, and (3) the interaction of mesoscale vortices with synoptic scale PV anomalies.

Dafis et al. [2020] investigated the organization of deep convection and its role in the strengthening of nine Medicanes that occurred between 2005 and 2018. Results showed that DC organization is significantly influenced by topography and vertical wind shear. In four cases of Medicanes, Dafis et al. [2020] found that prior to the cyclone maximum intensity, there is sustained and organized DC activity close to the cyclones’ centers.

## 3 Data

### 3.1 Cyclone tracks and clusters

The associated storm tracks used in this study were generated by Flaounas et al. [2023] in a composite approach that combines multiple tracking methods. The tracks are produced using ERA5 reanalysis (see below in Section 3.2) for the period 1979-2020, and the parameters considered include mean SLP minima, gradients, relative vorticity field at 850 hPa and geopotential height at 1000 hPa. The outputs from 10 separate cyclone tracking methods are filtered in order to keep just the tracks with the highest agreement among them. The “confidence level” is defined by the number of tracking methods utilized, which range from 2 to 10, to generate composite track points. The cyclones are monitored throughout their lifetime and their center position is identified as the minimum sea-level pressure (SLP) at each timestep. In our study, a confidence level of 5 was chosen that yielded 3190 cyclone tracks.

To offer a broader view of the atmospheric conditions in which the cyclones take place, the tracks were assembled into clusters and classified based on their upper-level potential vorticity (PV), a method proposed by Givon et al. [2023]. Self-organizing map (SOM) algorithm [Kohonen, 1990] was used to classify the clusters, with input being the isentropic upper-level PV averaged across 320-340 K at the moment of minimum SLP. The storm tracks were categorized in 9 clusters. Figure 4 shows the mean upper-level PV structure of each cluster and the mean frequency out of all cyclones. The longitude latitude box represents the selected region between 20°W-45°E and 30°-50°N.

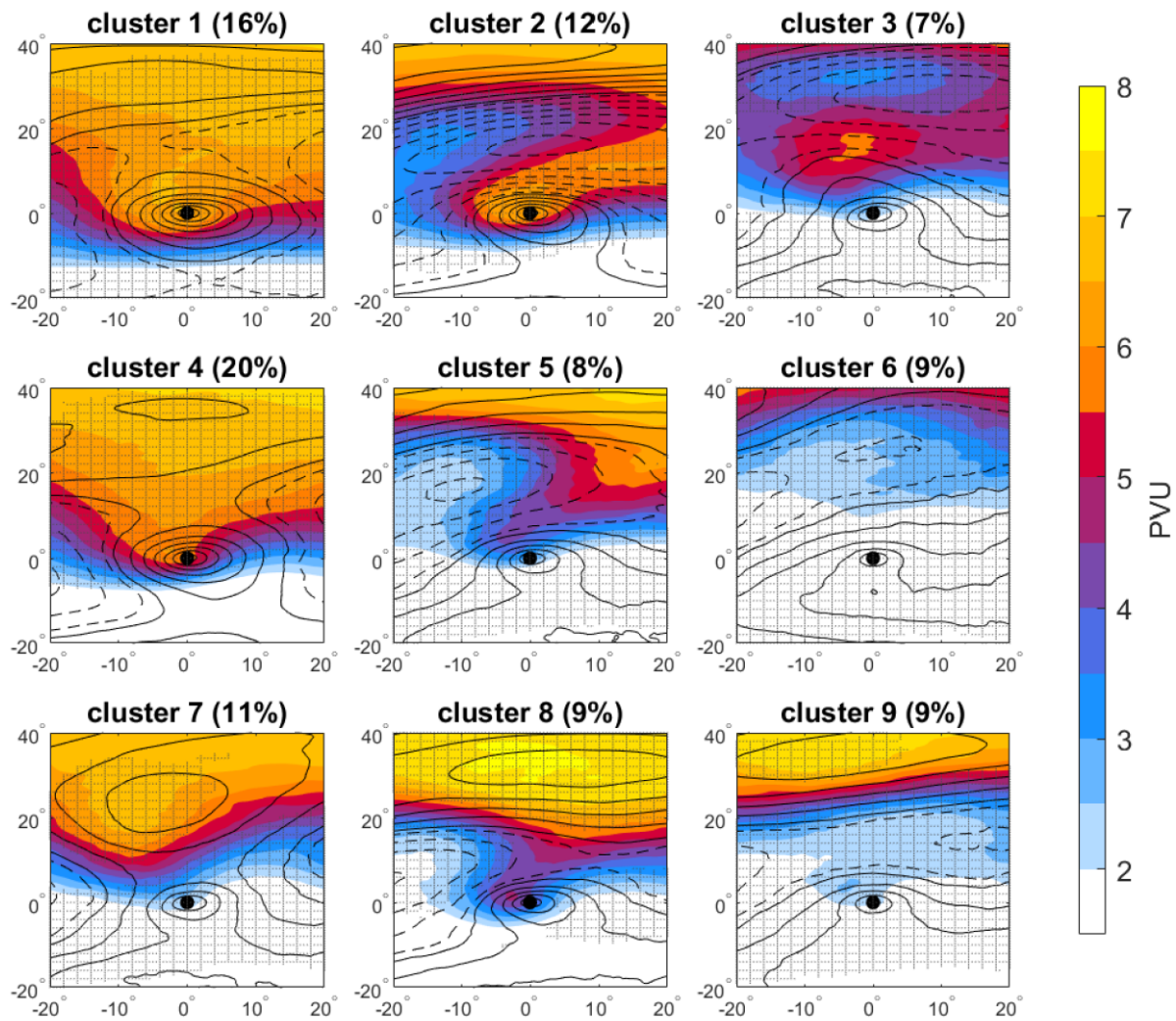


**Figure 4.** Cyclone-centered cluster composites of upper-level PV (PVU, shading) and SLP (black contours at 2-hPa intervals, dashed over 1015 hPa). Stippling indicates a 99% significance level of the PV field concerning the total cyclone average. The mean frequency of each cluster out of all cyclones considered is given in the title. Reprinted from Givon et al. [2023].

Features of the clusters including dynamical, seasonal and geographical distributions as well as certain surface impacts are described in detail in Givon et al. [2023]. A condensed overview of the cluster characteristics is provided in Figure 5. For a more comprehensive view, Figures 6-7 portray the seasonal and geographical distributions of these aforementioned clusters.

Cluster	(1) Stage A lee-low	(2) AWB+CWB low	(3) Long-wave cut-off low	(4) Stage B lee-low
Season	winter	winter	spring	winter
Genesis	Alps	Alps	Atlas	Alps
Peak	Ligurian Sea	diverse	Atlas	diverse
Cold sector	extreme	extreme	weak	strong
Warm sector	faint	Weak	strong	mild
Precipitation	heavy, LS+ C-	heavy, LS+ C+	mild, LS- C-	heavy, LS+ C+
Mobility	fast	slow	fast	fast
Trend	decrease	none	increase	decrease

Cluster	(5) AWB low	(6) Heat low (Sharav)	(7) Daughter low	(8) CWB low	(9) Short-wave cut-off low
Season	spring/autumn	summer	spring	autumn	summer
Genesis	Atlas	Atlas	diverse	Alps	diverse
Peak	Atlas	Sahara	diverse	Ligurian sea	diverse
Cold sector	mild	faint	weak	mild	faint
Warm sector	strong	extreme	extreme	mild	strong
Precipitation	mild, LS- C-	weak, LS- C-	mild, LS- C-	heavy, LS- C+	mild, LS- C-
Mobility	average	slow	fast	slow	slow
Trend	increase	increase	none	none	increase

Figure 5. Summary of the main cyclone class characteristics. Precipitation is summarized as the mean absolute pattern, large-scale (LS), and, convective (C) anomaly signs. Reprinted from Givon et al. [2023].

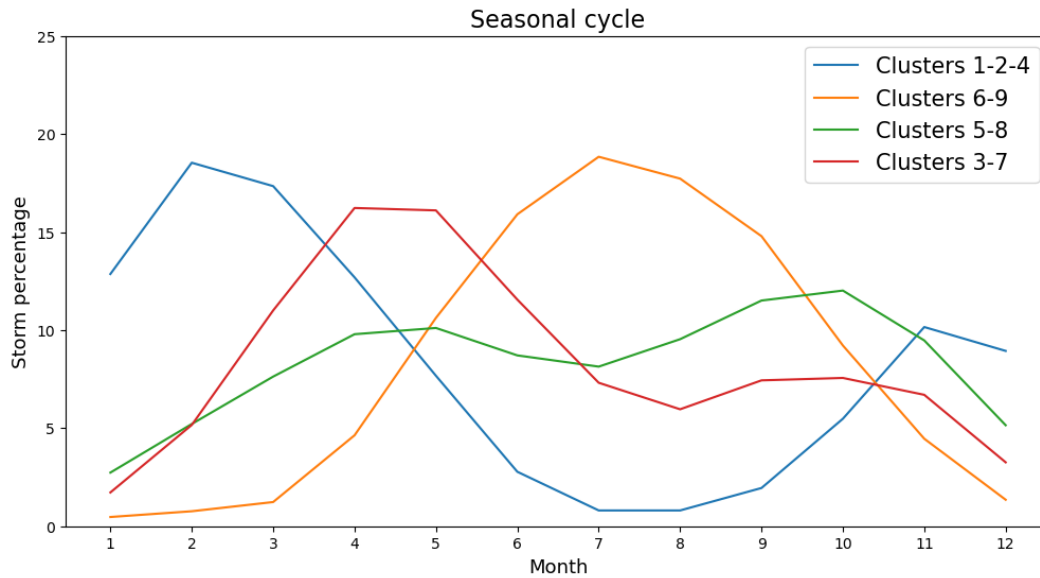
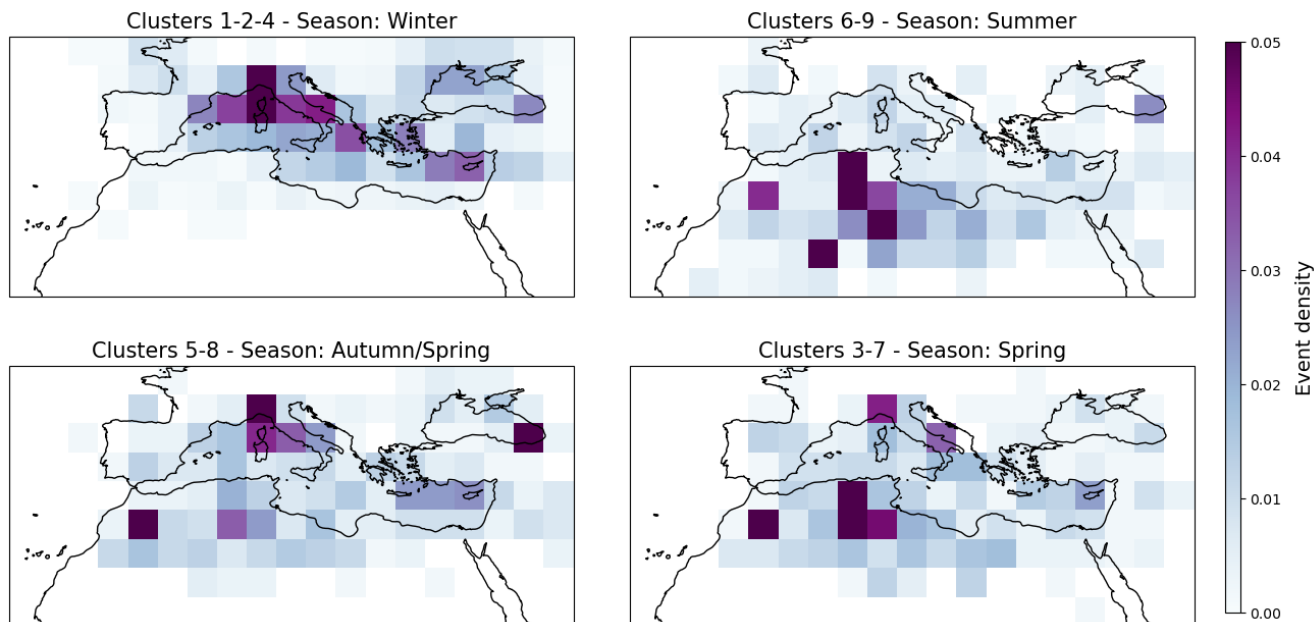


Figure 6. Shows the seasonal distribution of the different clusters. Clusters 1-2-4 mainly occur in winter, clusters 6-9 in summer, clusters 5-8 both in spring and autumn with higher density in autumn and clusters 3-7 mainly in spring.





**Figure 7.** Shows the geographical distribution of the different clusters grouped in their respective peak season.

Detailed discussion on cluster features like cold fronts, warm conveyor belts, and surface impacts will follow in Section 6, interlinked with the results of our study. In Appendix B, we offer supplementary composites of these additional features, which draw from the analysis conducted by Givon et al. [2023]. Finally, a concise introduction of each cluster follows, supported by Givon et al. [2023].

Cluster 1 has the strongest PV signal and is identified as Stage A lee cyclone that occurs in the Gulf of Genoa (Fig. 7). Cluster 4 are Stage B lee-lows and cluster 2 are AWB lows that initiate in the lee of Alps. However, the peaks of clusters 2 and 4 vary in location and favor marine environments. Clusters 1-2-4 have their highest occurrence in winter (Fig. 6) and are the most “explosive” with a fast deepening rate. A low-level PV signal is seen in these clusters giving rise to a “PV tower”.

Clusters 5 and 8 are AWB and CWB lows, respectively. Cluster 5 mainly occurs evenly in spring and autumn, while cluster 8 is most common in autumn (see Fig. 6). Cluster 5 mostly initiates near the Atlas in comparison to cluster 8, which is highly localized near the Alps and Ligurian Sea (see Fig. 7). Both clusters exhibit explosive systems, however, only cluster 8 has a low-level PV signal and “PV tower” build-up.

Clusters 3 and 7 are long-wave cut-off lows and daughter cyclones, respectively, that mainly occur in spring (see Fig. 6). Cluster 3 initiates and peaks at the Atlas, while cluster 7 has a diverse geographical distribution (Genoa and Northwest Africa). The clusters do not develop any mid-tropospheric PV signal, however, large PV values are identified near the surface.

Clusters 6 and 9 are more common in summer (see Fig. 6). Cluster 6 consists primarily of African heat lows (Sharav lows) and cluster 9 are short-wave cut-off lows that can occur both near Genoa and Africa (refer to Fig. 7). Although cluster 6 has the lowest PV signal, both clusters do not show any low-level PV.

Clusters 3, 6 and 9 tend to deepen more slowly, owing to the arid environment in which these cyclones form, lacking humidity fluxes to maintain high precipitation and latent heat release. Additionally, clusters

1, 3, 4, and 7 exhibit a quicker eastward propagation in comparison to clusters 2, 5, 6, 8, and 9 which are more static. Note that stationary cyclones pose a significant threat to extreme weather occurrence [Givon et al., 2023].

### 3.2 Reanalysis Data

The fifth-generation reanalysis data (ERA5) from the European Centre for Medium-Range Weather Forecast (ECMWF), spans from 1 January 1979 to the present. ERA5 is based on model forecasts from the ECMWF Integrated Forecast System (IFS) CY41R2 [Hersbach et al., 2020] and is constructed by a hybrid incremental four-dimensional variational assimilation (4D-Var; Courtier et al. [1994]) with a 12-hour assimilation window. It has an available spatial resolution of  $0.25^\circ$  in longitude and latitude (i.e. 31 km grid spacing), with 137 levels from the surface to 0.01 hPa. ERA5 data has an hourly temporal resolution for numerous atmospheric, ocean-wave and land-surface parameters.

Reanalysis data offers detailed and high-resolution information across climatological periods, enabling a comprehensive analysis of past conditions at each grid point and ensuring a complete picture of weather and climate data. However, it should be taken into consideration that uncertainty remains due to model parameterizations of small-scale physical processes [Urraca et al., 2018], such as for convective precipitation. Mainly, reanalysis is our best guess at the state of the atmosphere, but it should not be considered as reliable as observations.

**Table 1.** ERA5 variables used in the study.

Parameter	Units	Resolution	Coverage
Convective available potential energy (CAPE)	$\text{J kg}^{-1}$	$0.25^\circ/1 \text{ h}$	1979-2020
Convective precipitation (CP)	mm	$0.25^\circ/1 \text{ h}$	1979-2020
Wind components (u, v at 500hPa & u, v at 10m)	m/s	$0.25^\circ/6 \text{ h}$	1979-2020
Mean SLP	Pa	$0.25^\circ/1\text{h}$	1979-2020
Land-sea mask		$0.25^\circ$	

Table 1 shows the variables used in this study. Definitions of CAPE and convective precipitation, as described in ERA5, are given below:

- **CAPE:** CAPE is a measure of atmospheric instability, indicating the potential for convection and the development of severe weather like heavy rainfall and thunderstorms. In the ECMWF IFS, CAPE is calculated by comparing parcels of air at different model levels below 350 hPa. If a parcel is warmer and moister than its surroundings, it rises and cools until it loses buoyancy. The total excess buoyancy represents the potential energy of CAPE. Larger positive values of CAPE suggest greater buoyancy and potential for severe weather. The calculation assumes certain conditions like no mixing with surrounding air and pseudo-adiabatic ascent.
- **Convective precipitation:** Convective precipitation is generated by the convection scheme within ECMWF IFS. This scheme represents convection at spatial scales smaller than the grid box. Additionally, precipitation can also result from the cloud scheme in the IFS, which accounts for cloud formation, dissipation, and large-scale precipitation based on atmospheric quantities predicted at grid box scales or larger.

Furthermore, in order to account for environments influenced in the proximity of the cyclone tracks, the region examined here corresponds to  $\pm 10^\circ$  from the area selected in clustering (see Section 3.1). Therefore, we considered the Mediterranean region from  $30^\circ$  West to  $55^\circ$  East and  $10$ - $60^\circ$  North for all the variables in Table 1.

### 3.2.1 Derived variables

Using the above, we have calculated two additional variables as detailed below:

1. **Bulk shear (BS0-6)**: The wind components from ERA5 (refer to Table 1) were used to calculate the magnitude of bulk shear approximately between the near-surface level and 6 km. The shear accounts for the difference in 10 m winds at the surface and at 500 hPa ( $\sim 6$  km), as shown below:

$$\text{BS}(0-6) = \sqrt{(u_{500\text{hPa}} - u_{10\text{m}})^2 + (v_{500\text{hPa}} - v_{10\text{m}})^2} \quad (1)$$

Bulk shear is an important element in severe storm analysis because it causes storm updrafts to tilt in high-shear conditions, possibly leading to more persistent and well-structured storms. Low-level shear also leads to vorticity, supporting the development of rotating storms [Púčík et al., 2015].

2. **WMAXSHEAR**: A composite product of CAPE and bulk shear is computed [Taszarek et al., 2017] as follows:

$$\text{WMAXSHEAR} = \sqrt{2 \times \text{CAPE} \times \text{BS}(0-6)} \quad (2)$$

WMAXSHEAR is commonly used to study the climatological aspects of severe thunderstorm environments [Taszarek et al., 2020b].

## 3.3 Hail & Lightning proxies

In this study, we used hail and lightning probabilities as proxies for the aforementioned hazards. Probabilities for large hail ( $\geq 2$  cm) and lightning were developed by Battaglioli et al. [2023], calculated for the area of interest ( $10$ - $60^\circ\text{N}$ ;  $30^\circ\text{W}$ - $55^\circ\text{E}$ ) and period 1979-2020. The data has 3 hourly time resolution and a spatial resolution of  $0.25^\circ \times 0.25^\circ$ .

To generate the probabilities, Additive Regression Convective Hazard Models (AR-CHaMo; Rädler et al. [2018]) were trained with lightning observations, hail reports and predictor parameters from atmospheric variables in ERA5 reanalysis. The probability of hail ( $P_{\text{hail}}$ ) is taken as the product of the probability of a thunderstorm occurring ( $P_{\text{lightning}}$ ) and the conditional probability of hail given a storm ( $P_{\text{hail}|\text{lightning}}$ ). The selected predictor parameters for the regression models are listed in Table 2.

**Table 2.** Predictor parameters for the lightning and hail regression models developed by Battaglioli et al. [2023].

Model	Lightning	Hail $\geq$ 2cm
<b>Predictors</b>	MU_LI (K) RH_500-850hPa (%) 1h Acc. Conv. Precip. ( $\text{kg m}^{-2}$ ) MU_MIXR ( $\text{g kg}^{-1}$ ) Land-sea Mask	MU500_CAPE-10° ( $\text{J kg}^{-1}$ ) EFF_MU_BS ( $\text{m s}^{-1}$ ) MU_MIXR ( $\text{g kg}^{-1}$ ) 0° height (m)

Clarifications for the parameters shown in Table 2 are given below, supported by Battaglioli et al. [2023]:

- **MU\_LI & RH\_500-850hPa:** Most Unstable Lifted Index [Galway, 1956] and average relative humidity between 500 and 850 hPa, respectively. The two are considered critical factors for convective initiation, as they account for instability and mid-level moisture [Rädler et al., 2018].
- **Convective Precipitation:** Convective precipitation is essential in identifying scenarios with convective inhibition even in the presence of adequate instability and moisture.
- **MU\_MIXR:** Mixing ratio for the most unstable parcel. Battaglioli et al. [2023] states that the likelihood of lightning exhibits a bimodal distribution concerning MU\_MIXR. As instability and mid-level moisture increase, lightning probability rises with higher MU\_MIXR values up to 12-15 g/kg, depending on the level of instability (more pronounced in highly unstable environments). Subsequently, the probability of lightning decreases again.
- **Land-sea Mask:** A land-sea mask was incorporated to account for the observation that lightning occurs less frequently over the sea compared to land. This difference in occurrence could be influenced by varying aerosol load or LCL (lifting condensation level) height [Battaglioli et al., 2023].
- **MU500\_CAPE-10°:** CAPE for the most unstable parcel above 500 m from ground level and in the layer above the -10°C isotherm. This parameter exhibited superior performance as an instability predictor across Europe, the U.S., and its subregions. Its widespread effectiveness suggested that it might better capture the essential elements for hail formation, and particularly significant buoyancy at higher levels within the storm [Battaglioli et al., 2023].
- **EFF\_MU\_BS:** Effective Most Unstable Shear is the bulk wind shear between the height of the most unstable parcel and halfway to its Equilibrium Level (similar to Thompson et al. [2007]). It was chosen because it outperformed bulk wind shear between 0 and 6 km as a shear parameter.
- **0° height (m):** For hail with a diameter of 2 cm or greater the model accounts the higher of the 0° isotherm as for smaller hailstones, which are more prone to melting, the height of the freezing level becomes more crucial in the model’s predictions [Battaglioli et al., 2023].

## 4 Methods

The steps followed in Part I and Part II of this study are detailed below. Part I establishes the relationship between convective environments and hazards in Mediterranean cyclones through composite analysis. Further, Part II focuses on the temporal evolution of convective parameters and hazards around of the cyclone core.

### 4.1 Part I: Composite analysis

#### 4.1.1 Composite analysis

After pre-processing of the data (detailed in Section 3), we computed a composite analysis to highlight spatial structures associated with the convective environments and hazards along the Mediterranean cyclone tracks.

The composite method we followed is similar to the one described in the upcoming paper “A storm-relative climatology of compound hazards in Mediterranean Cyclones” by Dr. Raphaël Rousseau-Rizzi. One composite map for each cluster was obtained by averaging the variables over all storms belonging to that cluster and is shown on a  $10^\circ \times 10^\circ$  box centered at the cyclone core, i.e. from a Lagrangian cyclone-centered viewpoint. The variable fields, described in Sections 3.2-3.3, were linearly interpolated on the storm box at  $0.25^\circ$  resolution. Only one time step per storm was considered, corresponding to the time where the central pressure is minimal, selected among the times where data is available.

In practice, this method gave us one composite per cluster and per variable and that composite represented an average environmental field.

#### 4.1.2 Statistical significance

In order to determine the statistical significance of each gridpoint in the composite maps, we tested the null hypothesis that the storm-relative average variable belongs to the distribution of the variable at that point over all times, whether there are cyclone events or not.

To do this we generated 2000 Monte-Carlo samples for each of the parameters at the same sites as the storm samples, but at random times. While the times chosen for Monte-Carlo samples may appear arbitrary, they adhere to the seasonal distribution as that of the storm samples. This was performed similarly to Welker et al. [2014], where we introduced randomness by altering the day (spanning from 5 days prior to 5 days after the event’s original date) and the year of the event, however the month of the event remained unaltered throughout this process. Empirical p-values were estimated as one minus the quantile of that point among the relevant Monte-Carlo samples at each point of the composite maps. If the probability at the storm point was the highest, the p-value is set to 0.

To avoid a high false discovery rate (FDR) when performing multiple hypothesis tests, we followed the method suggested by Wilks [2016]. As a result, we adjusted for the FDR by sorting all  $N$  empirical p-values from  $p_1$  to  $p_N$  and by computing an effective p-value significance threshold ( $p_{FDR}$ ) provided by

$$p_{FDR} = \max_{i=1, \dots, N} [p_{(i)} : p_{(i)} \leq (i/N)a_{FDR}] \quad (3)$$

where  $a_{FDR} = 0.05$  is the FDR control threshold. The effective p-value results to approximately 0.005, which is far more restrictive than the conventional 0.05 criterion. The study will specifically address regions falling within the significant area delineated as a black contour on the composite maps in Section 5.1.

### 4.1.3 Contours

To facilitate our analysis in understanding the relationship between the variables and the dynamical and geographical features of the clusters, we included a composite analysis (detailed in Section 4.1.1) over the following fields:

- Mean sea level pressure (MSLP), which is the pressure at the surface adjusted to the height of the mean sea level.
- Land-sea mask, percentage of land in a grid box as opposed to ocean or inland waterways (lakes, reservoirs, rivers and coastal waters).

The above features were added as contour lines to the composite maps shown in Section 5.1. In detail, Fig. 8 represents the composite of land mask for each cluster. A value of more than 0.5 (i.e.  $> 50\%$ ) may include of a mix of land and inland water but not ocean. Therefore, areas colored brown in Fig. 8 have a land cover between 50% to 80%, whereas those colored in red have a land cover above 80%. The white areas in Fig. 8 signify regions with less than 50% land cover and hence can only be comprised of a water surface.

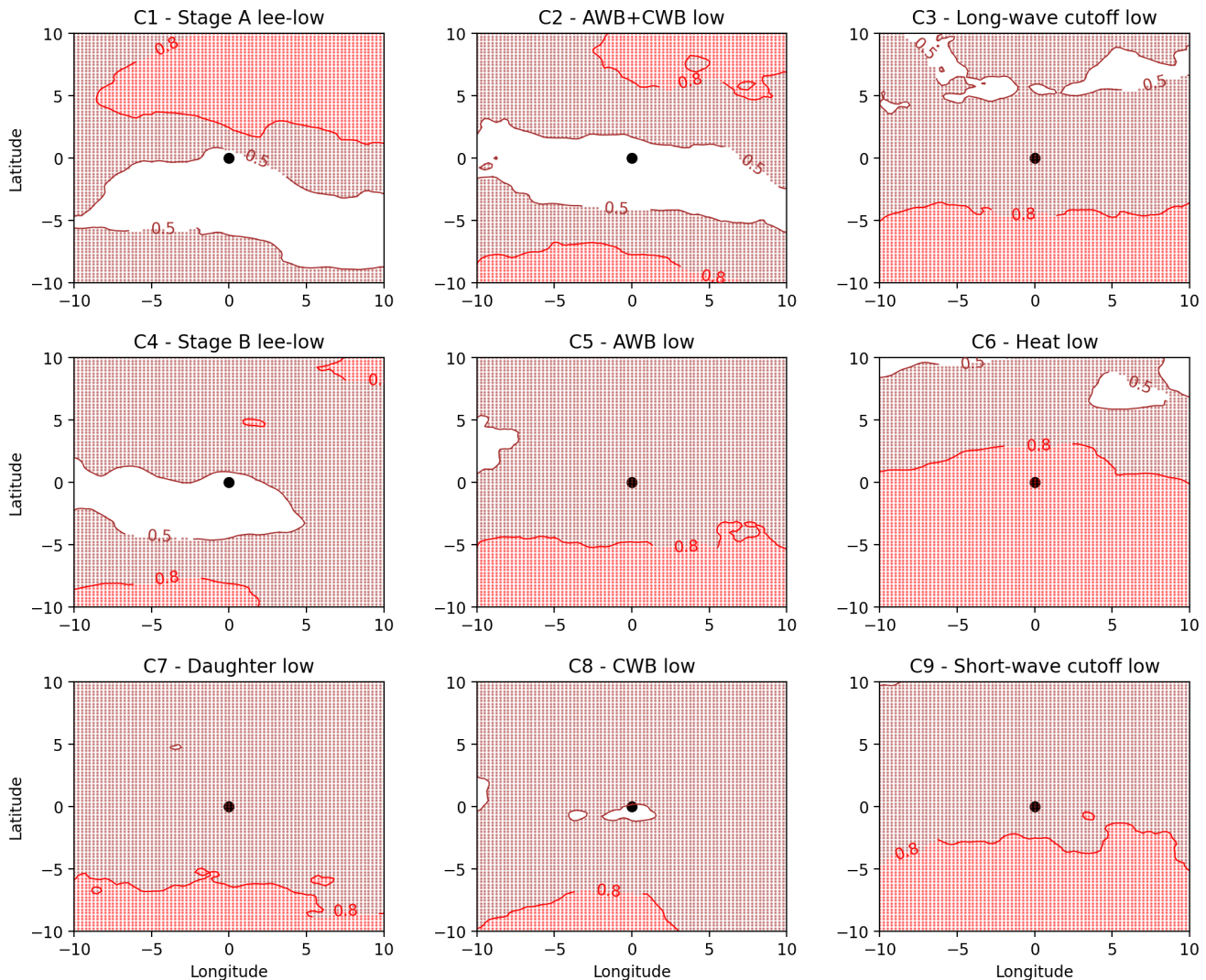


**Figure 8.** The brown and red contours identify the land-sea mask at levels 0.5 and 0.8, respectively. Brown stippling shows areas with land cover between 50% to 80% and red stippling shows areas with land cover above 80%.

## 4.2 Part II: Time Evolution

To analyze the time evolution of the parameters, we took the following steps:

1. We identified the time at which the cyclone is at its maximum intensity (i.e. at minimum pressure) for each event ID under each cluster. The time of minimum pressure is later defined as the zero hour (i.e.  $t=0$  h).
2. Starting from  $t=0$  h of each event ID, we have selected the times and locations of the storms from 24 hours before to 24 hours after, at 6 hourly timesteps.
3. The variables were then taken at the times determined in Step 2 and averaged over an area of 200 km radius from the cyclone core. The 200 km radius facilitates the correlation of cyclone core intensity with deep convection processes and the associated hazards near the cyclone center, where maximum rainfall and convection are anticipated [Flaounas et al., 2015]. However, the results of

the time evolution analysis were not sensitive to a radius definition between 200 and 500 km (not shown).

4. We then proceeded with boxplot analysis at each time step, to describe the distribution of the values within each group of clusters. Box-and-whisker plots represent groupings of the data based on their quantiles. The box spans from the 25<sup>th</sup> (Q1) to the 75<sup>th</sup> (Q3) percentiles, with a line at the median (Q2). The whiskers extend from the box's borders and represent the 10<sup>th</sup> and 90<sup>th</sup> percentiles.
5. As an additional step, we calculated the mean value over all cyclones in the cluster groups at each time step, shown as a solid red line (refer to Section 5.2). It is important to recognize that the mean line can deviate considerably from the median, mainly because the mean is sensitive to the influence of outliers.

The figures in Section 5.2 show the time series of spatially averaged CAPE, bulk shear, convective precipitation and lightning. In the time evolution figures, the clusters were grouped by their peak season since comparable evolution characteristics were presented in clusters with a similar seasonal distribution. Even so, plots by individual clusters are shown in Appendix A.1. The temporal evolution of the fields along cyclone tracks offers a convenient approach to measuring changes that occur during their life cycle. Additionally, we have computed the time evolution of surface winds at 10 m in order to explain the results we see for bulk shear. The time evolution figures for 10 m surface wind are presented in Appendix A.2.



## 5 Results

### 5.1 Part I: Composite maps

#### 5.1.1 CAPE

The climatology of CAPE in the Mediterranean displays a distinct seasonal cycle, with higher values during summer, peaking in July-August, and lower values during winter, reaching a minimum in January-February [Romero et al., 2007]. In the Mediterranean region, autumn has higher CAPE values than spring, attributed to the lingering warm Mediterranean Sea after peak summer insolation that acts as a significant heat and moisture source.

The composite of CAPE for each cluster is represented in Fig. 9.

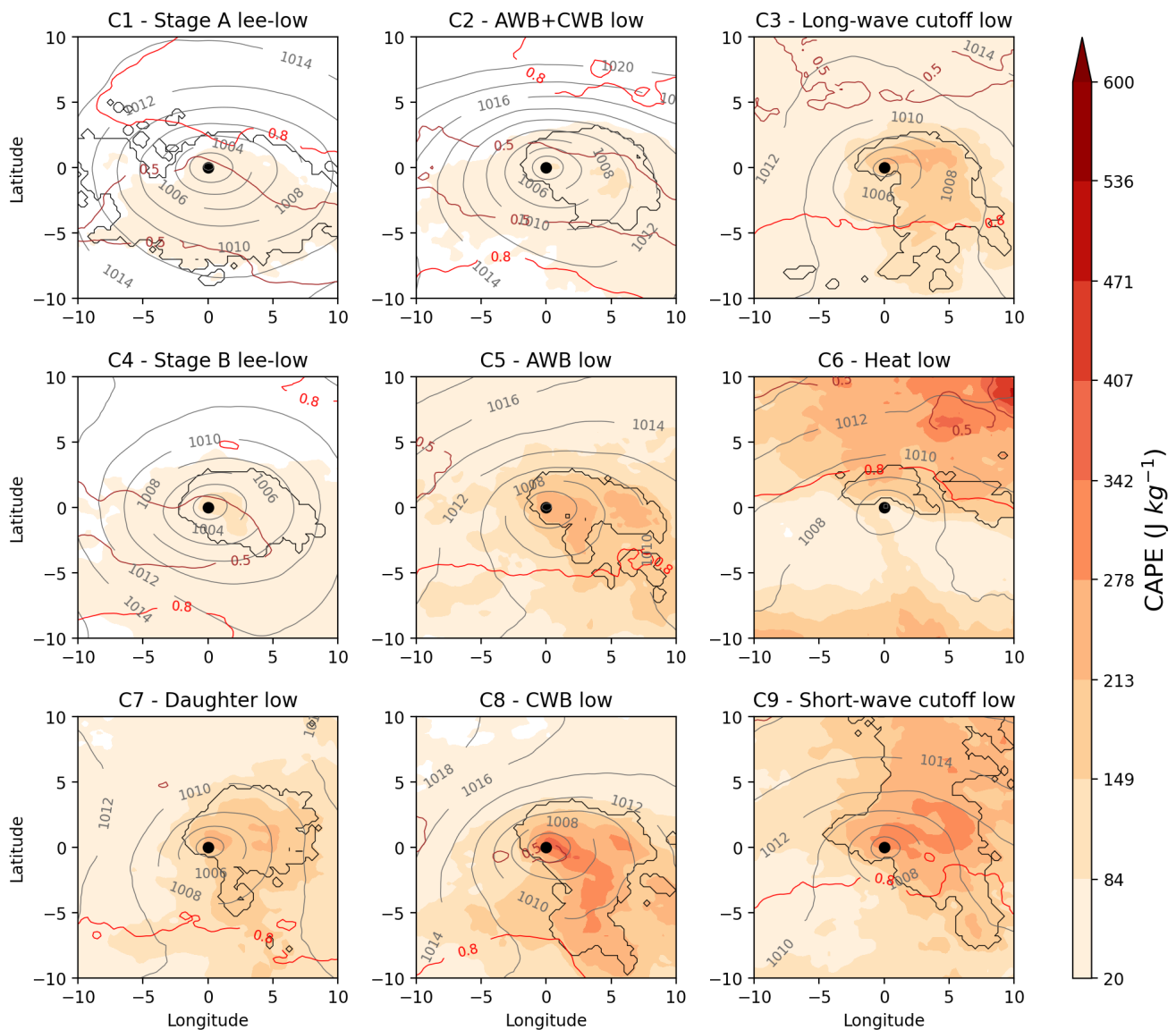


**Figure 9.** Composite mean of CAPE for each cluster (colored filled contours). The black contour identifies the statistically significant area. The brown and red contours identify the land-sea mask at levels 0.5 and 0.8, respectively. Mean sea-level pressure is represented by the grey contours at 200 Pa intervals.

Clusters 1, 2 and 4 show the lowest values of CAPE in Fig. 9 because they mainly occur in winter, when CAPE is close to its seasonal minimum. For the summer clusters (6 and 9), we see high values of CAPE to the north of the cyclones' center and over an area of 50% land cover, in the range of 213-342 J kg<sup>-1</sup>. Clusters 3 and 7 occur mostly in spring, where CAPE values are in the range of 84-213 J kg<sup>-1</sup> and significant values extend from the south to the east of the storm's center. Further, clusters 5 and 8 have higher CAPE values than clusters 3 and 7 in Fig. 9, with a similar spatial pattern. Cluster 8, which mainly occurs in autumn, shows the highest values of CAPE in the range of 213-407 J kg<sup>-1</sup>.

Clusters 3, 5, 7, 8, and 9 have a significant CAPE structure where the fraction of land cover is comprised between 50% and 80% (land mask detailed in Section 4.1.3). For cluster 6, the significant structure is seen over 80% land cover and hence shows the surface heating of the heat low during summer. Finally, clusters 1, 2, and 4 have CAPE values over areas with less than 50% land cover (i.e. water surface). This is expected as warm SSTs are important in producing CAPE in winter [Romero et al., 2007].

### 5.1.2 Bulk shear

The composite of bulk shear between 0-6 km is represented for each cluster in Fig. 10.

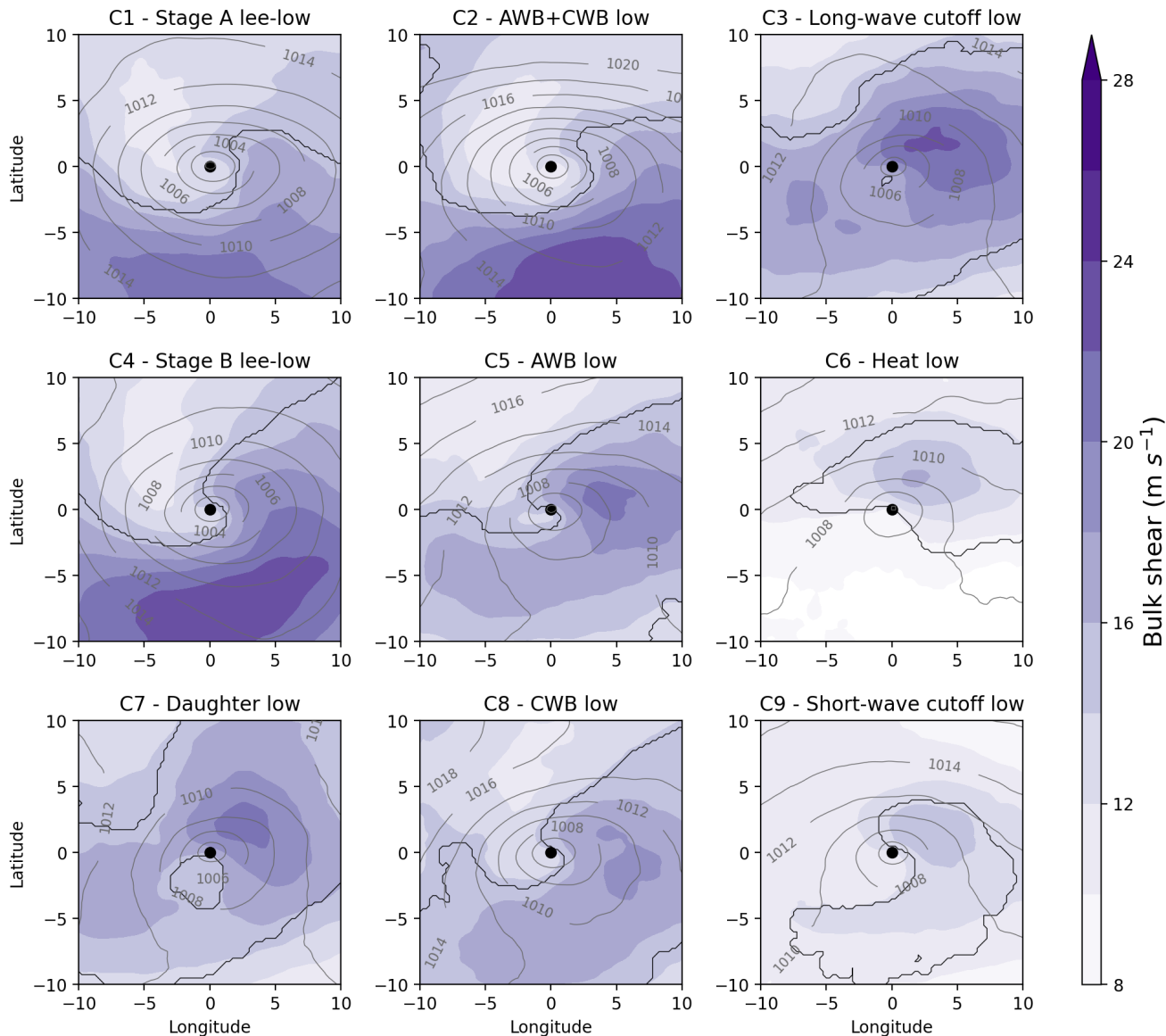


**Figure 10.** As in Fig. 9 but for bulk shear between 0-6 km. Land mask omitted.

The winter clusters in Fig. 10 exhibit high shear to the south of the storm centers: clusters 2 and 4 have values in the range of 18-26 m/s, while cluster 1 ranges between 18-22 m/s, even though its spatial structure is similar. Clusters 6 and 9 mostly occur in summer and have the lowest bulk shear. In cluster 6, bulk shear ranging from 10-16 m/s is found to the north-northeast of the storm centers, coinciding with the strongest pressure gradient. In contrast, cluster 9 exhibits a structure that encircles the center, extending from the south to the northeast, which may be linked to the dynamics of the cut-off low. Further, clusters 3 and 7 show high values of bulk shear to the northeast side of the storm centers, co-located with high-pressure gradients. Clusters 5 and 8 present a structure wrapping around itself from the south to the northeast. The bulk shear values within the significant areas of clusters 3, 5, 7 and 8

range between 14-24 m/s.

### 5.1.3 WMAXSHEAR

The composite of WMAXSHEAR for each cluster is shown below in Fig. 11.

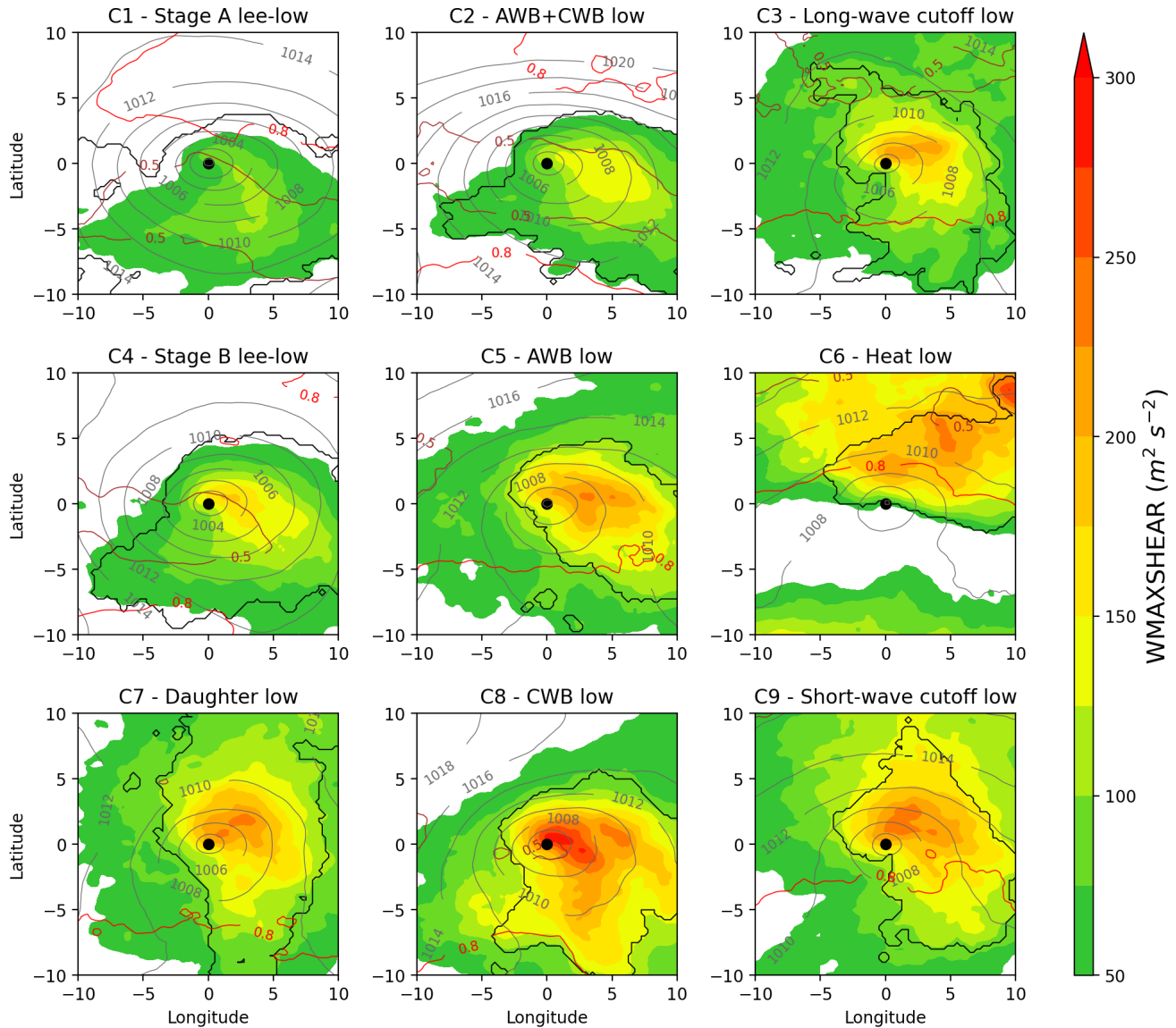


**Figure 11.** As in Fig.9 but for WMAXSHEAR.

WMAXSHEAR composites in Fig.11 exhibit similar structural features as the CAPE composites in Fig.9 (described in Section 5.1.1). However, the bulk shear shows a strong contribution for clusters with weak CAPE (i.e. clusters 1, 2 and 4). Clusters 3 and 7 exhibit high WMAXSHEAR values primarily to the northeast of the storm centers, where the bulk shear maximum coincides with the CAPE maximum. In contrast to cluster 3, WMAXSHEAR in cluster 7 extends farther away from the storm center, indicating a bigger region conducive to the development of severe convective storms. Clusters 6 and 9 show large WMAXSHEAR values to the northeast of the storm centers, mainly due to high CAPE. However, we

will see below in Sections 5.1.4-5.1.6, convective hazards within these clusters, especially in cluster 6, are relatively limited. This is attributed to the arid environment that clusters 6 and 9 form (refer to Fig. 7 for their spatial distribution).

Cluster 8 in Fig. 11 shows the highest values of WMAXSHEAR in the range of 150-300  $m^2s^{-2}$  and above, wrapping around the cyclone center from the south to the north-northeast, with the maximum located to the northeast of the cyclone center. Notably, Taszarek et al. [2017] showed that for very large hail events, the WMAXSHEAR presented values higher than 300  $m^2s^{-2}$ . This was attributed to the fact that very large hailstones are predominantly associated with supercell thunderstorms, which are more likely to form under conditions of high WMAXSHEAR values. Specifically, WMAXSHEAR takes into account both CAPE (i.e. instability) and bulk shear between 0-6 km and captures effectively the likelihood of severe thunderstorms [Markowski and Richardson, 2011; Taszarek et al., 2020b]. This is important as high shear and high CAPE environments might not happen at the same time, hence the combined parameter takes care of this issue.

### 5.1.4 Convective Precipitation

Figure 12 displays the composite for 1h accumulated convective precipitation for each cluster, specifically at the 1-hour mark when the cyclone reached its maximum intensity.

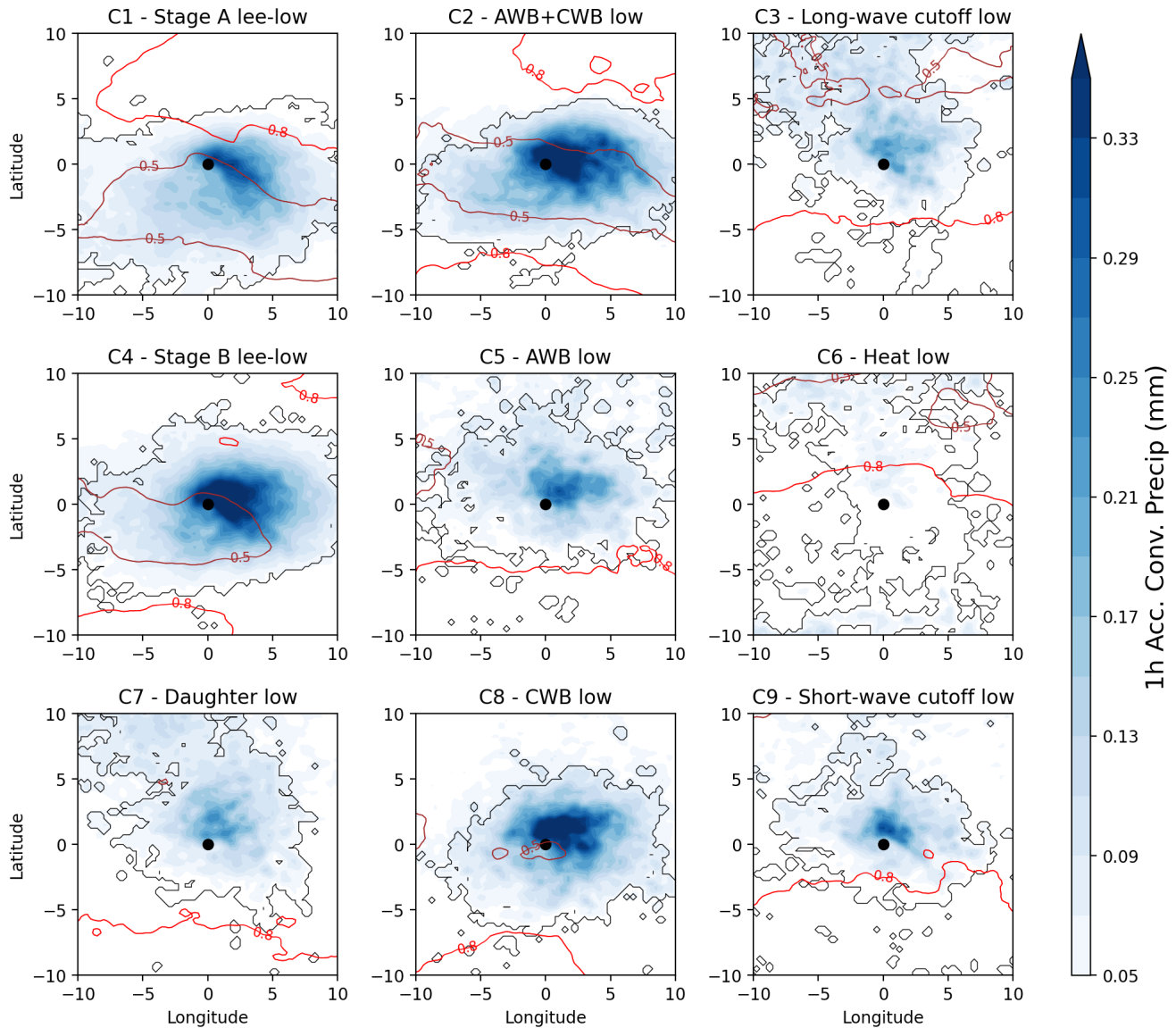


**Figure 12.** As in Fig. 9 but for 1h accumulated convective precipitation. MSPL contours omitted.

Clusters 2 and 4 in Fig. 12, show the highest values of convective precipitation (above 0.33 mm/h), extending from the north to the east of the storm's center. Cluster 1 has values from 0.17-0.23 mm/h, in the northeast and extending further south with respect to the cyclones' center. In cluster 8 (autumn), convective precipitation is concentrated to the north-northeast of the storm's center with values above 0.33 mm/h, similar to winter clusters 2 and 4. Cluster 5 has lower convective precipitation values up to 0.25 mm/h, close to the cyclone core. Furthermore, clusters 3, 7 and 9 (spring and summer) have lower amounts of convective precipitation than the preceding clusters discussed. Even so, they share a similar spatial pattern, with most rain falling to the north and northeast of the storm centers. Finally,

convective precipitation is considerably lower in cluster 6, with values below 0.09 mm/h.

It is worth noting that there is a region around the cyclone center of clusters 2 and 4 with less than 50% land cover representing water surface (as detailed in Section 4.1.3) and this may be important for the convective precipitation, because of the energy and moisture provided by the warm sea surface. On the other hand, clusters 3, 5, and 7 are mostly positioned over regions with more than 50% land coverage (refer to Section 4.1.3), indicating their frequent occurrence in northwest Africa (see Fig. 7). This positioning signifies that the cyclone core and associated hazards tend to concentrate above areas with higher land coverage.

### 5.1.5 Lightning Proxy

Figure 13 shows the composite for the lightning proxy.

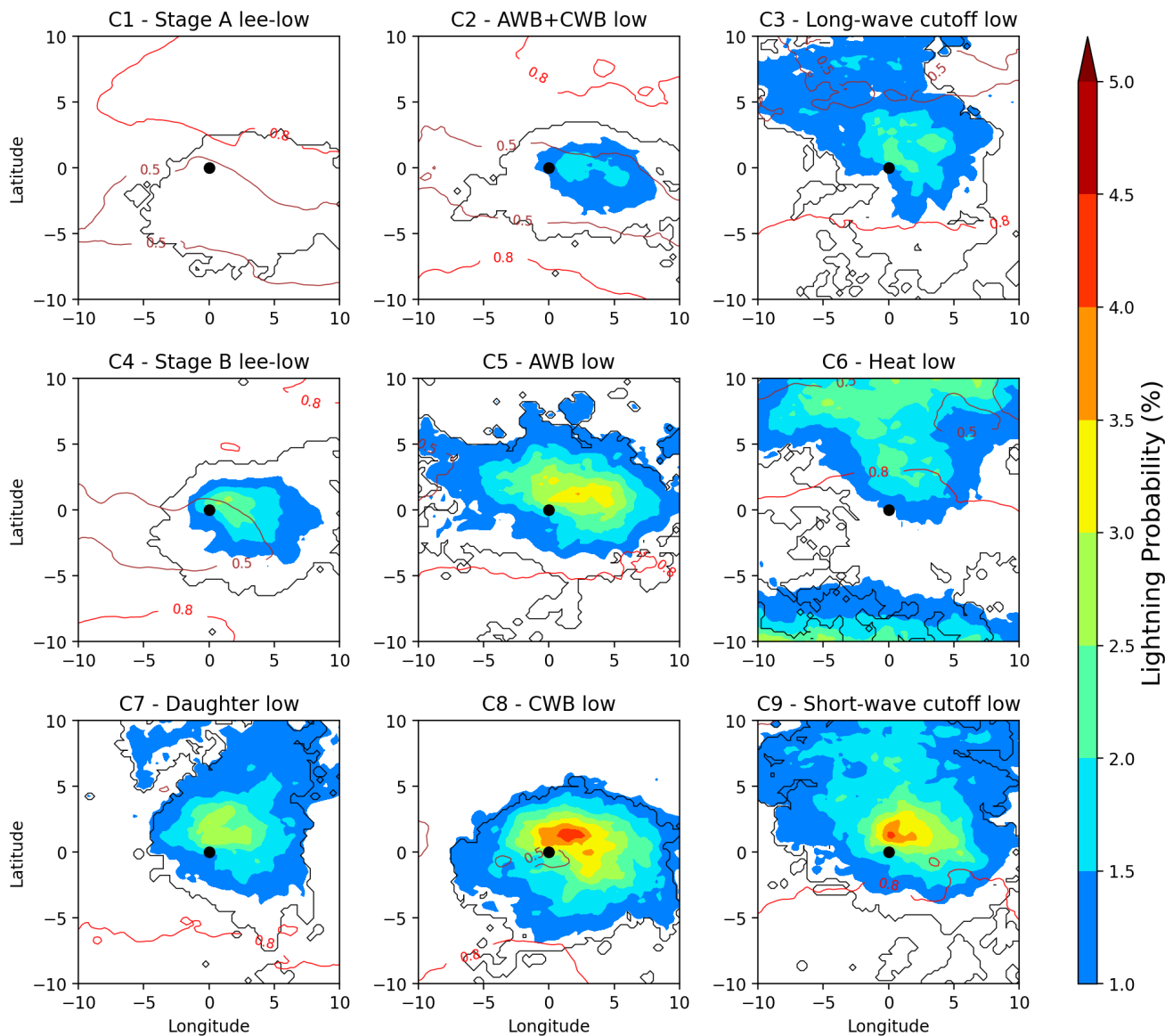


**Figure 13.** As in Fig. 9 but for the lightning proxy. MSPL contours omitted.

We see in Fig. 13 that cluster composites of lightning proxy have similar structural features to the averaged environmental field of convective precipitation (see Section 5.1.4). However, in the case of the winter clusters (1, 2, and 4), the magnitude of lightning seen in Fig. 13 does not align with the level of high convective precipitation exhibited in these clusters shown in Fig. 12.

Clusters 8 and 9 exhibit the highest lightning probabilities. Specifically, Cluster 8 has the greatest probability of lightning flashes close to the center of the storm and to the northeast, up to an average probability of 4.5%. The similarity with the WMAXSHEAR composite map (Fig. 11) is consistent with prior findings, stating that the lightning probability increases with WMAXSHEAR [Taszarek et al., 2020b]. Cluster 9 shows a high lightning probability north of the storm center, in the region of highest WMAXSHEAR (Fig. 11) and convective precipitation (Fig. 12). The alignment between WMAXSHEAR and lightning proxy holds for all clusters.



### 5.1.6 Hail Proxy

The composite of hail probabilities for each cluster is shown in Fig. 14.

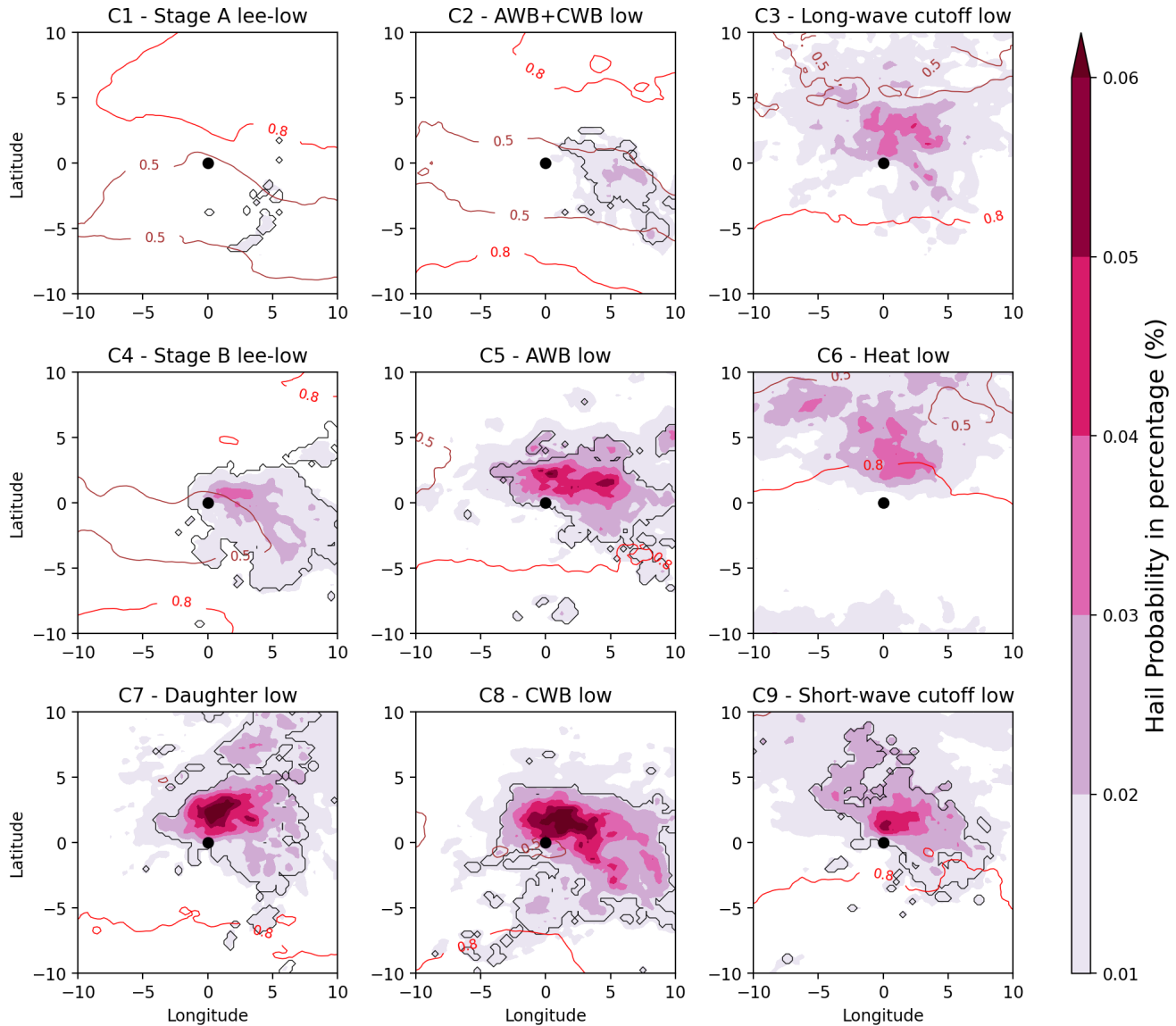


**Figure 14.** As in Fig. 9 but for the hail proxy. MSPL contours omitted.

In Fig. 14, significant areas of hail risk occur in clusters 8, 5, 7 and 9, which are clusters that mainly occur in autumn, spring and summer. Risk of hail appears to the north and east of the storms' center in all mentioned clusters and only in cluster 8 do the probabilities extend further southeast.

Clusters 5 and 9 exhibit a probability of hail in the range of 0.02% to 0.06%, while clusters 8 and 7 also have areas of probabilities above 0.06%. Because of the sparsity of the event, the probability of occurrence in Fig. 14 is low; however, if we consider the cumulative probability of hail occurrence over a larger area, consisting in the sum of multiple local grid-point probabilities, the values are substantially larger.

Clusters 5, 7 and 9 are associated with occurrences in northwest Africa. Even so, it is not unexpected

to see hail probabilities in these clusters, given the findings of Battaglioli et al. [2023], which state that northern Africa experiences the highest modeled hail occurrence, aligning with the findings of Punge et al. [2017] based on overshooting top detections. However, the lack of ground-truth observations in this region makes it challenging to verify this prediction. Nevertheless, there are known reports of very large hail events in the Atlas region.

Finally, in cluster 4, we notice an area of higher hail probability in comparison to the other winter clusters (1 and 2). Nonetheless, the probabilities are in the lower range with respect to the clusters discussed above.

## 5.2 Part II: Time evolution

In Part II of the study, we look at the time evolution of CAPE, bulk shear, convective precipitation and lightning. The clusters are grouped based on their peak season, as individual clusters sharing similar seasonal distributions revealed a comparable evolution in time. The cluster groupings are as follows: 1, 2, and 4 are winter clusters; 5 and 8 are spring and autumn clusters; 3 and 7 are spring clusters; and summer clusters consist of 6 and 9. Finally, the plots represent the spatially averaged variables in the 200 km radius around the cyclone core at time steps before and after the maximum cyclone intensity (details in Section 4.2).

### 5.2.1 CAPE

The time evolution for CAPE is illustrated in Fig. 15.

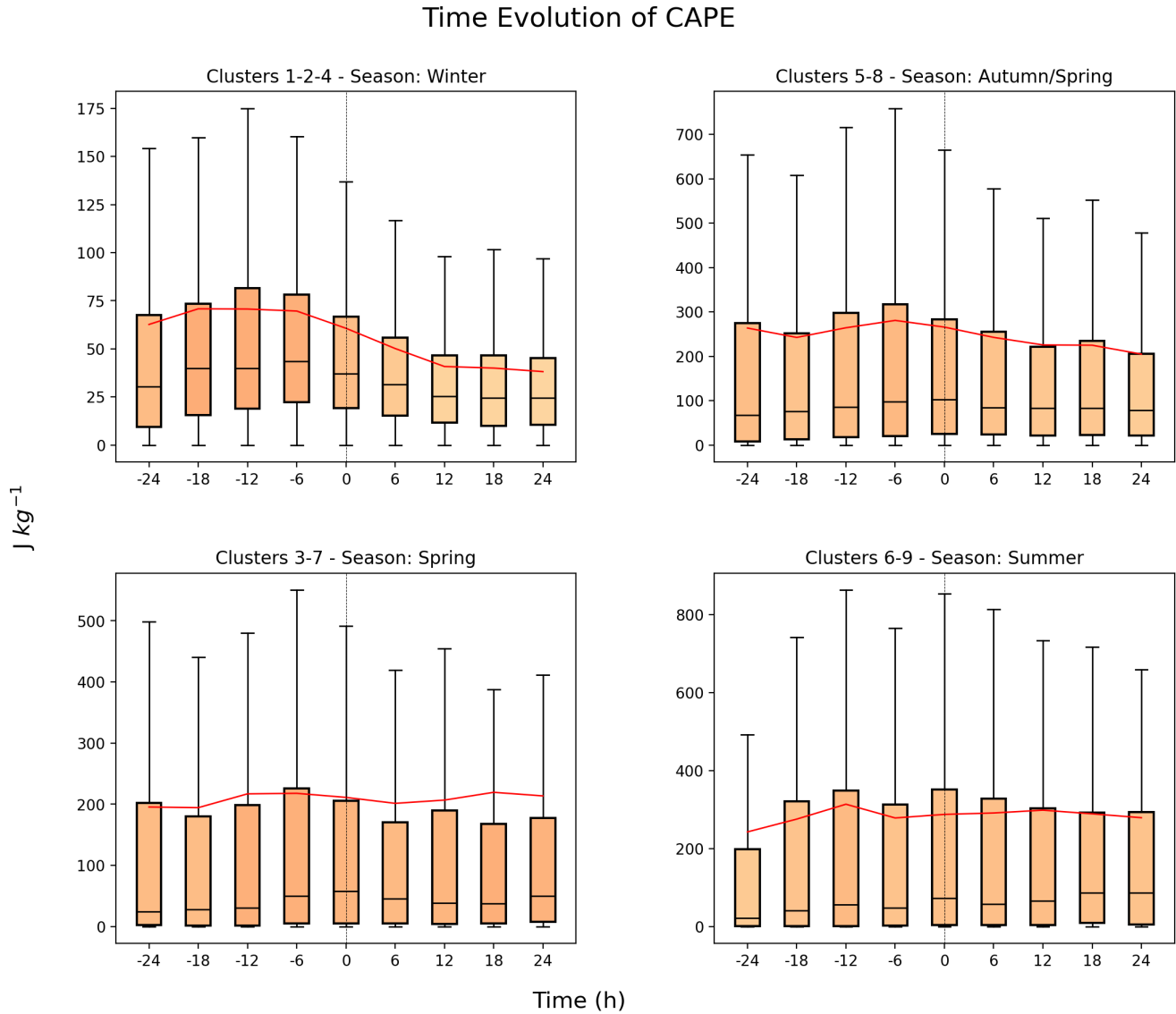


**Figure 15.** Spatial average (200 km radius around cyclone center) of CAPE at time steps before and after the minimum pressure ( $t=0$  h). Clusters are grouped based on their dominant occurrence season. The y-axis limits vary for each plot. Red line shows the mean value of the cyclones belonging to the relevant clusters at each time step. Box plots represent the interquartile range, the line inside the box denoting the median, and the whiskers indicating the 10<sup>th</sup> and 90<sup>th</sup> percentiles. The box-plot shades change according to normalized values using the respective color scheme of the parameter. Outliers are omitted.

In winter, CAPE shows a build-up before the maximum intensity of the storms. In clusters 5-8, there is a gradual increase of CAPE from  $t=-18$  h until the peak at  $t=-6$  h after which it gradually decreases. There is less variability in the evolution of CAPE in the spring and summer clusters.

CAPE levels are high in the summer clusters throughout the time series, with the mean value (red line) around  $300 \text{ J kg}^{-1}$ . Similar high mean values of CAPE are seen in clusters 5-8 at times before the minimum pressure (i.e. before  $t=0$  h). Further, it is worth noticing how the 90<sup>th</sup> percentile at the peak

of clusters 5-8 (i.e. at  $t=-6$  h) reaches above  $700 \text{ J kg}^{-1}$ .

### 5.2.2 Bulk shear

Figure 16 shows the time series of spatially averaged bulk shear (0-6 km) around the storms' center.

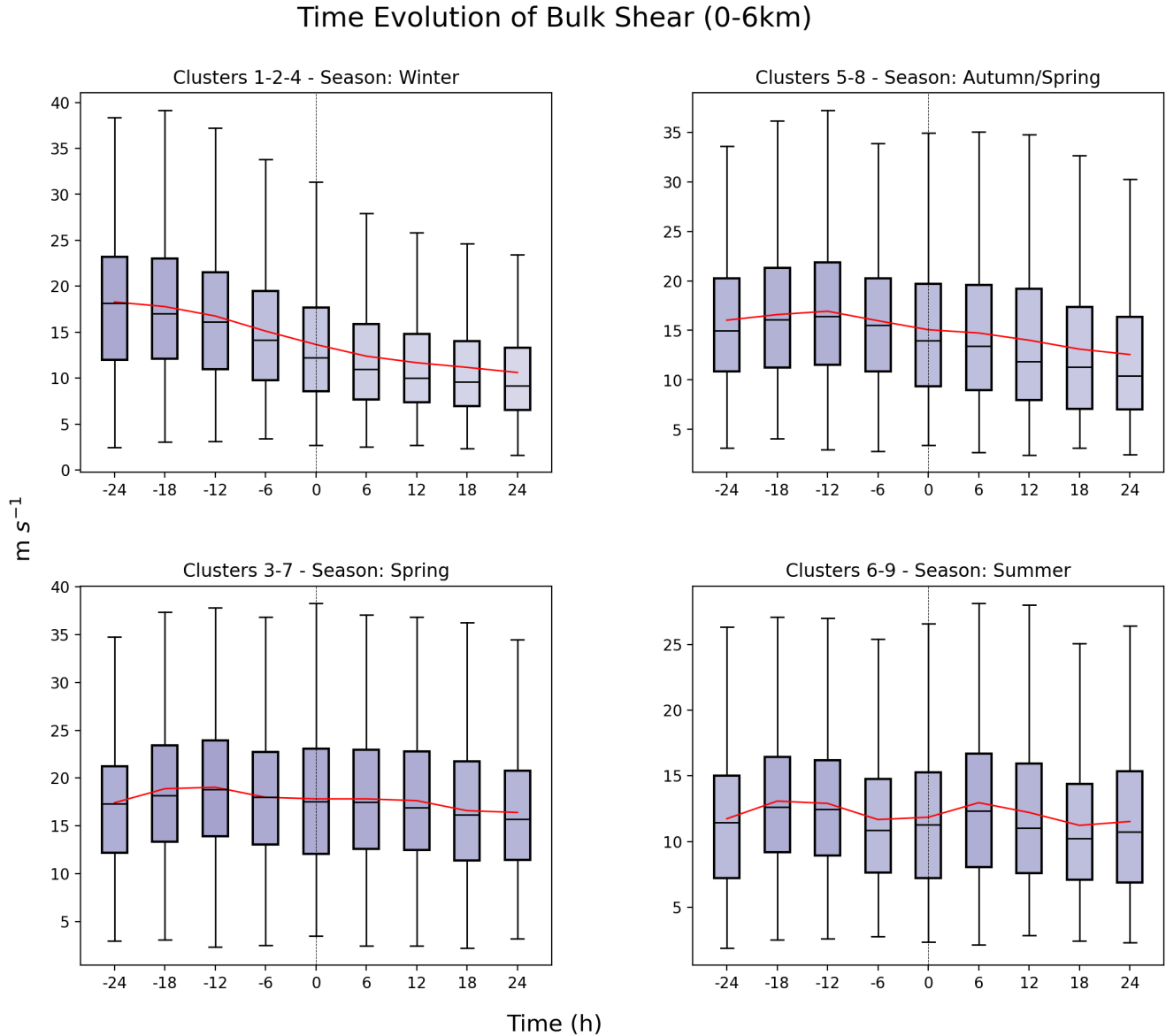


**Figure 16.** As in Fig. 15 but for bulk shear between 0-6 km.

The bulk shear in clusters 1-2-4, displays a gradual decrease from the start to the end of the time series, indicating the presence of an upper-level PV streamer playing an important role in the genesis and development of the cyclones [Flaounas et al., 2015]. To further understand the time evolution of bulk shear, we also performed the same analysis for 10 m surface wind presented in Fig. 30. Specifically, for clusters 1, 2, and 4 we see a gradual increase of surface winds from  $t=-24$  h until the mature stage of the cyclones at  $t=0$  h, accounting for at least some of the bulk shear decrease. Clusters 5-8 show a peak of bulk shear at  $t=-12$  h, followed by a moderate decrease. Again, the surface wind (Fig. 30) plays a role in

decreasing the shear by peaking at  $t=-6$  h until  $t=0$  h. It is worth noticing in Fig. 27, that bulk shear for cluster 8 alone resembles to some extent the time evolution of winter clusters. Bulk shear in spring (clusters 3-7) shows a smaller variability in its time evolution, with a slight peak at  $t=-12$  h. Finally clusters 6-9 (summer) show a non-monotonic development of the bulk shear. The same applies to the summer surface wind, where fluctuations are seen throughout the time series (refer to Fig. 30).

The magnitude of bulk shear in Fig. 16 is high for winter, autumn and spring clusters, with 90<sup>th</sup> percentile reaching 35 m/s. In winter, the magnitude of mean bulk shear starts from approximately 18 m/s at  $t=-24$  h and decreases to just above 10 m/s at 24 hours after the mature stage ( $t=24$  h). The mean bulk shear in summer clusters remains between 10-15 m/s at all time steps, and for autumn and spring, the mean generally remains between 15-20 m/s.

### 5.2.3 Convective Precipitation

The time evolution for 1h accumulated convective precipitation is presented in Fig. 17.

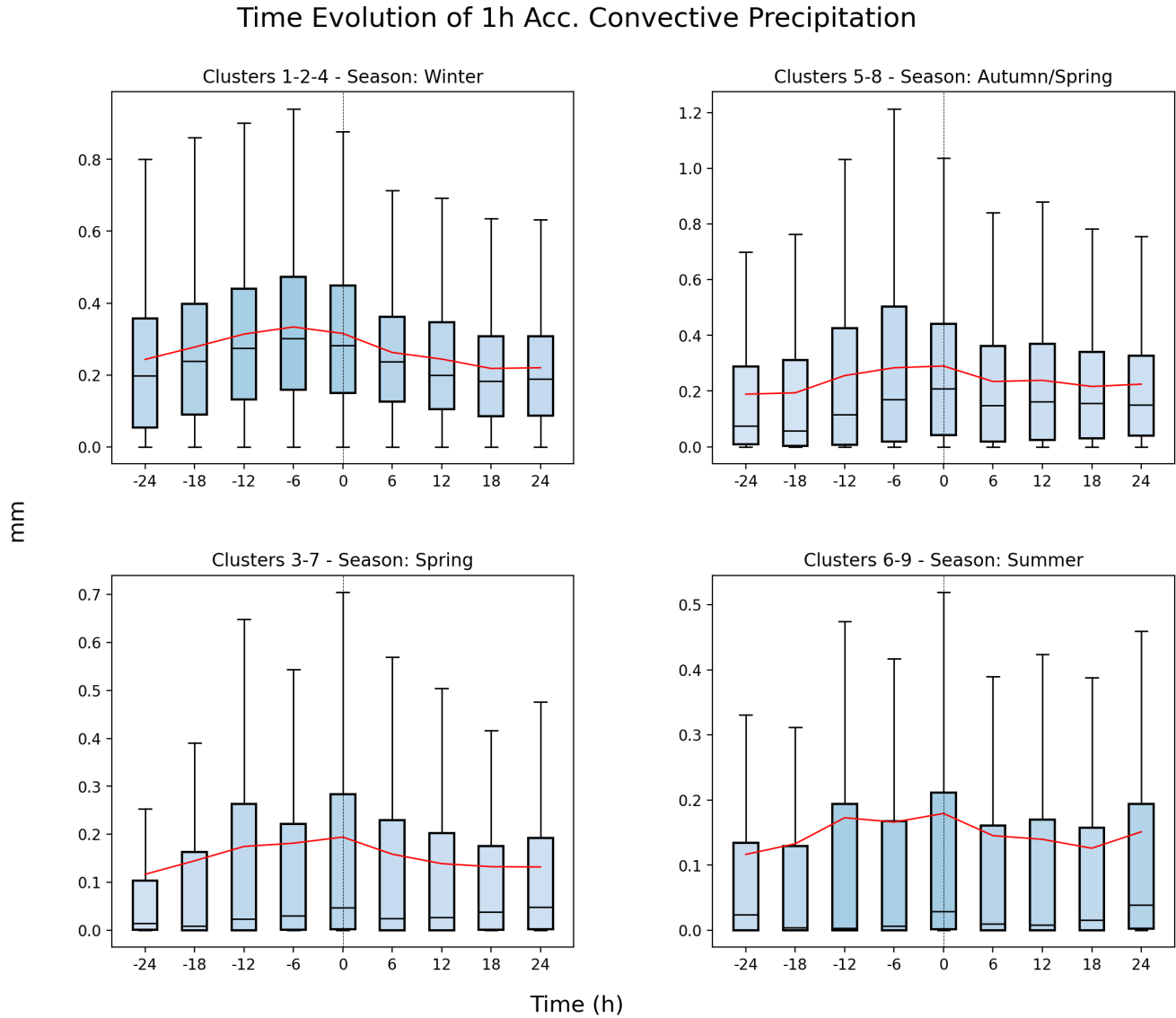


**Figure 17.** As in Fig. 15 but for 1h accumulated convective precipitation.

Figure 17 shows a maximum of convective precipitation for the winter clusters 1-2-4 at 6 hours before the minimum pressure (i.e.  $t=-6$  h). This may be related to the build-up of the convective environment before  $t=-12$  h, described in Sections 5.2.1-5.2.2. In clusters 5-8, convective precipitation gradually increases until  $t=0$  h. However, between  $t=-6$  h to  $t=0$  h, the mean values are substantially constant, and at  $t=-6$  h the variability among the cyclones is highest, with the 90<sup>th</sup> percentile reaching 1.2 mm/h. Spring clusters 3-7 exhibit a peak in convective precipitation at the time of minimum pressure. However, the mean convective precipitation values for these clusters are relatively low, ranging between 0.1-0.2 mm/h. Summer clusters 6-9 exhibit convective precipitation patterns mainly influenced by the behavior of cluster 9 (see Fig. 28), characterized by its elevated convective precipitation activity seen in Fig. 12.

### 5.2.4 Lightning Proxy

Figure 18 displays the time evolution of lightning probabilities.

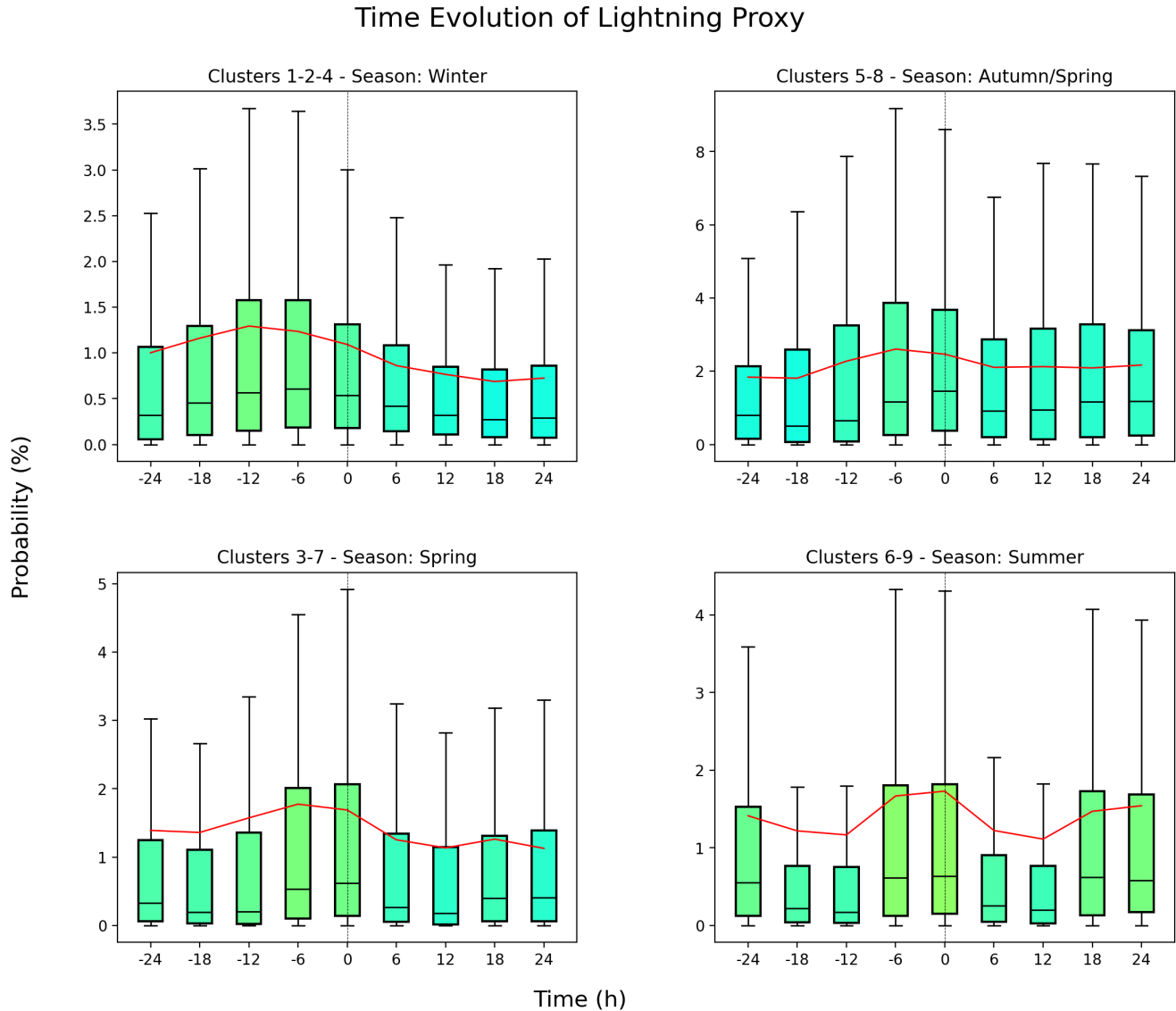


**Figure 18.** As in Fig. 15 but for the lightning proxy.

Lightning for winter clusters in Fig. 18, peaks at  $t=-12$  h, before the peak of convective precipitation (refer to Section 5.2.3) and is followed by a decrease in probability. A similar situation occurs for the other cluster groups. Mean lightning probability in clusters 5-8 peaks at  $t=-6$  h, just before the smooth maximum of convective precipitation during  $t=-6$  h to  $t=0$  h. Likewise, in clusters 3-7, mean lightning probability peaks at  $t=-6$  h before the mature stage of the cyclone and maximum convective precipitation. It should be noted, however, that the highest 90<sup>th</sup> percentile of lightning in Fig. 18 for clusters 5-8 (time step  $t=-6$  h) and clusters 3-7 (time step  $t=0$  h), coincides with the highest 90<sup>th</sup> percentile of convective precipitation for the respective cluster groupings (see Fig. 17). In summer clusters, even though there are fluctuations in convective precipitation, we see a peak of the lightning proxy at  $t=-6$  h and until the time of minimum pressure ( $t=0$  h).



## 6 Discussion

The convective parameters (CAPE, bulk shear and WMAXSHEAR) take into account stability and shear. High values represent the increasing intensity of the convective hazards (convective precipitation, lightning and hail proxies) along Mediterranean cyclone tracks. The results section above (Section 5) primarily presents specific values and findings on the composite maps and time evolution of the clusters. In the following discussion, we explore the interplay between convective parameters and hazards in relation to the clusters' spatial and seasonal distributions and their dynamical features. It is important that these three factors are taken into consideration together since the PV structure of the clusters exhibits pronounced seasonal and geographic discrepancies. For example, clusters similarly classified as Rossby wave-breaking lows may occur in different locations with distinct environments (i.e. moist vs. dry) with effects on the hazards' intensity.

### 6.1 Winter Clusters 1-2-4

Clusters 1 and 4 mainly occur near mountainous areas (refer to Figs. 5 and 7) where the highest cyclogenesis frequency is located on the lee side of mountains (e.g. the Alps in western Mediterranean). For both clusters, convective rainfall is seen close to the core of the cyclone, north and east of the centre along the cold front region (cf. with Fig. 36), and is in agreement with the spatial characteristics of precipitation around the Mediterranean cyclones presented by Raveh-Rubin and Wernli [2016] and Flaounas et al. [2018]. Specifically, Fig. 2 from Raveh-Rubin and Wernli [2016] shows convective precipitation in the cyclone center (feature 7) and along the cold front (feature 6). Even though CAPE is not strong in these clusters, the bulk shear provides the necessary environmental forcing. Stronger convective environments (i.e. magnitude in WMAXSHEAR) are observed in cluster 4 compared to cluster 1 (see Fig. 11), indicating that stronger hazards are prone to form within the former (see the summary of cluster 4's convective environment and hazards in Fig. 19).

## Winter Cluster 4 - Stage B lee-low

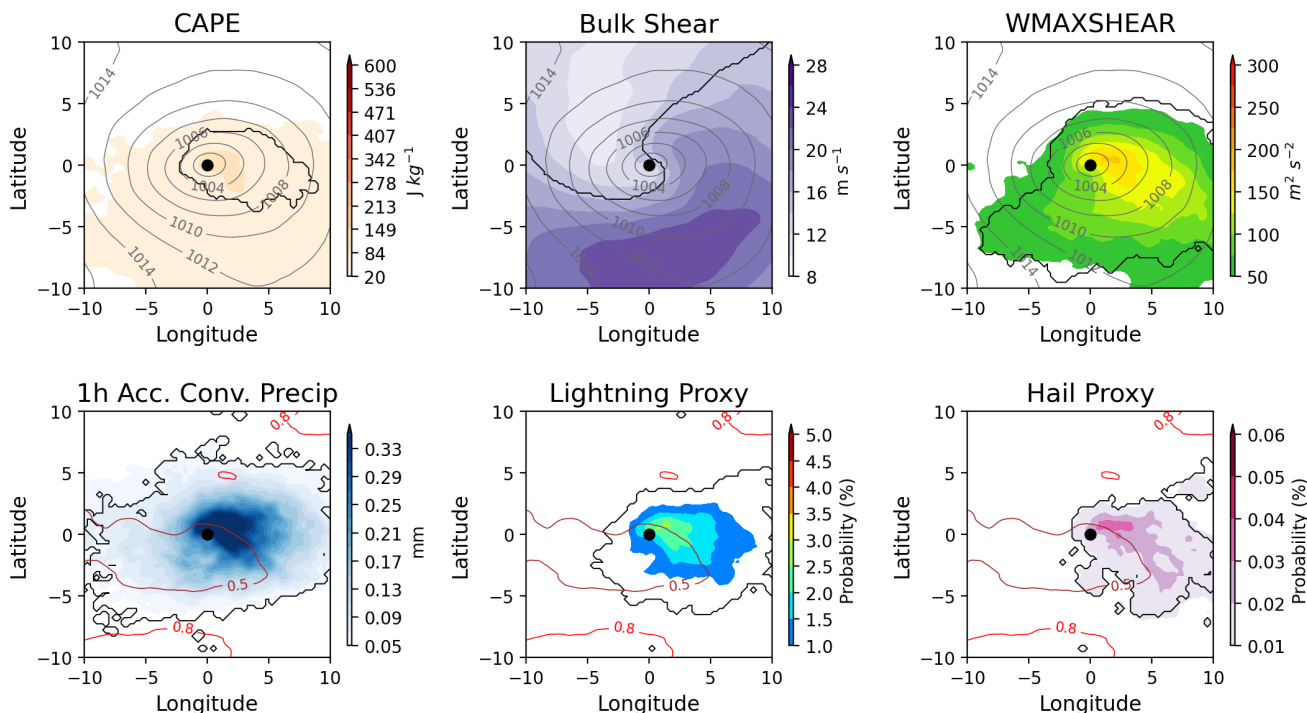


**Figure 19.** Summary for Cluster 4’s composites of CAPE, bulk shear, WMAXSHEAR, 1h accumulated convective precipitation, lightning and hail proxies (colored filled contours), as shown in Section 5.1. The black contour identifies the statistically significant area. The brown and red contours identify the land-sea mask at levels 0.5 and 0.8, respectively. Mean sea-level pressure is represented by the grey contours at 200 Pa intervals.

The above findings may be further connected to the dynamics of cluster 4. Specifically, from Fig. 33 we can see strong baroclinicity and a frontal structure due to strong gradients in 2m-temperature. Further, cluster 4 exhibits a warm occlusion, characterized by the wrapping of warm air from the south and around the cyclone core (illustrated in Fig. 35). Warm air occlusion is a critical phase in the life cycle of mid-latitude cyclones. During this phase, the warm air mass originally located ahead of the cyclone’s cold front becomes elevated above the cooler air near the ground [Neiman and Shapiro, 1993], leading to the establishment of a warm front aloft characterized by rising warm air and distinct cloud and precipitation patterns. This phase of the cyclone’s development can have significant implications, potentially contributing to the hazards we see in cluster 4 (Fig. 19).

Cluster 4’s heightened convective activity in comparison to cluster 1, may be attributed to its elevated moisture content [Givon et al., 2023]. This increased moisture availability leads to a notable rise in lightning and hail probabilities within cluster 4 (see Fig. 19), as it provides the necessary fuel for more vigorous convection. The diabatic processes and increased cyclone intensities in this context are further supported by cluster 4’s deep PV structure (see Fig. 32), similarly as discussed in Section 2.2.2. Additionally, the higher hail probability in cluster 4 in comparison to the other winter clusters (1 and 2), may also be related to its diverse spatial distribution. For example, Taszarek et al. [2020a] finds that large hail is predominantly observed across much of Europe during the months of June and July, however, there is an exception for southern Italy and Greece, where the highest frequency of large hail events occurs during the winter season.

In cluster 4, peak WCB activity (see Fig. 34) is likely linked to moist air advection as the lee-low separates from stage A lee-low over the Mediterranean Sea. Additionally, Flaounas et al. [2018] showed that deep convection-induced rainfall predominantly concentrates around the cyclone’s center and eastern flanks, while WCB-related rainfall primarily occurs to the northeast. Furthermore, a significant portion of deep convection is associated with embedded convection in WCBs. These spatial patterns align with cluster 4’s convective precipitation and lightning composites, detailed in Fig. 19, which show elevated values to the north-northeast and east of the storm’s center.

Cluster 2’s convective environment and hazards are summarized in Fig. 20. Its dynamical structure is related to an anticyclonic wave breaking, and later to a cyclonic wave breaking low. Givon et al. [2023] showed that cluster 2 is a more static cyclone, with the possibility of increased hazard risk (second row of Fig. 20). Despite the lower WMAXSHEAR in cluster 2 compared to cluster 4, the two have comparable features of CAPE and bulk shear, leading to similar levels of convective precipitation (cf. Fig. 19 and Fig. 20).

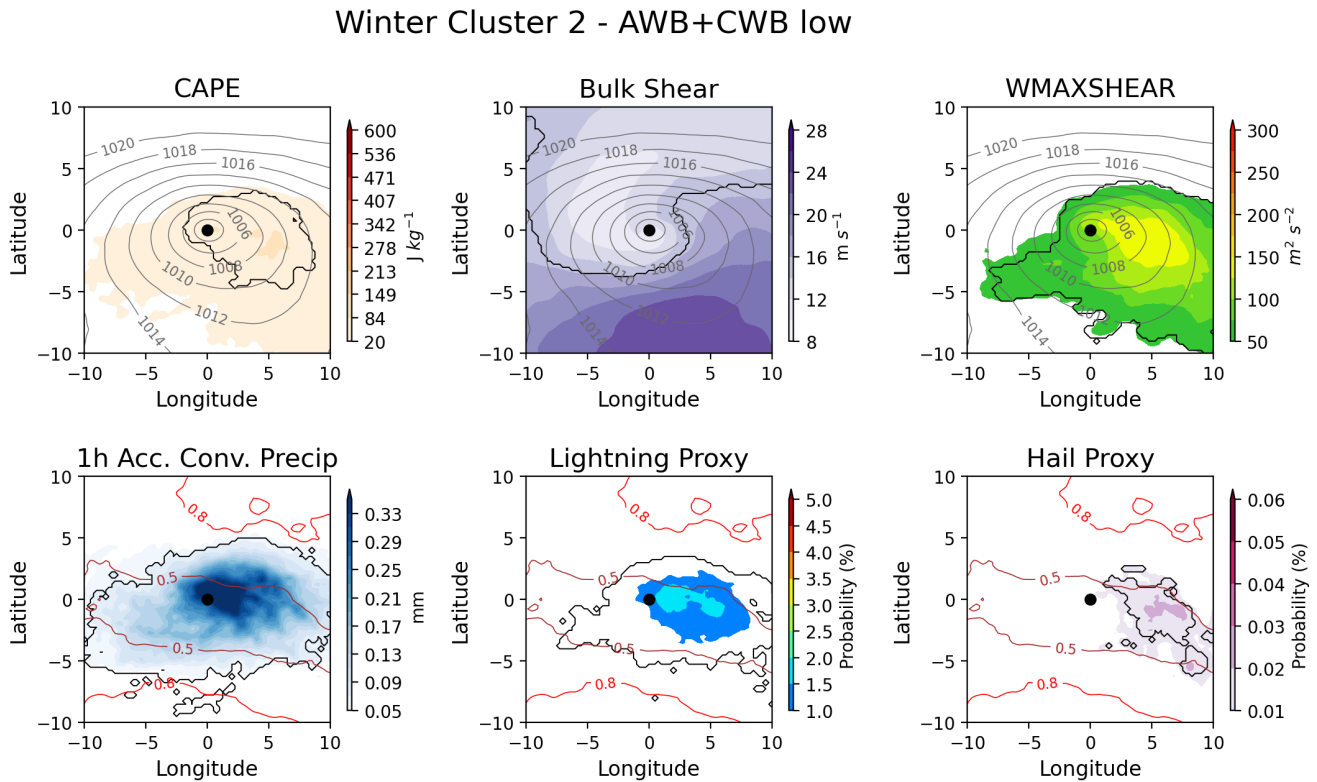


**Figure 20.** As in Fig. 19 but for Cluster 2.

Cluster 2 is not the deepest in terms of MSLP, however, it exhibits a contracted shape with pronounced MSLP gradients (grey contours in Fig. 20). This deepening structure is driven by the southward extension of AWB lows, forming a tilting cyclonic pattern above the surface cyclone (detailed in Section 2.2.3.2). Notably, in Fig. 32, cluster 2 extends farthest from the primary PV reservoir, resulting in a distinct PV tower formation (defined in Section 2.2.2). According to Givon et al. [2023], this supports the presence of precipitation and surface-wind maxima within cluster 2. Cluster 2’s hazards, as seen in the second row of Fig. 20, extend eastward from the cyclone center. This can be attributed to several factors. Firstly,

the presence of a trailing cold front (as seen in Fig. 36) to the east of the cyclone center, as depicted in Fig. 2, contributes to hazard development. Secondly, the occurrence of hazards to the east of the storms' center may be linked to the PV dynamics of cluster 2, particularly the southward extension of the PV streamer and the concurrent formation of a PV tower over the cyclone center during its mature stage. This development aligns with the wrapping of the PV streamer around the cyclone center and the shifting of surface fronts to the east, facilitating convection at the PV streamer's tip and contributing to eastward hazard extension [Flaounas et al., 2015]. Finally, the geographical distribution of cluster 2 plays a role, with hazards occurring more over water than on land (details on the land mask in Section 4.1.3), thereby enhancing cyclone development through increased moisture uptake.

Overall, Givon et al. [2023] states that clusters 1-2-4 are the most explosive. Diabatic processes play an important role in explosive cyclones (as mentioned in Section 2.2). This may suggest a connection between diabatic processes and the convective hazards seen in clusters 1-2-4, with intensity variations depending also on their dynamical features. Specifically, Flaounas et al. [2021] commented that the behavior of convection may vary between two cyclones due to the influence of different large-scale forced ascents. For example, when examining Fig. 33, we can see that clusters 2 and 1 are both cold cyclones with negative 2-m temperature anomalies across their domain, however, cluster 2 is the most impactful due to its deep PV structure and slow propagation. Furthermore, cluster 1 has a weaker convective environment and hazards (refer to Section 5.1). Cyclones in this cluster are confined to the lee of Alps (stage A) with a faint warm sector, as evident in Fig. 33 and Fig. 35. Consequently, these conditions may lead to reduced moisture availability, which further contributes to the noted lower convective activity and hazards in cluster 1, compared to the other winter clusters. Givon et al. [2023] also claims that convective precipitation is reduced in cluster 1, due to downdrafts on the lee side of the mountains. Downdrafts are projected to promote stability due to cooler and drier air, and hence decrease convective precipitation.

### 6.1.1 Time evolution of Clusters 1-2-4

Figure 21 provides a summary of the temporal variability in bulk shear, CAPE, convective precipitation and lightning, for the winter clusters.

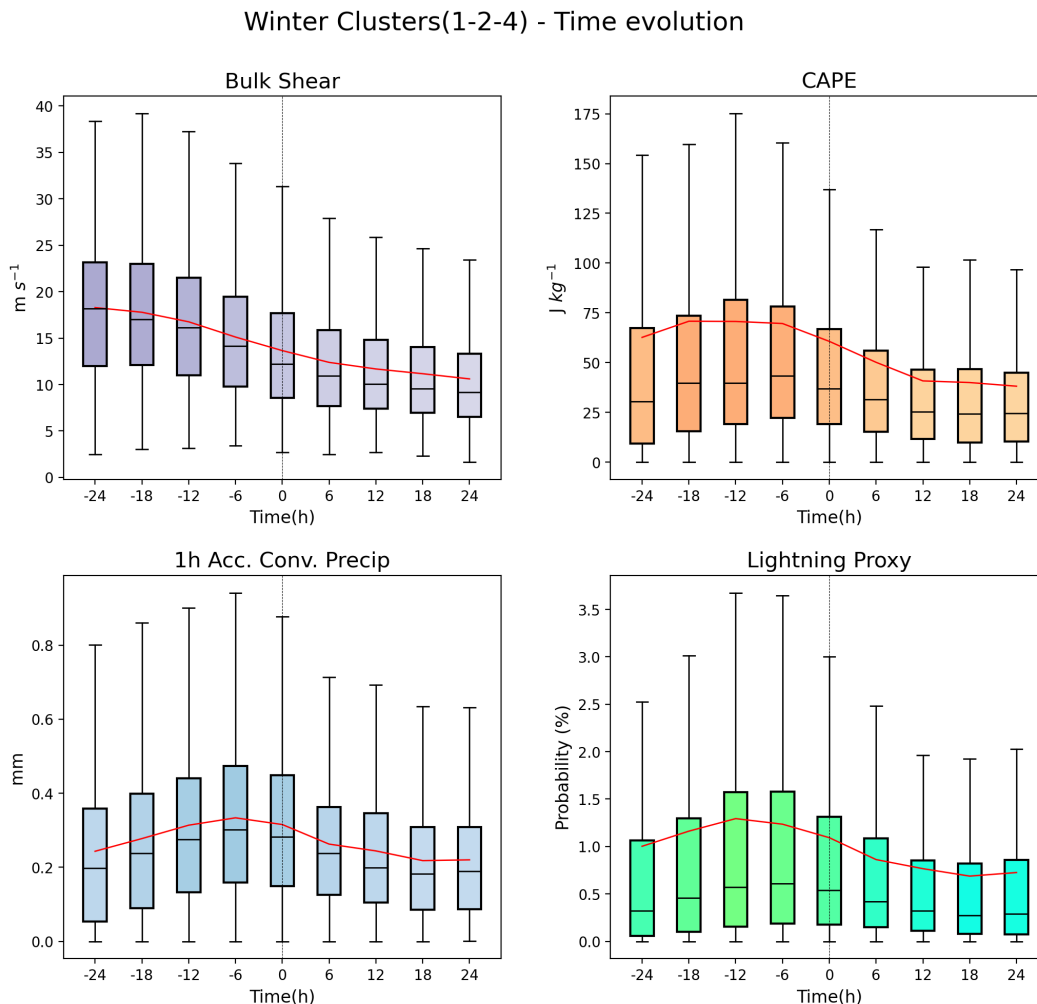


**Figure 21.** Summary of spatial average (200 km radius around cyclone center) of bulk shear, CAPE, 1h accumulated convective precipitation, and lightning proxy at time steps before and after the minimum pressure ( $t=0$  h) for winter clusters, as shown in Section 5.2. Red line shows mean value of the cyclones belonging to the relevant clusters at each time step. Box plots represent the interquartile range, the line inside the box denoting the median, and the whiskers indicating the 10<sup>th</sup> and 90<sup>th</sup> percentiles. The box-plot shades change according to normalized values using the respective color scheme of the parameters. Outliers are omitted.

In Section 5.2, we noted the evolution of convective conditions, with a build-up of bulk shear and CAPE from -24 h to the cyclone’s mature stage ( $t=0$  h). This aligns with Flaounas et al. [2015], which emphasized the role of the PV streamer in directing moist and warm air toward the cyclone center before its mature stage. In the study by Galanaki et al. [2016] on intense Mediterranean cyclones, a decrease in cloud content was observed from 0 h to +6 h, implying that convection must have occurred prior to cyclones reaching their maximum intensity. While this is in agreement with the overall result on the convective environment in Fig. 21, it does not directly correlate with the peak convective precipitation at  $t=-6$  h in Fig. 21. Additionally, Galanaki et al. [2016] showed that cyclone-induced lightning activity drops significantly after  $t=-6$  h, reaching its lowest point at  $t=+6$  h. This is comparable to our results in Fig. 21, where the lightning probability decreases from -6 h and reaches a constant low at +12 h. Lastly, Flaounas et al. [2018] found that precipitation tends to increase from -24 h to around -6 h and then gradually decreases to  $t=0$  h, similar to our results in Fig. 21 for convective precipitation.

Looking at the intensity of the convective parameters, bulk shear and CAPE in Fig. 21, we can relate their values to the results by Pacey et al. [2021] for severe convective windstorms occurring in the cold season. According to Fig. 21, the bulk shear begins at a mean value of approx 18 m/s, with individual maxima reaching values up to 40 m/s. Likewise, Pacey et al. [2021] found for a selection of storms, a wind shear within the range between 21-39 m/s and CAPE values less than  $100 \text{ J kg}^{-1}$  in 72% of the instances. The average CAPE values for winter clusters in Fig. 21, range below  $100 \text{ J kg}^{-1}$ , with some extreme cases reaching  $175 \text{ J kg}^{-1}$ .

## 6.2 Autumn & Spring Clusters 5-8

In autumn, sea surface temperature (SST) is climatologically higher, inducing a higher land-sea temperature contrast. This contrast creates regions of high atmospheric instability favorable to the release of heat and moisture, thus assisting the development of convection and heavy rainfall. Flaounas et al. [2018] showed that intense cyclones associated with high rainfall occur mostly in autumn and winter, in agreement with Fig. 12, showing highest convective precipitation in winter clusters 1-2-4 and autumn cluster 8.

Cluster 8's convective environment and hazards are summarized in Fig. 22. It predominantly occurs in autumn and is linked to CWB lows. The PV streamer's dynamic forcing and instability encourage heavy convection [Flaounas et al., 2015], similar to the processes described for cluster 2 in Section 6.1. On average, the PV streamer is located west of the cyclone center, resulting in cyclonic breaking on the poleward side of the jet (as detailed in Section 2.2.3.2). This supports the low-level cyclonic circulation around the storm center. The eastward displacement of the warm sector is associated with the CAPE structure observed in Fig. 22, characterized by strong warm advection from the south to the east of the storm center and ahead of the cold front (cluster 8's cold front composite is shown in Fig. 36). This is also consistent with the findings of Flaounas et al. [2015], where moist values are often seen on the cyclone's eastern flank and along the surface warm front. Likewise, Givon et al. [2023] linked cluster 8 to strong convective activity and weak large-scale precipitation, possibly due to topography allowing the PV streamer to extend southward, inducing convection towards its tip. Furthermore, the westward propagation of CWB lows against the mean flow allows the formation of quasi-stationary cyclones, which is in agreement with Givon et al. [2023] that identified cluster 8 as a more stationary cyclone and hence associated with elevated hazard risks, as shown in Fig. 22. Additionally, cluster 8, similarly to cluster 2 discussed above, exhibits a deep PV structure and is classified as an explosive cyclone [Givon et al., 2023], again contributing to the hazards in Fig. 22.

## Autumn Cluster 8 - CWB low

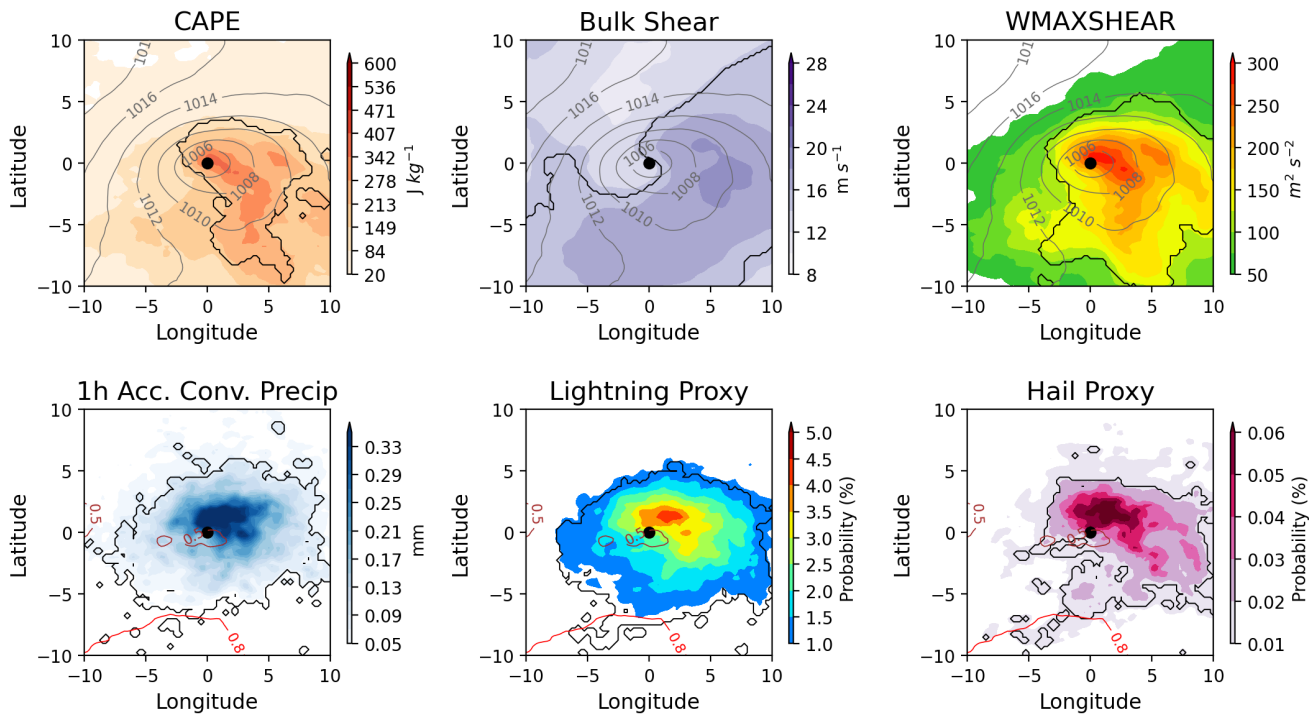


**Figure 22.** As in Fig. 19 but for Cluster 8.

In view of the above, we have a sharp and strong structure of WMAXSHEAR for cluster 8 (shown in Fig. 22), with its peak close to the center-east of the cyclone core and decreasing as it extends southwards and eastwards. This intense convective environment results in significant hazards (second row of Fig. 22), including convective precipitation and lightning concentrated to the northeast of the storm center. This aligns with the findings by Flaounas et al. [2018], who showed that DC is favored around the cyclone core and on their eastern side, where WCBs generate rainfall on the north-east of a storm's center. Further, Flaounas et al. [2018] showed that a considerable portion of DC relates to embedded convection in WCBs. The position of WCBs in cluster 8 (see Fig. 34) corresponds to the spatial distribution of its convective hazards (second row of Fig. 22). Additionally, cluster 8 exhibits a frontal structure (shown in Fig. 33) with both cold and warm anomalies, contributing to atmospheric instability and enhancing the convective environment. Furthermore, cluster 8 features a warm occlusion, similar to cluster 4, with warm sector air from the south wrapping around the cyclone center, contributing to the development of convective hazards. Notably, cluster 8 presents a greater hail risk, with the highest probabilities located northeast of the cyclone center and some risk extending southward.

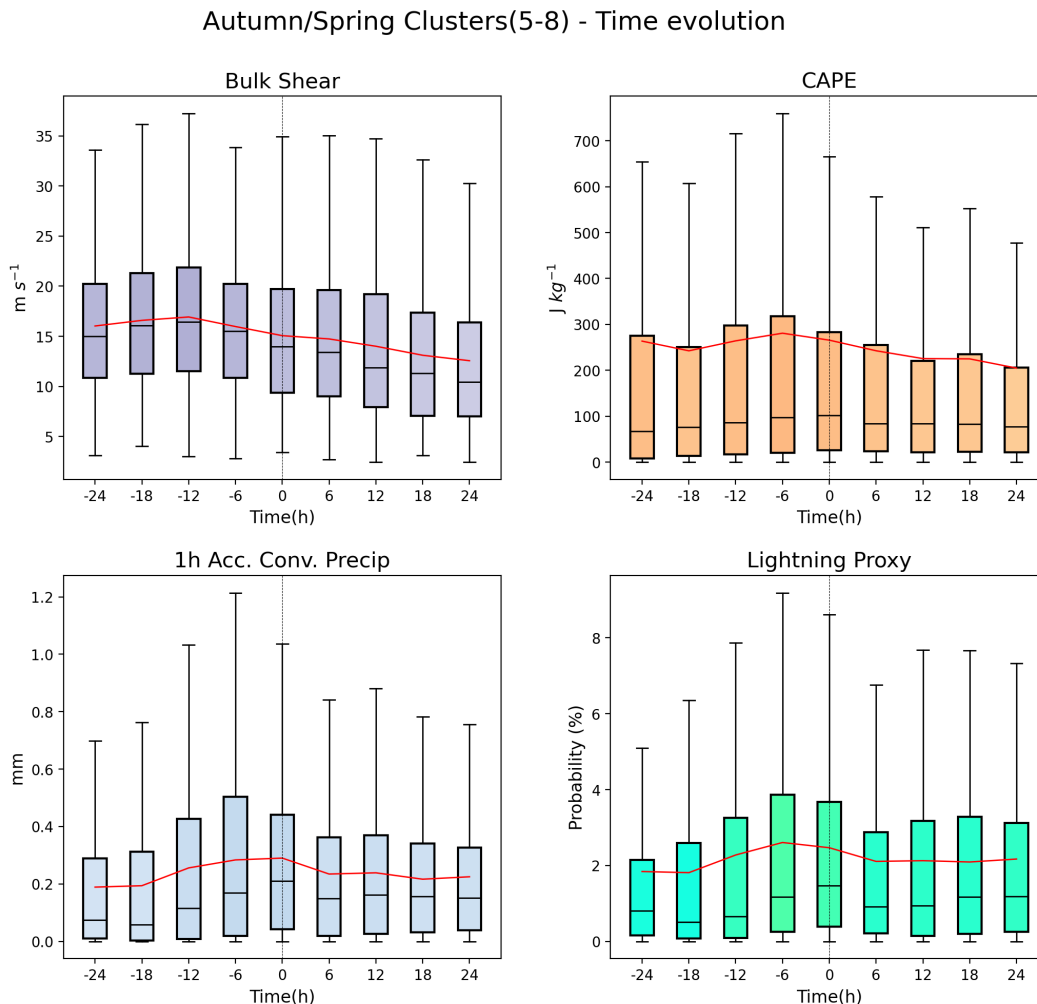
Cluster 5 are AWB lows that mainly occur in the subtropics, near the Atlas Mountains, with even distribution in spring and autumn. The CAPE values are lower compared to cluster 8, however, cluster 5 has higher bulk shear wrapping the cyclone centre from south-west to its east (shown in Fig. 10). WMAXSHEAR is lower in cluster 5 than cluster 8, however high values can be seen concentrated to the east of the cyclone core (refer to Fig. 11). Due to the prevalent high land fraction in the area where cluster 5 predominates (see Fig. 8), there is restricted moisture availability. Consequently, cluster 5 exhibits lower convective precipitation compared to cluster 8. Cluster 5 does not exhibit any low-level PV signal (see

Fig. 32), however a fraction of cluster 5 shows explosive systems given the AWB dynamics. Furthermore, cluster 5 propagates eastwards slower [Givon et al., 2023], hence it may allow for the development of severe hazards. High bulk shear and moderate CAPE values can contribute to a conducive environment for the formation of hail. This is in agreement with the hail probabilities seen in Fig. 14 and as discussed in Section 5.1.6 for cluster 5, where high modeled hail occurrences by Battaglioli et al. [2023] were presented in northern Africa. The highest hail probabilities are found near the stronger WMAXSHEAR area, north-east of the storm center.

### 6.2.1 Time evolution of Clusters 5-8

The time evolution of clusters 5-8 is summarized in Fig. 23. We can see that the convective parameters and hazards evolve in a similar manner as discussed for the winter clusters above (refer to Section 6.1.1). However, the bulk shear and CAPE show less temporal variability in their evolution for clusters 5-8, compared to the winter clusters. Flaounas et al. [2021] highlighted that both baroclinic and diabatic processes should be accounted for the development of cyclones, given that sea surface fluxes and latent heat release can significantly alter the cyclone evolution even when baroclinic instability is the primary forcing. Consequently, the reduced fluctuations in bulk shear and CAPE may be argued to be associated with cyclones that deviate from the conventional baroclinic life cycle, likely due to the influence of these diabatic processes.





**Figure 23.** As in Fig. 21 but for autumn/spring Clusters 5-8.

Lightning probabilities are higher for clusters 5-8 than the rest cluster groupings, with a maximum at -6 h. This aligns with Galanaki et al. [2016], finding the peak lightning at  $t=-6$  h and higher activity altogether in winter and autumn. Further, Galanaki et al. [2016] showed that the average CAPE at 0 h, for storms producing lightning, is in the order of  $700 \text{ J kg}^{-1}$ , compared to  $200 \text{ J kg}^{-1}$  for cyclones that do not produce lightning. At  $t=0$  h in Fig. 23, the 90<sup>th</sup> percentile of CAPE reaches between 600-700  $\text{J kg}^{-1}$  and is consistent with Galanaki et al. [2016] who considered only very intense cyclones.

### 6.3 Spring Clusters 3-7

Clusters 3 and 7 are classified as cut-off lows and daughter cyclones, respectively. Both clusters mainly occur in spring, with cluster 3 showing a local maximum in northwest Africa, on the lee-side of the Atlas Mountains; the dry environment of cluster 3 reflects in its hazard composites (Figs.12-14). Cluster 7 has a more diverse spatial distribution with occurrences both in northwest Africa and the Gulf of Genoa.

In clusters 3 and 7, a frontal structure is evident as shown in Fig. 33. Notably, the warm sector exhibits elevated CAPE values that extend from the southeast to the east of the storm center (see Fig. 9). Further, we see the bulk shear for both clusters to the northeast of the storms' center, at the location of the

highest pressure gradients (Fig. 10). Even though CAPE has moderate values, bulk shear is considerably high. Specifically, WMAXSHEAR, as seen in Fig. 11, is presented to the northeast of the storms' center at the location of maximum bulk shear. High frequency of WCBs is also present in clusters 3 and 7 (shown in Fig. 34), even though their precipitation is limited [Givon et al., 2023]. The inconsistency between the high frequency of WCBs in clusters 3 and 7 and their weak precipitation patterns arises from their predominant occurrence over northwest Africa, where moisture availability is scarce. Additionally, Fig. 32 reveals that these clusters have high PV values near the surface but lack mid-level tropospheric PV. This suggests a deficit in PV production from diabatic heating and, consequently, weak convection, since diabatic processes typically act as a PV sink near the surface and as a source in the lower-to-middle troposphere, followed by another PV sink in the upper levels [Flaounas et al., 2015, 2021].

In agreement with the discussion above, we see low values in convective precipitation and lightning for clusters 3 and 7 (refer to Figs.12-13). Significant hail probabilities are seen only in cluster 7 (see Fig. 14) as certain cases occur in Northwest Africa (discussed in Section 5.1.6) and also in the Gulf of Genoa with higher moisture availability.

### 6.3.1 Time evolution of Clusters 3-7

Figure 24 summarizes the time evolution of convective parameters and hazards for clusters 3-7. Similarly to clusters 5-8 above (refer to Section 6.2.1), we see even less temporal variability in the evolution of bulk shear and CAPE. Further, there is a contrast with the findings by Flaounas et al. [2018], which show that cyclones with low rainfall production, as in the case of clusters 3-7 (see Fig. 12), tend to reach their peak at -6 h, as opposed to the gradual increase in mean convective precipitation seen in Fig. 24 from -24 h to its peak at t=0 h. However, the differences in the cyclone sample and in the variables (convective instead of total precipitation) are expected to account for such divergence.

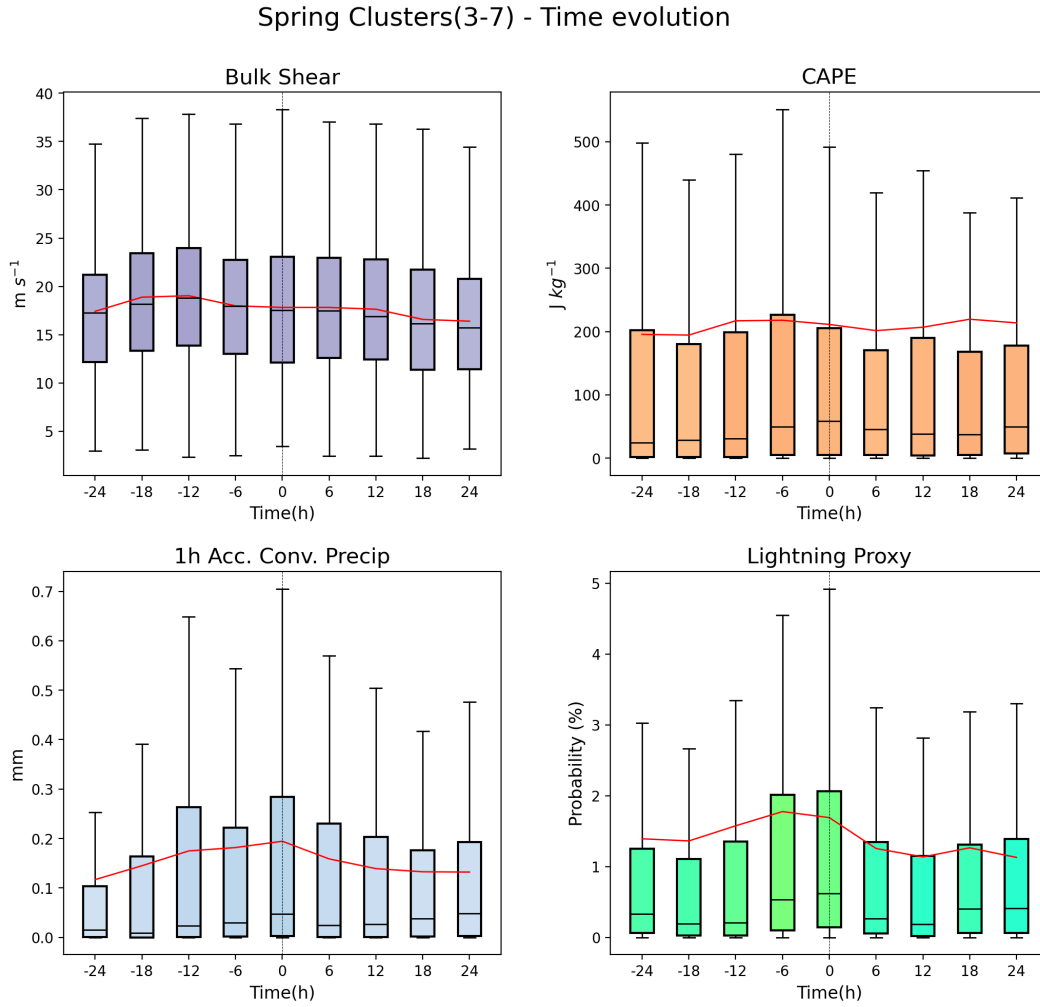


Figure 24. As in Fig. 21 but for spring Clusters 3-7.

## 6.4 Summer Clusters 6-9

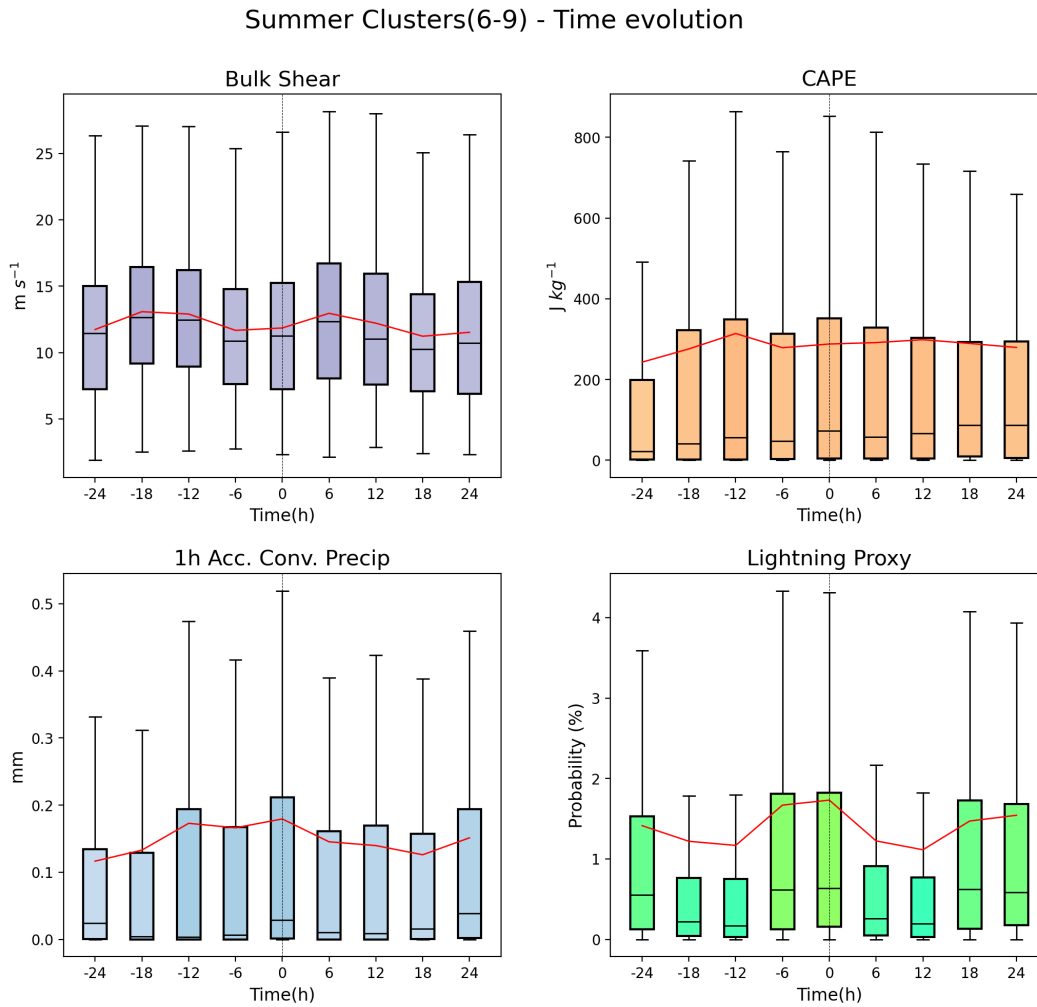
Cluster 6 primarily occurs over land in northern Africa and corresponds to continental heat lows known as Sharav lows. It exhibits weak upper-level and no low-level PV anomalies. They arise mostly during the summer season due to significant surface heating over land (seen in Fig. 33) and limited surface evaporation [Trigo et al., 2002]. Despite high CAPE values seen in Fig. 9, it lacks significant convective precipitation, lightning activity, and hail probabilities due to moisture limitations (refer to Section 5.1). Givon et al. [2023] links cluster 6 to substantial convective precipitation anomalies further south related to the African monsoon (not shown here).

Cluster 9 is associated with cut-off lows in northwest Africa, the Mediterranean Sea and the Gulf of Genoa. Similarly to cluster 6 above, cluster 9 presents a uniform warm anomaly (Fig. 33) and no frontal structure. Stronger CAPE values than cluster 6, are seen in cluster 9 to the northeast of the cyclone center which indicates high atmospheric instability. As a result, the WMAXSHEAR in Fig. 11 suggests the possibility for a severe convective environment to the northeast, which is also supported by the wrapping bulk shear structure (see Fig. 10). Favorable conditions due to warm sea waters, possibly influenced by the diverse spatial distribution of cluster 9 with incidents over the Mediterranean Sea,

may lead to severe thunderstorm development within the cluster. This aligns with the higher convective precipitation, lightning activity, and hail risk seen in cluster 9 compared to cluster 6 (refer to Section 5.1). Cluster 9 has high PV values near the surface but low PV values at upper and mid-levels as shown in Fig. 32. Nonetheless, Raveh-Rubin and Wernli [2016] highlighted that shallow convection and interactions with orography contribute greatly to heavy rainfall, which may be connected to the hazards we find in cluster 9.

#### **6.4.1 Time evolution of Clusters 6-9**

We can see the time evolution for the convective environment and hazards of the summer clusters 6-9 in Fig. 25. The variability of the convective parameters, especially in bulk shear and hazards, display fluctuations before and after the minimum pressure of the storm. Trigo et al. [2002] showed that the diurnal cycle plays an important role in the development of cyclones throughout spring and summer and mentions that Saharan depressions are associated with stationary thermal lows (similar to cluster 6), which are primarily caused by substantial diurnal oscillations in inland surface temperature. This is consistent with the standalone time evolution results of cluster 6, showing even higher temporal fluctuations (seen in Appendix A.1). Convective precipitation and lightning for cluster 9 alone show weaker fluctuations, where this may be associated with the diverse geographical distribution of cluster 9, including occurrences also in the Gulf of Genoa. Specifically, this agrees with Trigo et al. [2002], which states that the diurnal fluctuations of Genoa lows are much smoother than over any of the other areas, where thermal processes predominantly govern the behavior.



Finally, we can also compare the magnitude of bulk shear and CAPE for the summer clusters, with the results by Pacey et al. [2021] for warm season severe convective windstorms (Type 1 environment detailed in Section 2.1). The mean bulk shear ranges between 10-15 m/s, whereas in the study of Pacey et al. [2021] the IQR is very similar, with values between 10-20 m/s. The mean CAPE reaches  $300 \text{ J kg}^{-1}$  at  $t=-12 \text{ h}$  and stays constant thereafter, where certain cases reach a CAPE of  $800 \text{ J kg}^{-1}$  at the 90<sup>th</sup> percentile. This is comparable with the IQR results for CAPE by Pacey et al. [2021], which are in the range of 200-1040  $\text{J kg}^{-1}$ .

## 7 Conclusion

Mediterranean cyclones are responsible for the majority of the weather impacts in the region [Flaounas et al., 2022]. Despite advances in understanding the genesis and large-scale features of Mediterranean cyclones, our knowledge of their associated hazards and seasonal and spatial distribution is quite limited. Analysing the hazards embedded in the Mediterranean cyclones involves studying the convective environments, and hence the mesoscale characteristics of such cyclones. This study highlights how large-scale dynamics and seasonal and spatial characteristics interact with convective environments along the cyclone tracks. The analysis makes use of 9 cyclone clusters selected based on the Mediterranean cyclones' upper-level PV structure [Givon et al., 2023]; the resulting classification allows a further cluster grouping based on the respective peak seasons and time evolution: winter clusters 1-2-4, autumn/spring clusters 5-8, spring clusters 3-7, and summer clusters 6-9.

Clusters 1 and 4 (stage A and stage B lee-lows, respectively) with maximum frequency during winter, are closely linked to topography, exhibiting convective rainfall close to the core of the cyclones, north and east of the center. Cluster 4 shows a stronger convective environment, with elevated WMAXSHEAR, and higher hazard intensities compared to cluster 1, due to its warm occlusion and deep PV structure. Cluster 2, ascribable to an AWB cyclone, exhibits a similar convective environment as cluster 4, however, its hazards extend further east due to the presence of a trailing cold front, the influence of the PV dynamics and interaction with the sea. Overall, clusters 2 and 4 were found as the most explosive [Givon et al., 2023], with our hypothesis, discussed in Section 6.1, pointing to a crucial role of diabatic processes for the intensity of their convective hazards.

Cluster 8, associated with CWB lows and peaking in autumn, shows severe convective environments, with elevated values in CAPE, bulk shear and WMAXSHEAR, leading to high-intensity hazards, mainly positioned to the northeast of the cyclones' center. This is attributed to its favorable seasonal and geographical distribution, coupled with frequent WCB occurrences, which potentially increased moisture availability. The deep PV structure of cluster 8, similar to cluster 2 above, is also believed to have influenced its convective environments and hazards.

Clusters not covered above (3, 5, 6, 7 and 9) displayed relatively milder convective hazard characteristics in diverse seasons and regions (detailed in Section 6). For instance, cluster 5 (AWB low), which occurs evenly in spring and autumn, shows lower hazard intensities due to its western African distribution. Furthermore, it is noteworthy that cluster 9 (short-wave cutoff low), in contrast to the other summer cluster 6, exhibits higher convective hazards, including significant hail risk. A similar pattern emerges with cluster 7 (daughter cyclone), primarily occurring in spring with distinct characteristics.

The time evolution analysis revealed a build-up of the convective environment (bulk shear and CAPE) as the clusters progressed from -24 hours to the mature stage ( $t=0$  h). However, winter clusters (1, 2, and 4) stood out by exhibiting higher variability in bulk shear at times before the mature stage of the cyclones, whereas spring and autumn clusters (3, 5, 7 and 8) show a more uniform temporal evolution. Summer clusters (6 and 9), particularly cluster 6, show fluctuations that may be related to the diurnal cycle. In terms of the convective hazards (convective precipitation and lightning), clusters 1-2-4 show a peak between  $t=-12$  h and  $t=-6$  h, whereas clusters 5 and 8 show a peak between  $t=-6$  h and  $t=0$  h. For clusters 3-7 and 6-9, the peak of convective hazards is mainly seen at the maximum intensity of the

storms ( $t=0$  h).

The temporal evolution characterises the dynamic nature of convective systems and their diverse development. Understanding these variations in time is crucial for accurate forecasting and early warning systems. Specifically, further investigation into the drivers of these temporal changes, such as diabatic processes, large-scale forced ascent, PV dynamics, and topography, can provide valuable insights into the underlying mechanisms governing convective weather phenomena. Nevertheless, it is worth noting that the temporal variations seen in all clusters, while important to study, are not exceedingly substantial. Consequently, choosing the mature stage as the focal point for analysis can still provide valuable information.

The main limitation of this study is the parametrization of the small-scale physical processes from the reanalysis dataset. Future research on the topic would benefit from incorporating observational reports into the analysis and looking at a more local scale. Further, while it addresses moisture availability by examining spatial distribution and convective precipitation composites for each cluster, an assessment of the relative humidity for each cluster would enhance the validity of our findings.

Examining additional convective variables, especially those that contribute to the proxies for hail and lightning, can offer more comprehensive insights into the atmospheric conditions that give rise to these hazards and help to focus on additional hazards, such as damaging winds by downdrafts. Furthermore, analysing the frequency of strong convective environments and hazards (exceeding specific thresholds) can provide valuable cluster-wise information and give emphasis to the occurrence of cyclones characterised by intense convective activity. Finally, future work could focus on identifying tropical-like Mediterranean cyclone (Medicanes) within each cluster and discerning their unique environmental features, as Medicanes are closely associated with convective environments. Such investigations may aid in characterising Medicanes compared to conventional Mediterranean cyclones, and gain further understanding of the environmental conditions that lead to their development.

In conclusion, the study demonstrated the significance of considering both stability and shear in understanding the convective hazards along Mediterranean cyclone tracks. The findings also emphasize the importance of taking into account the seasonal, spatial and dynamical characteristics of cyclones when assessing their potential hazards. These results can be valuable for forecasting and mitigating the impacts of extreme weather events associated with Mediterranean cyclones, particularly in enhancing early warning systems and preparedness measures by exploring the interactions between various convective hazards and their regional effects.

## A Appendix

### A.1 Time evolution of all clusters

#### A.1.1 CAPE

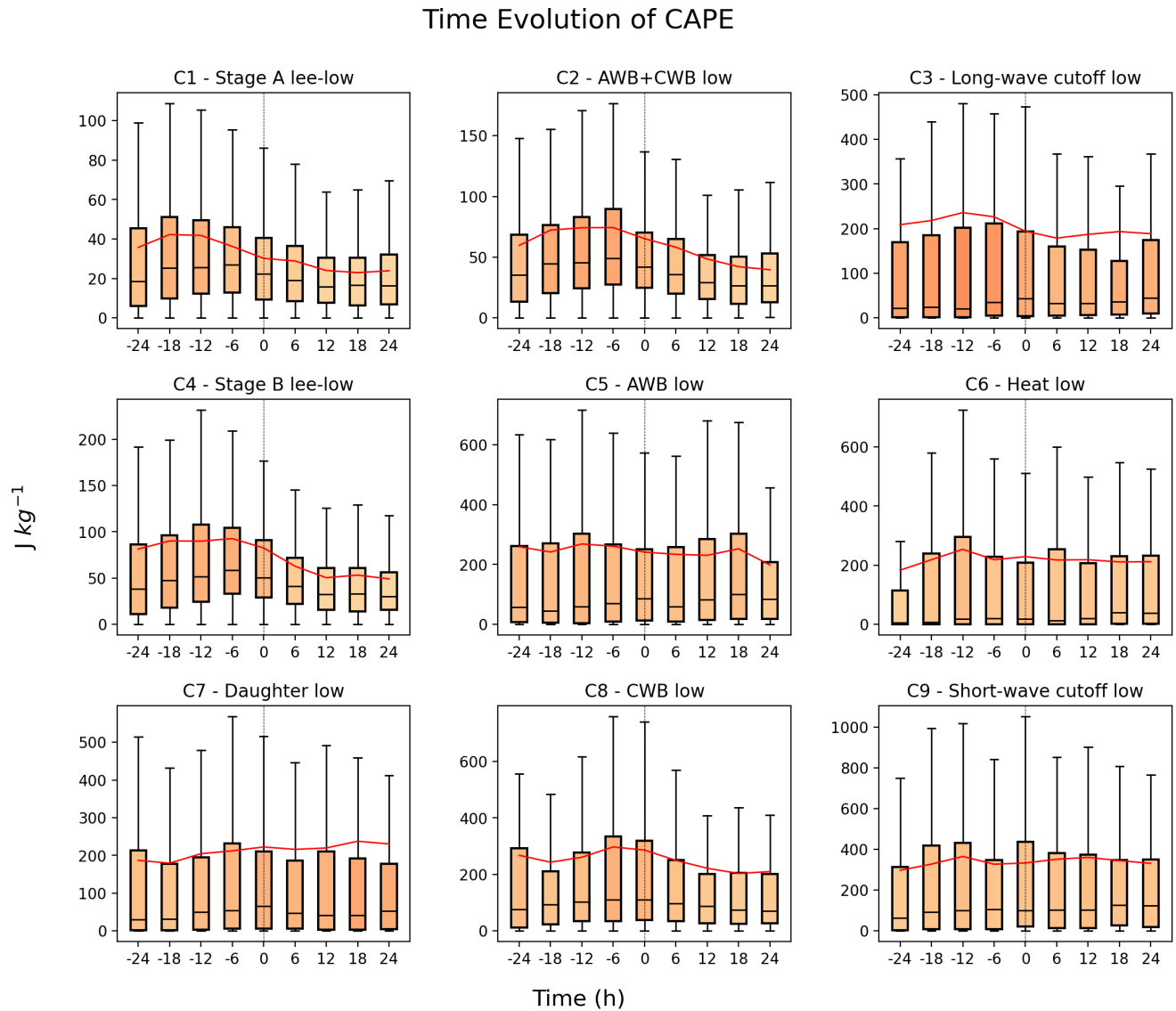


Figure 26. As in Fig. 15 but for each cluster separately.



A.1.2 Bulk Shear

Time Evolution of Bulk Shear (0-6km)

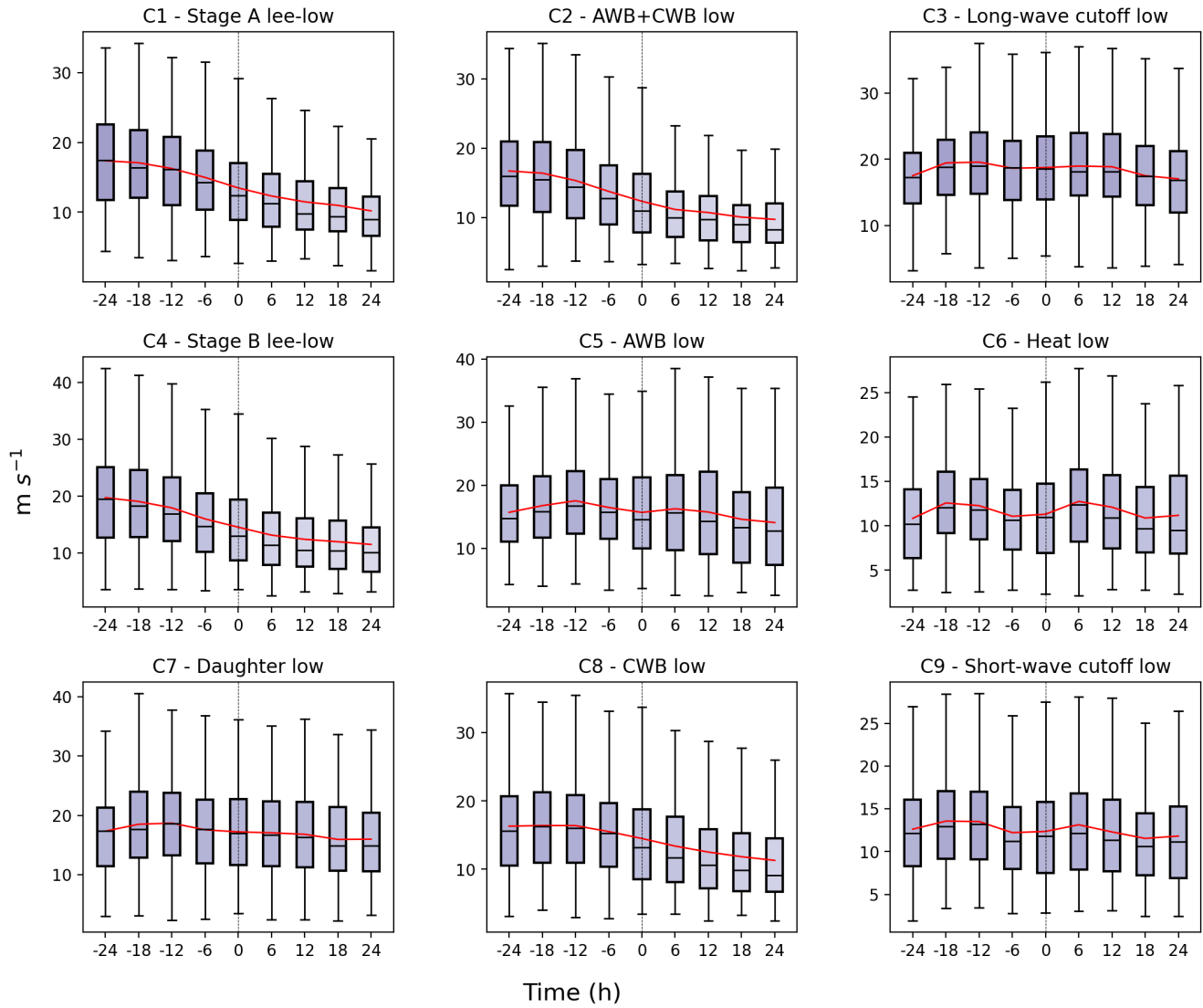


Figure 27. As in Fig. 16 but for each cluster separately.

A.1.3 Convective precipitation

Time Evolution of 1h Acc. Convective Precipitation

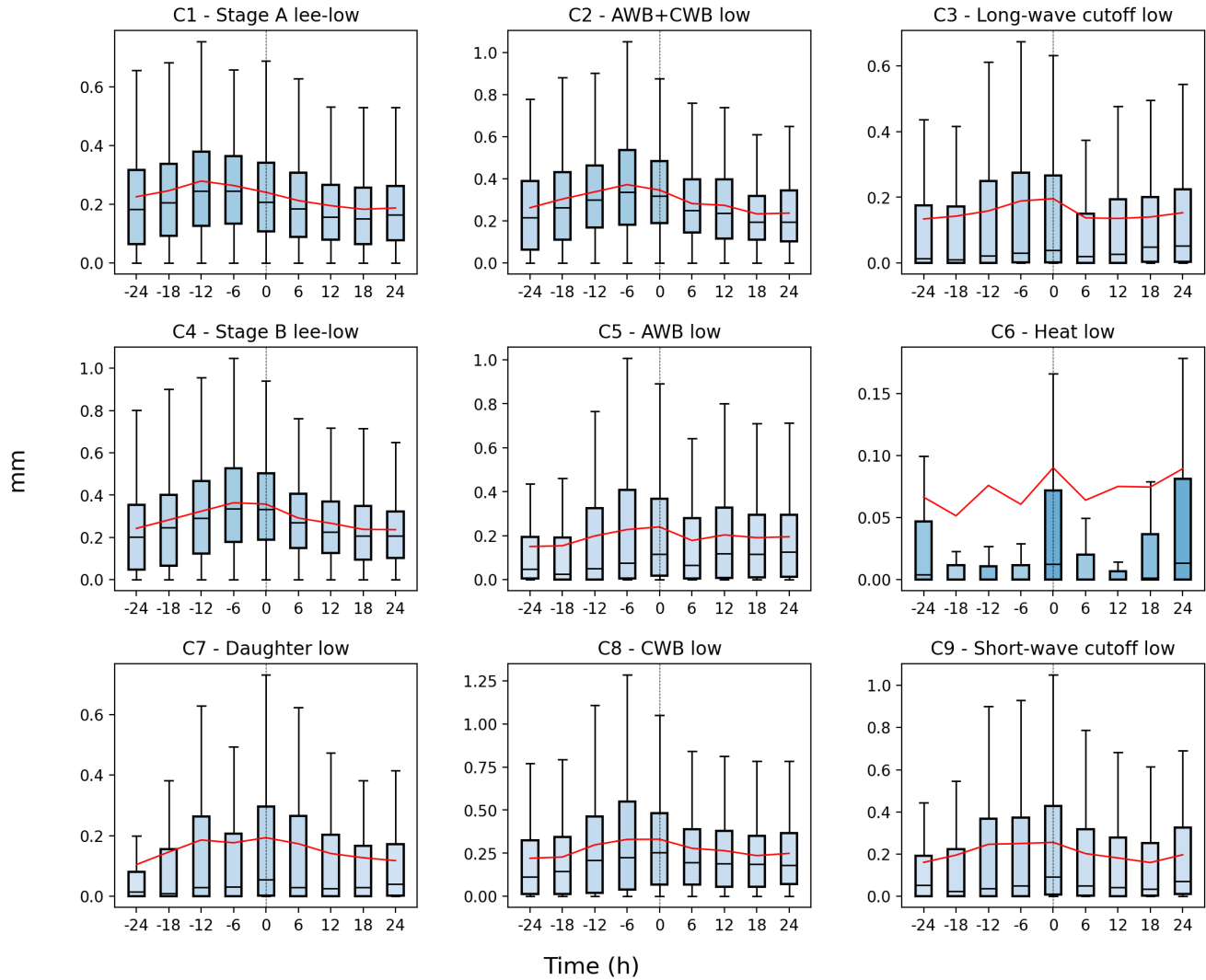


Figure 28. As in Fig. 17 but for each cluster separately.

A.1.4 Lightning Proxy

Time Evolution of Lightning Proxy

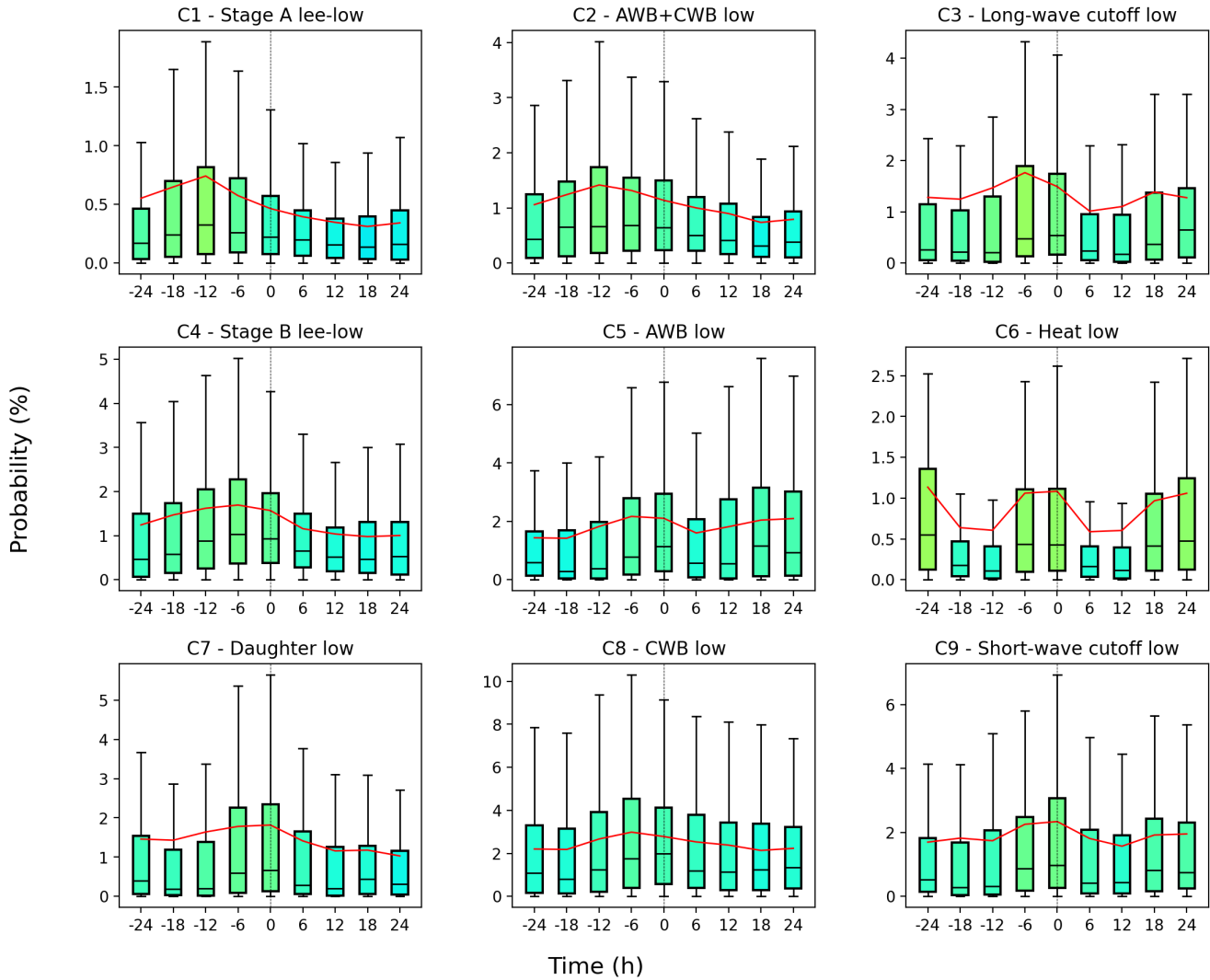


Figure 29. As in Fig. 18 but for each cluster separately.

### A.2 Time evolution of 10m surface wind

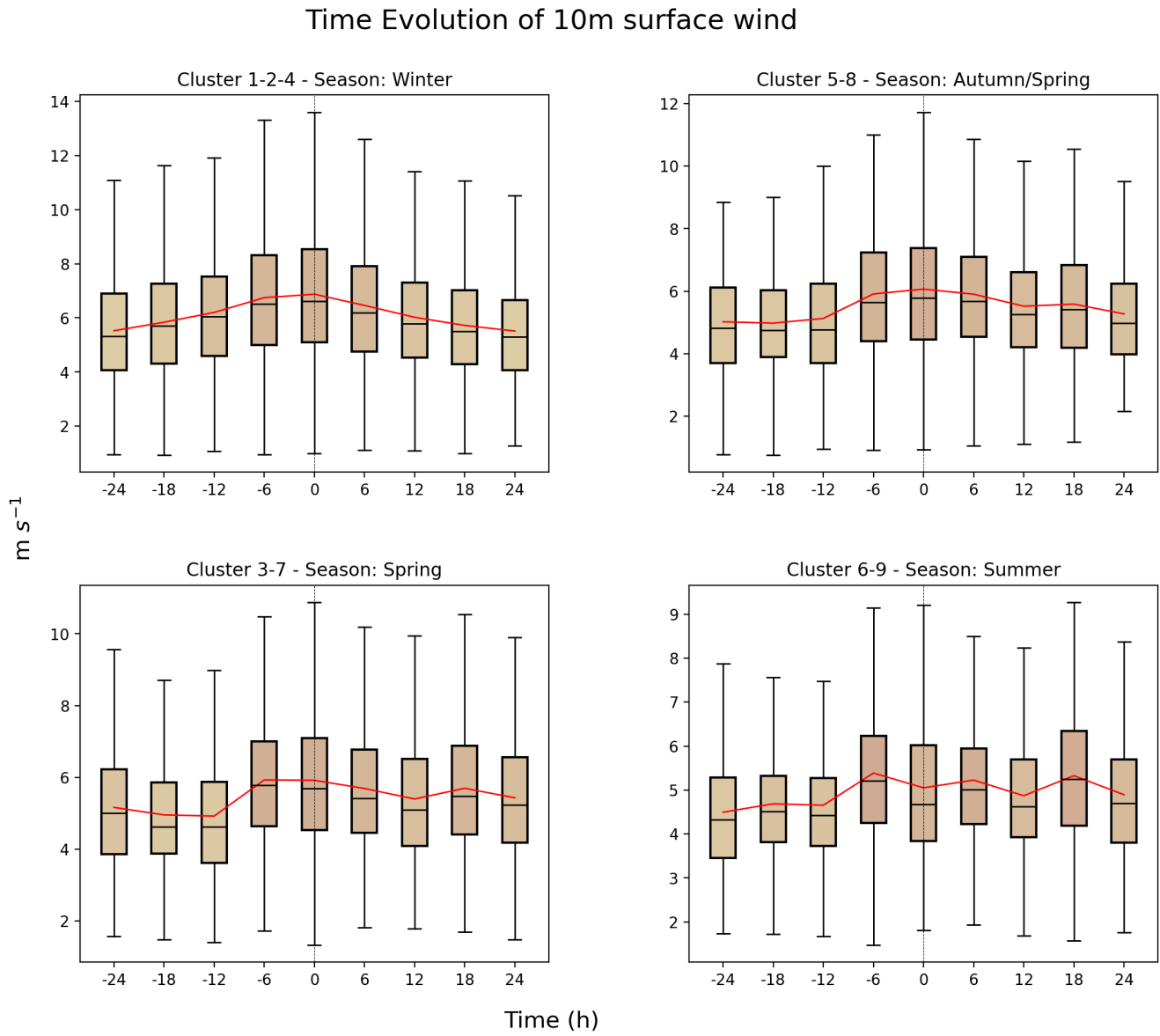


Figure 30. As in Fig. 15 but for 10 m surface wind.

### Time Evolution of 10m surface wind

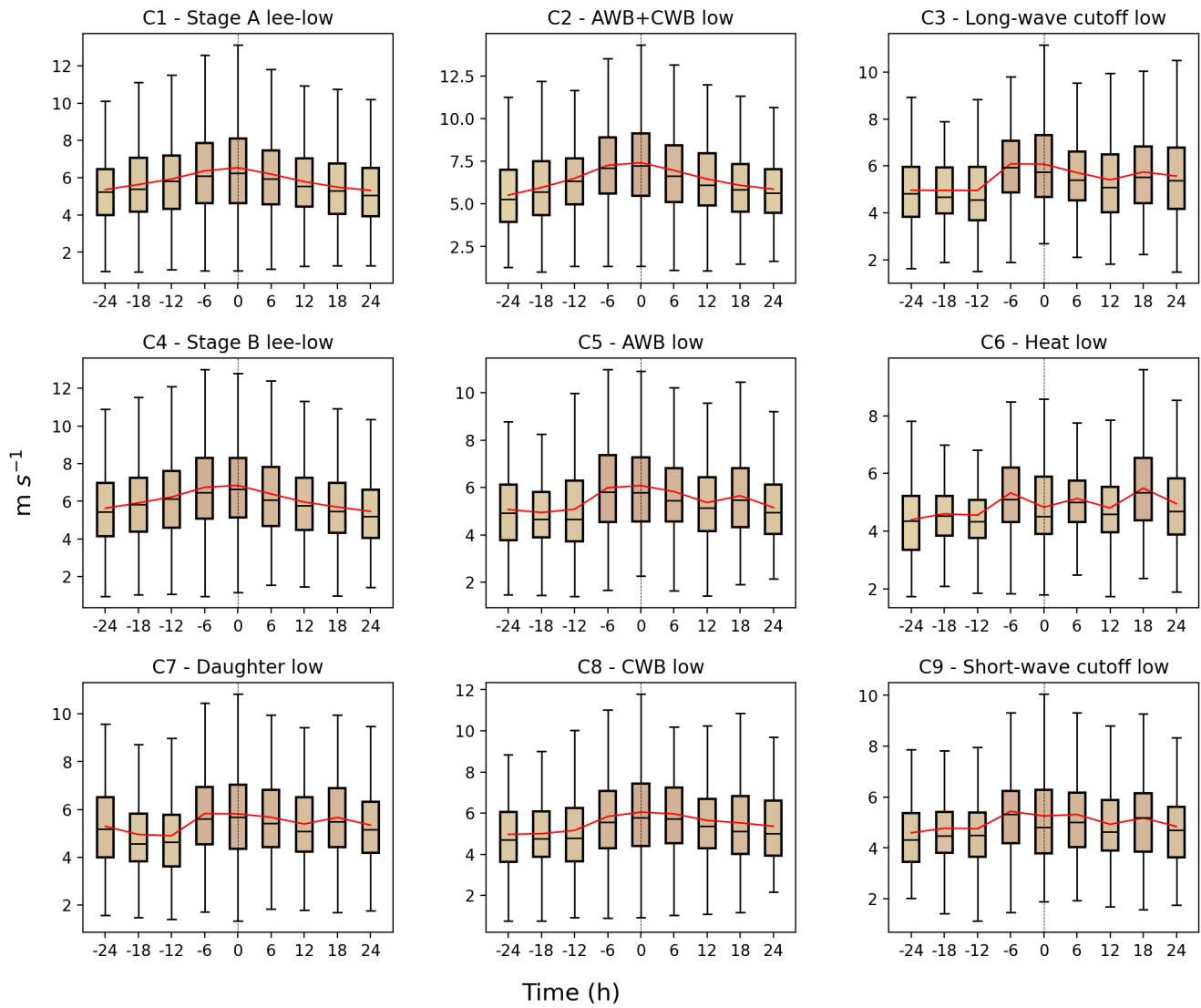
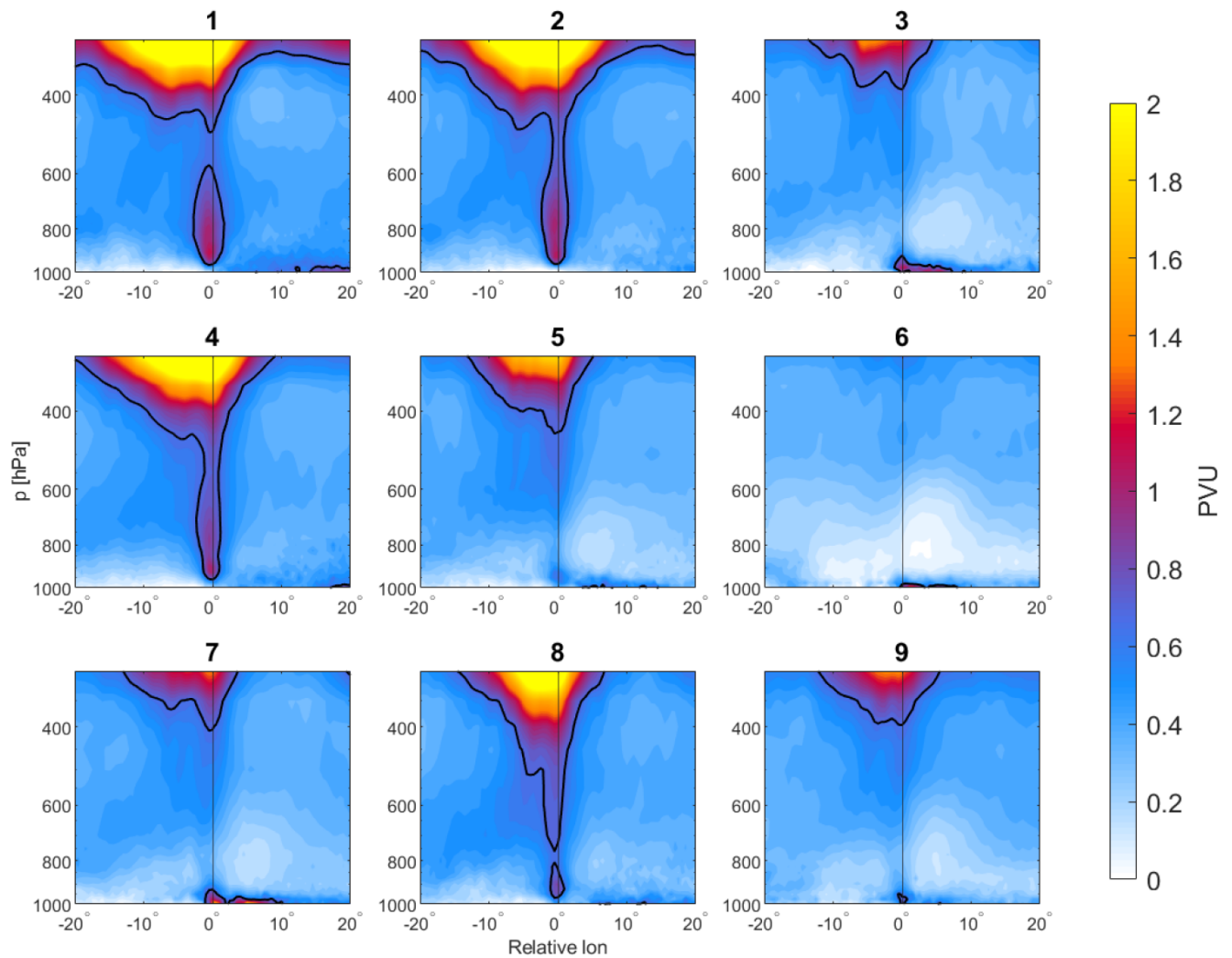


Figure 31. As in Fig. 30 but for each cluster separately.

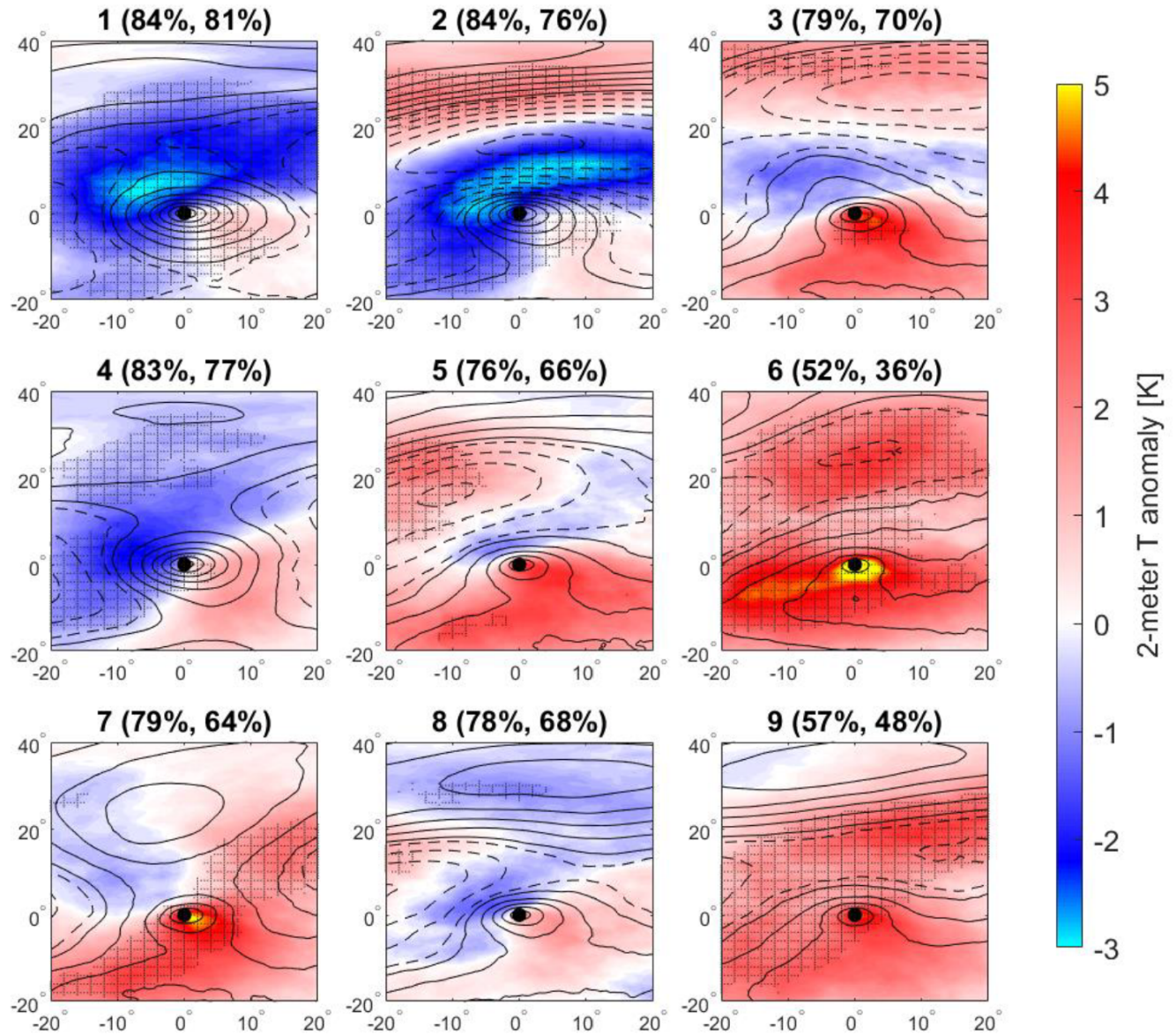
## B Appendix

### B.1 Composite of vertical cross-section of PV



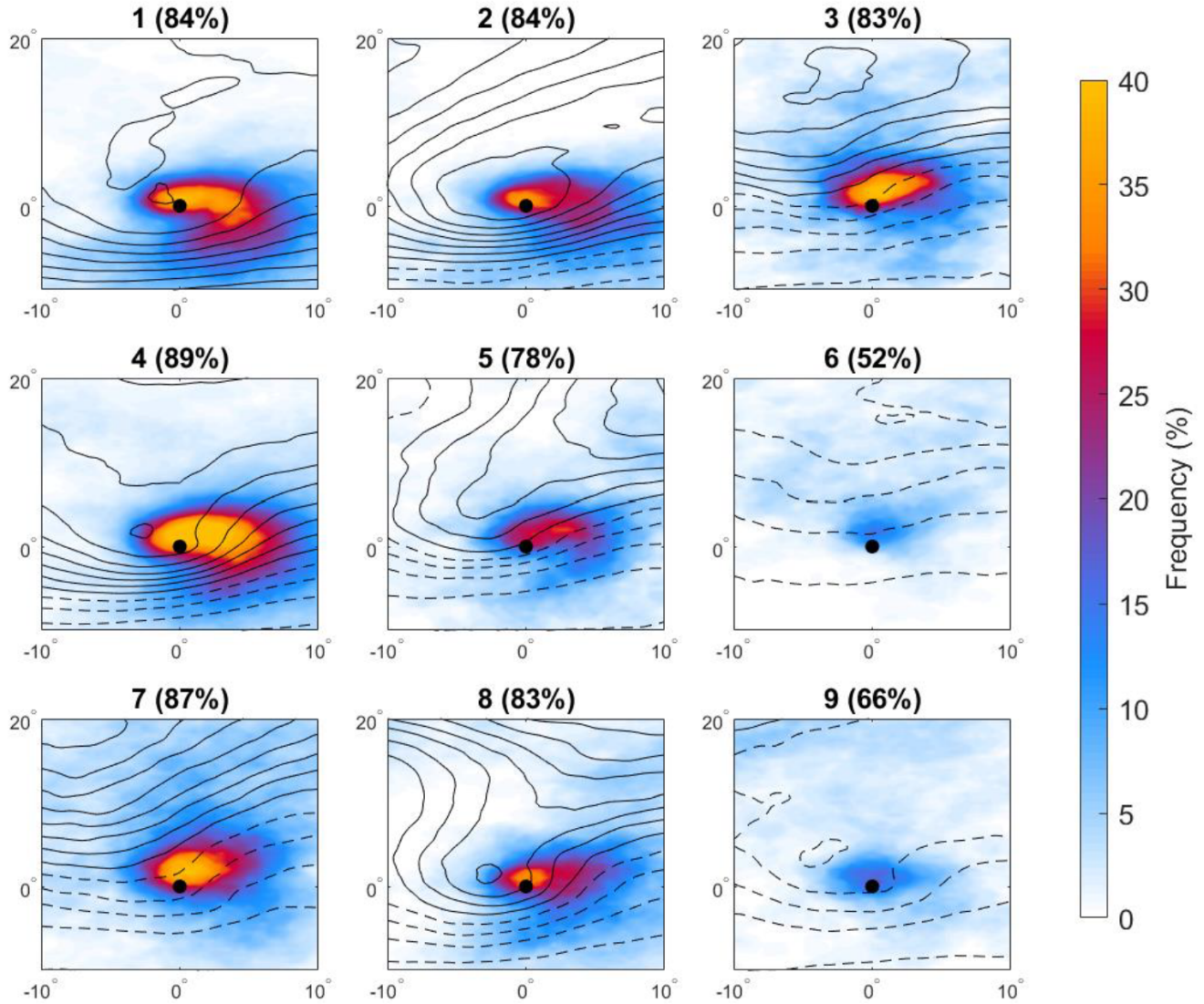
**Figure 32.** Zonal vertical cross-section composites through the center of the cyclones, by cluster. PV is shaded (PVU) with 0.7 PVU denoted in black contour. Reprinted from Givon et al. [2023].

## B.2 Composite of 2-m temperature anomaly



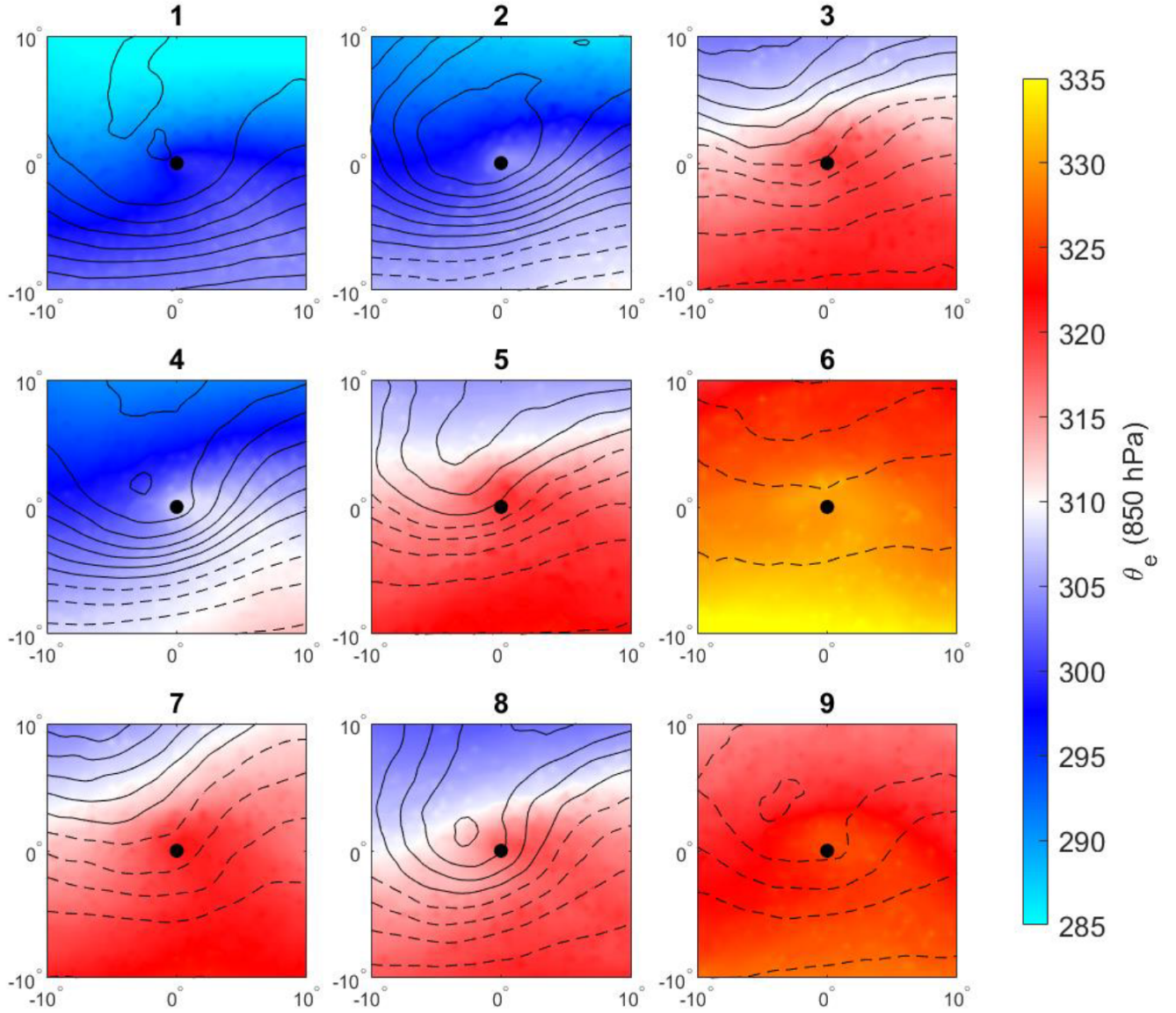
**Figure 33.** Composites of 2-m temperature anomaly from the local monthly climatology (K, shading) by cluster. Stippling denotes the 99% confidence level compared to the averaged field. Cold and warm front occurrence frequencies in  $\pm 5^\circ$  degree box around the cyclone are given in the title. Black contours are SLP at 2-hPa intervals, dashed over 1015 hPa. Reprinted from Givon et al. [2023].

## B.3 Composite of WCBs



**Figure 34.** Composite for mid-troposphere (800-400 hPa) warm conveyor belt masks (WCB). The cluster-mean frequency where a WCB is detected somewhere in the domain is reported in the panel titles. Black contours show cluster PV composites (as in Fig.(4), 0.5 PV intervals), with dashed contours for values below 3 PVU. Reprinted from Givon et al. [2023].



B.4 Composite of equivalent potential temperature ( $\theta_e$ )

**Figure 35.** Composite for 850-hPa  $\theta_e$  (K, shading). Black contours show cluster PV composites (as in Fig.(4), 0.5 PV intervals), with dashed contours for values below 3 PVU. Reprinted from Givon et al. [2023].

## B.5 Composite of cold fronts and warm fronts

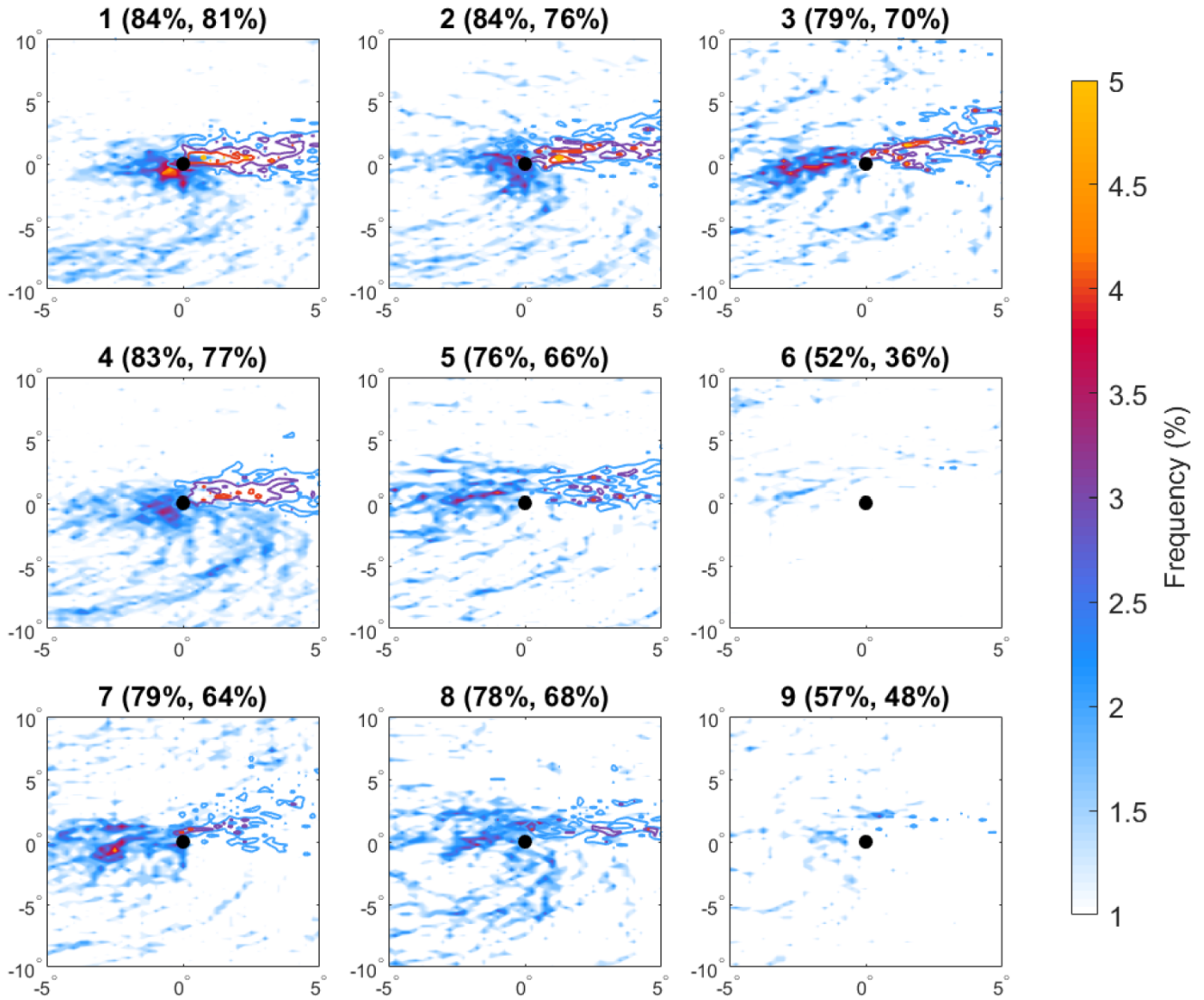


**Figure 36.** Composite cluster frequencies of cold fronts (shading) and warm fronts (contours). The cluster-mean frequencies of a nonzero signal are reported in the panel titles (left-cold, right-warm), corresponding to the fraction of cyclones showing a front present somewhere in a 10° box around the cyclone. Reprinted from Givon et al. [2023].

## References

- Alpert, P. and Ziv, B. (1989). The sharav cyclone: observations and some theoretical considerations. *Journal of Geophysical Research: Atmospheres*, 94(D15):18495–18514.
- Battaglioli, F., Groenemeijer, P., Púčík, T., Taszarek, M., Ulbrich, U., and Rust, H. (2023). Reconstructing long-term (1950-2021) trends in convective hazards using additive logistic regression models. Technical report, Copernicus Meetings.
- Berthet, C., Dessens, J., and Sánchez, J. L. (2011). Regional and yearly variations of hail frequency and intensity in france. *Atmospheric Research*, 100(4):391–400.
- Berthet, C., Wesolek, E., Dessens, J., and Sanchez, J. (2013). Extreme hail day climatology in southwestern france. *Atmospheric Research*, 123:139–150.
- Buzzi, A. and Tibaldi, S. (1978). Cyclogenesis in the lee of the alps: A case study. *Quarterly Journal of the Royal Meteorological Society*, 104(440):271–287.
- Campins, J., Genovés, A., Picornell, M., and Jansà, A. (2011). Climatology of mediterranean cyclones using the era-40 dataset. *International Journal of Climatology*, 31(11):1596–1614.
- Claud, C., Alhammoud, B., Funatsu, B. M., Lebeaupin Brossier, C., Chaboureau, J.-P., Béranger, K., and Drobinski, P. (2012). A high resolution climatology of precipitation and deep convection over the mediterranean region from operational satellite microwave data: development and application to the evaluation of model uncertainties. *Natural Hazards and Earth System Sciences*, 12(3):785–798.
- Courtier, P., Thépaut, J.-N., and Hollingsworth, A. (1994). A strategy for operational implementation of 4d-var, using an incremental approach. *Quarterly Journal of the Royal Meteorological Society*, 120(519):1367–1387.
- Dafis, S., Claud, C., Kotroni, V., Lagouvardos, K., and Rysman, J.-F. (2020). Insights into the convective evolution of mediterranean tropical-like cyclones. *Quarterly Journal of the Royal Meteorological Society*, 146(733):4147–4169.
- Emanuel, K. (2005). Genesis and maintenance of “mediterranean hurricanes”, *adv. geosci.*, 2, 217–220.
- Fiedler, S., Schepanski, K., Knippertz, P., Heinold, B., and Tegen, I. (2014). How important are atmospheric depressions and mobile cyclones for emitting mineral dust aerosol in north africa? *Atmospheric Chemistry and Physics*, 14(17):8983–9000.
- Fita, L., Romero, R., Luque, A., Emanuel, K., and Ramis, C. (2007). Analysis of the environments of seven mediterranean tropical-like storms using an axisymmetric, nonhydrostatic, cloud resolving model. *Natural Hazards and Earth System Sciences*, 7(1):41–56.
- Fita, L., Romero, R., and Ramis, C. (2006). Intercomparison of intense cyclogenesis events over the mediterranean basin based on baroclinic and diabatic influences. *Advances in Geosciences*, 7:333–342.

- Flaounas, E., Aragão, L., Bernini, L., Dafis, S., Doiteau, B., Flocas, H., L Gray, S., Karwat, A., Kouroutzoglou, J., Lionello, P., et al. (2023). A composite approach to produce reference datasets for extratropical cyclone tracks: Application to mediterranean cyclones. *Weather and Climate Dynamics Discussions*, pages 1–32.
- Flaounas, E., Davolio, S., Raveh-Rubin, S., Pantillon, F., Miglietta, M. M., Gaertner, M. A., Hatzaki, M., Homar, V., Khodayar, S., Korres, G., et al. (2022). Mediterranean cyclones: Current knowledge and open questions on dynamics, prediction, climatology and impacts. *Weather and Climate Dynamics*, 3(1):173–208.
- Flaounas, E., Gray, S. L., and Teubler, F. (2021). A process-based anatomy of mediterranean cyclones: from baroclinic lows to tropical-like systems. *Weather and Climate Dynamics*, 2(1):255–279.
- Flaounas, E., Kotroni, V., Lagouvardos, K., Gray, S. L., Rysman, J.-F., and Claud, C. (2018). Heavy rainfall in mediterranean cyclones. part i: contribution of deep convection and warm conveyor belt. *Climate dynamics*, 50(7):2935–2949.
- Flaounas, E., Lagouvardos, K., Kotroni, V., Claud, C., Delanoë, J., Flamant, C., Madonna, E., and Wernli, H. (2016). Processes leading to heavy precipitation associated with two mediterranean cyclones observed during the hymex sop1. *Quarterly Journal of the Royal Meteorological Society*, 142:275–286.
- Flaounas, E., Raveh-Rubin, S., Wernli, H., Drobinski, P., and Bastin, S. (2015). The dynamical structure of intense mediterranean cyclones. *Climate Dynamics*, 44:2411–2427.
- Flocas, H. (2000). Diagnostics of cyclogenesis over the aegean sea using potential vorticity inversion. *Meteorology and Atmospheric Physics*, 73(1-2):25–33.
- Galanaki, E., Flaounas, E., Kotroni, V., Lagouvardos, K., and Argiriou, A. (2016). Lightning activity in the mediterranean: quantification of cyclones contribution and relation to their intensity. *Atmospheric Science Letters*, 17(9):510–516.
- Galway, J. G. (1956). The lifted index as a predictor of latent instability. *Bulletin of the American Meteorological Society*, 37(10):528–529.
- Givon, Y., Hess, O., Flaounas, E., Catto, J. L., Sprenger, M., and Raveh-Rubin, S. (2023). Process-based classification of mediterranean cyclones using potential vorticity. *EGUsphere*, 2023:1–36.
- Hersbach, H., Bell, B., Berrisford, P., Hirahara, S., Horányi, A., Muñoz-Sabater, J., Nicolas, J., Peubey, C., Radu, R., Schepers, D., et al. (2020). The era5 global reanalysis. *Quarterly Journal of the Royal Meteorological Society*, 146(730):1999–2049.
- Homar, V., Jansà, A., Campins, J., Genovés, A., and Ramis, C. (2007). Towards a systematic climatology of sensitivities of mediterranean high impact weather: a contribution based on intense cyclones. *Natural Hazards and Earth System Sciences*, 7(4):445–454.
- Houze Jr, R. A. (2004). Mesoscale convective systems. *Reviews of Geophysics*, 42(4).

- Johns, R. H. and Doswell III, C. A. (1992). Severe local storms forecasting. *Wea. Forecasting*, 7(4):588–612.
- Johnson, R. (2003). Thermal low. *Encyclopedia of Atmospheric Science*, pages 2269–2273.
- Kohonen, T. (1990). The self-organizing map. *Proceedings of the IEEE*, 78(9):1464–1480.
- Kouroutzoglou, J., Avgoustoglou, E. N., Flocas, H. A., Hatzaki, M., Skrimizeas, P., and Keay, K. (2018). Assessment of the role of sea surface fluxes on eastern mediterranean explosive cyclogenesis with the aid of the limited-area model cosmo. gr. *Atmospheric Research*, 208:132–147.
- Lionello, P., Bhend, J., Buzzi, A., Della-Marta, P., Krichak, S., Jansa, A., Maheras, P., Sanna, A., Trigo, I., and Trigo, R. (2006). Cyclones in the mediterranean region: climatology and effects on the environment. In *Developments in earth and environmental sciences*, volume 4, pages 325–372. Elsevier.
- Markowski, P. and Richardson, Y. (2011). *Mesoscale meteorology in midlatitudes*. John Wiley & Sons.
- Michaelides, S., Karacostas, T., Sánchez, J. L., Retalis, A., Pytharoulis, I., Homar, V., Romero, R., Zanis, P., Giannakopoulos, C., Bühl, J., et al. (2018). Reviews and perspectives of high impact atmospheric processes in the mediterranean. *Atmospheric Research*, 208:4–44.
- Miglietta, M. M. and Rotunno, R. (2019). Development mechanisms for mediterranean tropical-like cyclones (medicanes). *Quarterly Journal of the Royal Meteorological Society*, 145(721):1444–1460.
- Neiman, P. J. and Shapiro, M. (1993). The life cycle of an extratropical marine cyclone. part i: Frontal-cyclone evolution and thermodynamic air-sea interaction. *Monthly Weather Review*, 121(8):2153–2176.
- Pacey, G. P., Schultz, D. M., and Garcia-Carreras, L. (2021). Severe convective windstorms in europe: Climatology, preconvective environments, and convective mode. *Weather and Forecasting*, 36(1):237–252.
- Petterssen, S. (1956). *Weather analysis and forecasting, 2nd Edition*, volume 1. McGraw-Hill, New York, USA.
- Petterssen, S. and Smebye, S. (1971). On the development of extratropical cyclones. *Quarterly Journal of the Royal Meteorological Society*, 97(414):457–482.
- Pfahl, S., Madonna, E., Boettcher, M., Joos, H., and Wernli, H. (2014). Warm conveyor belts in the era-interim dataset (1979–2010). part ii: Moisture origin and relevance for precipitation. *Journal of Climate*, 27(1):27–40.
- Pinto, J. G., Karremann, M. K., Born, K., Della-Marta, P. M., and Klawe, M. (2012). Loss potentials associated with european windstorms under future climate conditions. *Climate Research*, 54(1):1–20.
- Porcù, F., Carrassi, A., Medaglia, C. M., Prodi, F., and Mugnai, A. (2007). A study on cut-off low vertical structure and precipitation in the mediterranean region. *Meteorology and Atmospheric Physics*, 96:121–140.

- Púčík, T., Groenemeijer, P., Rýva, D., and Kolář, M. (2015). Proximity soundings of severe and nonsevere thunderstorms in central europe. *Monthly Weather Review*, 143(12):4805–4821.
- Punge, H., Bedka, K., Kunz, M., and Reinbold, A. (2017). Hail frequency estimation across europe based on a combination of overshooting top detections and the era-interim reanalysis. *Atmospheric Research*, 198:34–43.
- Rädler, A. T., Groenemeijer, P., Faust, E., and Sausen, R. (2018). Detecting severe weather trends using an additive regressive convective hazard model (ar-chamo). *Journal of Applied Meteorology and Climatology*, 57(3):569–587.
- Raveh-Rubin, S. and Flaounas, E. (2017). A dynamical link between deep atlantic extratropical cyclones and intense mediterranean cyclones. *Atmospheric Science Letters*, 18(5):215–221.
- Raveh-Rubin, S. and Wernli, H. (2016). Large-scale wind and precipitation extremes in the mediterranean: dynamical aspects of five selected cyclone events. *Quarterly Journal of the Royal Meteorological Society*, 142(701):3097–3114.
- Reale, M. and Lionello, P. (2013). Synoptic climatology of winter intense precipitation events along the mediterranean coasts. *Natural Hazards and Earth System Sciences*, 13(7):1707–1722.
- Rigo, T., Berenguer, M., and del Carmen Llasat, M. (2019). An improved analysis of mesoscale convective systems in the western mediterranean using weather radar. *Atmospheric research*, 227:147–156.
- Romero, R., Gayà, M., and Doswell III, C. A. (2007). European climatology of severe convective storm environmental parameters: A test for significant tornado events. *Atmospheric Research*, 83(2-4):389–404.
- Saaroni, H., Harpaz, T., and Ziv, B. (2017). A new classification algorithm for daughter cyclone formation with respect to the parent’s frontal system—application for the mediterranean basin. *International Journal of Climatology*, 37(2):1050–1065.
- Scherrmann, A., Wernli, H., and Flaounas, E. (2023). Origin of low-tropospheric potential vorticity in mediterranean cyclones. *Weather and Climate Dynamics*, 4(1):157–173.
- Taszarek, M., Allen, J. T., Groenemeijer, P., Edwards, R., Brooks, H. E., Chmielewski, V., and Enno, S.-E. (2020a). Severe convective storms across europe and the united states. part i: Climatology of lightning, large hail, severe wind, and tornadoes. *Journal of Climate*, 33(23):10239–10261.
- Taszarek, M., Allen, J. T., Púčík, T., Hoogewind, K. A., and Brooks, H. E. (2020b). Severe convective storms across europe and the united states. part ii: Era5 environments associated with lightning, large hail, severe wind, and tornadoes. *Journal of Climate*, 33(23):10263–10286.
- Taszarek, M., Brooks, H. E., and Czernecki, B. (2017). Sounding-derived parameters associated with convective hazards in europe. *Monthly Weather Review*, 145(4):1511–1528.
- Thompson, R. L., Mead, C. M., and Edwards, R. (2007). Effective storm-relative helicity and bulk shear in supercell thunderstorm environments. *Weather and forecasting*, 22(1):102–115.

- Thorncroft, C., Hoskins, B., and McIntyre, M. (1993). Two paradigms of baroclinic-wave life-cycle behaviour. *Quarterly Journal of the Royal Meteorological Society*, 119(509):17–55.
- Toreti, A., Giannakaki, P., and Martius, O. (2016). Precipitation extremes in the mediterranean region and associated upper-level synoptic-scale flow structures. *Climate dynamics*, 47:1925–1941.
- Tous, M. and Romero, R. (2013). Meteorological environments associated with medicane development. *International Journal of Climatology*, 33(1):1–14.
- Trigo, I. F., Bigg, G. R., and Davies, T. D. (2002). Climatology of cyclogenesis mechanisms in the mediterranean. *Monthly Weather Review*, 130(3):549–569.
- Trigo, I. F., Davies, T. D., and Bigg, G. R. (1999). Objective climatology of cyclones in the mediterranean region. *Journal of climate*, 12(6):1685–1696.
- Urraca, R., Huld, T., Gracia-Amillo, A., Martinez-de Pison, F. J., Kaspar, F., and Sanz-Garcia, A. (2018). Evaluation of global horizontal irradiance estimates from era5 and cosmo-rea6 reanalyses using ground and satellite-based data. *Solar Energy*, 164:339–354.
- Welker, C., Martius, O., Froidevaux, P., Reijmer, C. H., and Fischer, H. (2014). A climatological analysis of high-precipitation events in dronning maud land, antarctica, and associated large-scale atmospheric conditions. *Journal of Geophysical Research: Atmospheres*, 119(21):11–932.
- Wernli, H. and Sprenger, M. (2007). Identification and era-15 climatology of potential vorticity streamers and cutoffs near the extratropical tropopause. *Journal of the atmospheric sciences*, 64(5):1569–1586.
- Wilks, D. (2016). “the stippling shows statistically significant grid points”: How research results are routinely overstated and overinterpreted, and what to do about it. *Bulletin of the American Meteorological Society*, 97(12):2263–2273.
- Yano, J.-I. and Emanuel, K. (1991). An improved model of the equatorial troposphere and its coupling with the stratosphere. *Journal of Atmospheric Sciences*, 48(3):377–389.
- Ziv, B., Harpaz, T., Saaroni, H., and Blender, R. (2015). A new methodology for identifying daughter cyclogenesis: application for the mediterranean basin. *International Journal of Climatology*, 35(13):3847–3861.

## Acknowledgements

I would like to thank my co-supervisors Dr. Raphaël Rousseau-Rizzi and Dr. Alice Portal, for their valuable time in helping me through this master thesis. The quality of this study has greatly improved as a result of their input and conversations. I would also like to thank Prof. Dr. Olivia Romppainen-Martius for her insightful remarks and for the feeling of inclusiveness within the Climate Impact group.

The study is based upon work from COST Action CA19109 “MedCyclones”, supported by COST - European Cooperation in Science and Technology (<https://www.cost.eu/>). Thereby, I want to give my thanks to Yonatan Givon for sharing with me his research on cyclone clusters. I would also like to extend my thanks to Francesco Battaglioli for the novel data on hail and lightning proxies and his support.

Finally, I want to thank my family for providing me the opportunity and support to pursue this study, and my friends for making this the best experience.



## Declaration of consent

on the basis of Article 30 of the RSL Phil.-nat. 18

Name/First Name: Angelidou Andrea

Registration Number: 21-117-304

Study program: MSc in Climate Sciences

Bachelor       Master       Dissertation

Title of the thesis: Convective environments along Mediterranean cyclone tracks:  
exploring severe surface weather

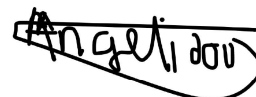
Supervisor: Prof. Dr. Olivia Romppainen-Martius

I declare herewith that this thesis is my own work and that I have not used any sources other than those stated. I have indicated the adoption of quotations as well as thoughts taken from other authors as such in the thesis. I am aware that the Senate pursuant to Article 36 paragraph 1 litera r of the University Act of 5 September, 1996 is authorized to revoke the title awarded on the basis of this thesis.

For the purposes of evaluation and verification of compliance with the declaration of originality and the regulations governing plagiarism, I hereby grant the University of Bern the right to process my personal data and to perform the acts of use this requires, in particular, to reproduce the written thesis and to store it permanently in a database, and to use said database, or to make said database available, to enable comparison with future theses submitted by others.

Bern, 30.08.2023

Place/Date



Signature